Solar Cell

Byungwoo Park

Department of Materials Science and Engineering
Seoul National University

http://bp.snu.ac.kr

Solar Energy Applications

Solar Car
Auburn Univ.

Solar Arrays
http://www.solar.org/solar/array

Solar Roof
http://thefraserdomain.typepad.com/energy

165,000 TW of sunlight hits the earth every day

Prof. Smalley's Group (Rice University)

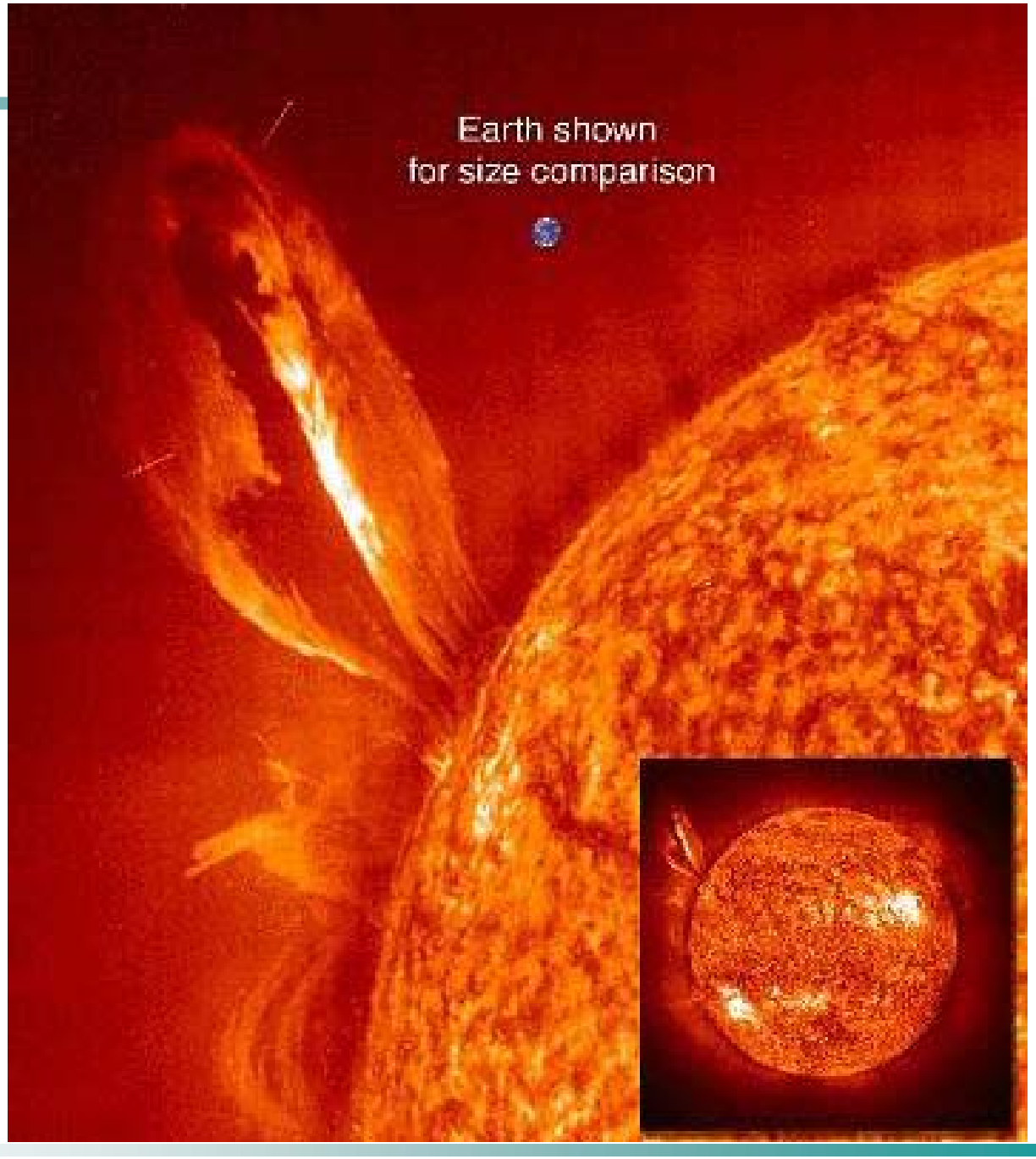

Solar-Cell Land Area Requirements

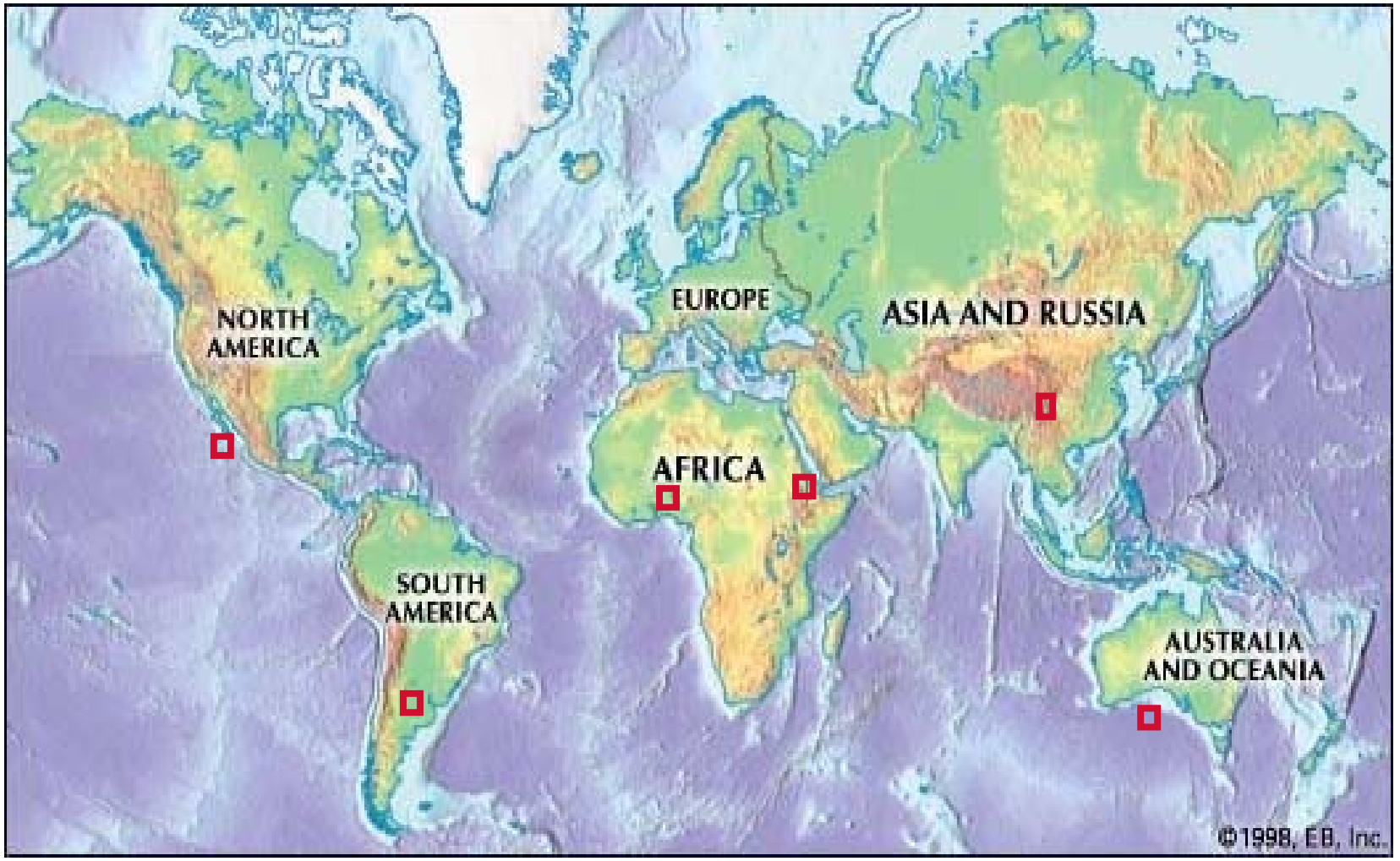

6 Boxes at 3.3 TW Each = 20 TW

Solar Cell Plants

Germany, Brandis (24 MW)
(40 MW is planned.)

Spain, Calaveron (21.2 MW)

Spain, Beneixama (20 MW)

Korea, Sinan (19.6 MW)

The largest solar-power plant is located in Spain, Murcia (26 MW).
Among top 50 solar-power plants, 31 plants are in Spain.
(cf. Germany: 14, U.S.A : 2, Korea: 1, Japan: 1, and Portugal: 1)
Korea's solar pant is the 7th in the world.

Photovoltaic Applications and Technologies
http://www.pvresources.com

Solar Cell

Advanced Inorganic Materials for Photovoltaics

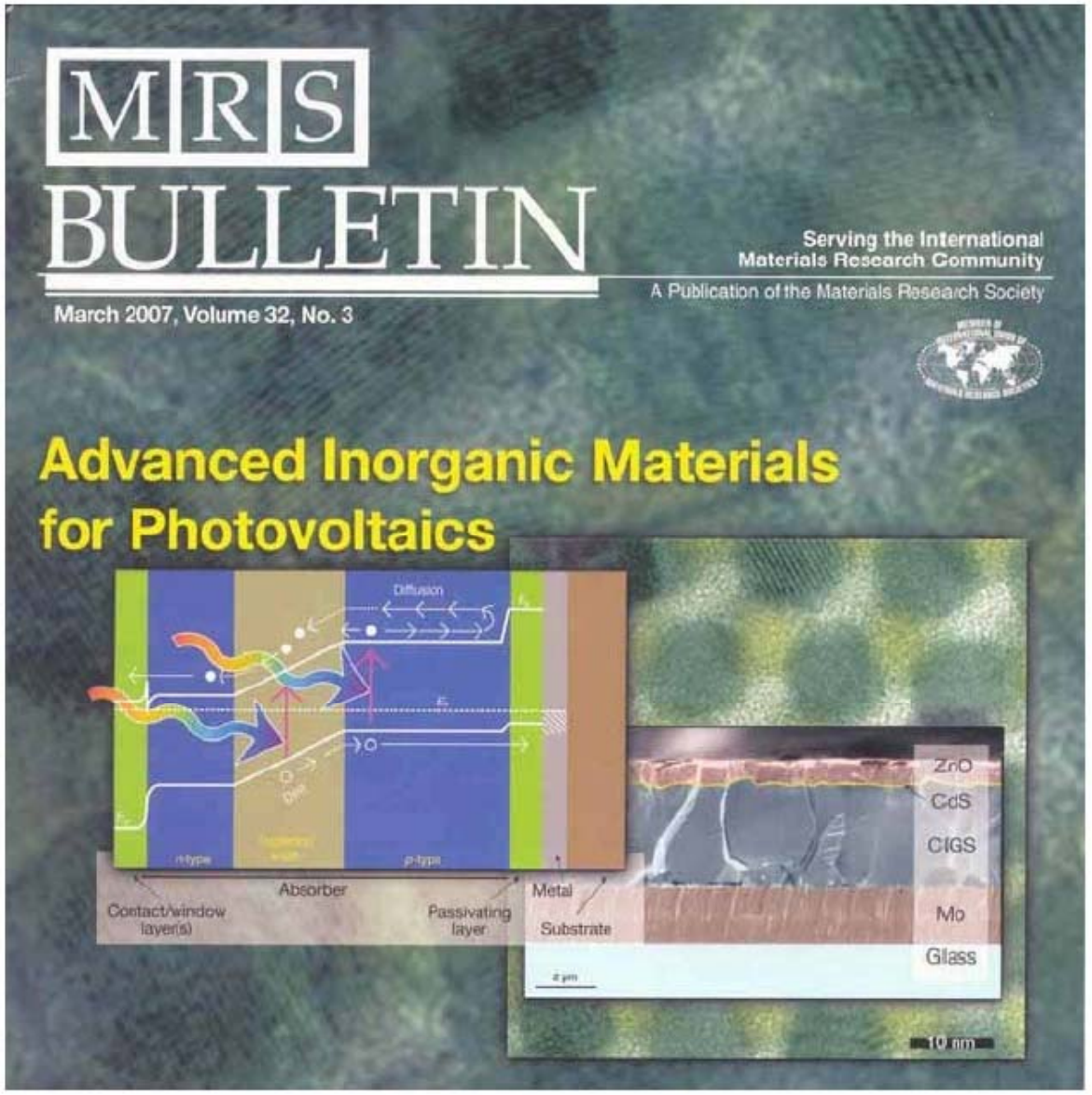

Solar Energy Conversion

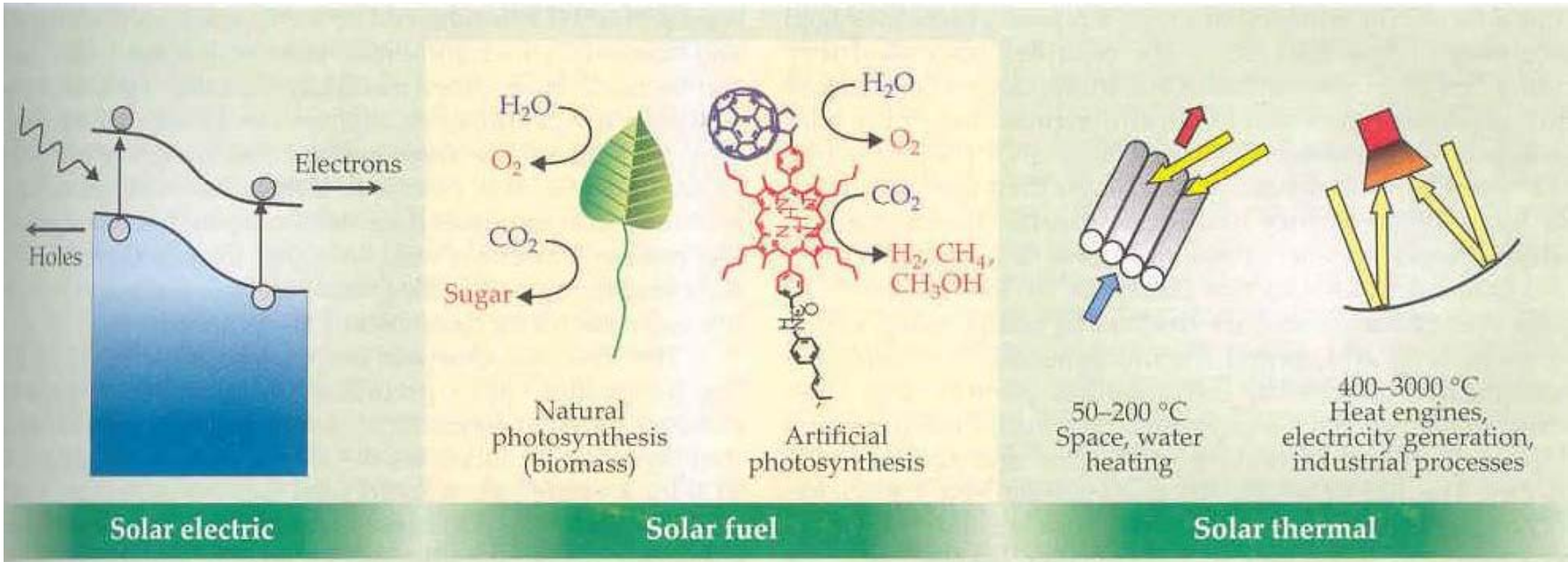

Figure 1. Solar photons convert naturally into three forms of energy—electricity, chemical fuel, and heat—that link seamlessly with existing energy chains. Despite the enormous energy flux supplied by the Sun, the three conversion routes supply only a tiny fraction of our current and future energy needs. Solar electricity, at between 5 and 10 times the cost of electricity from fossil fuels, supplies just 0.015% of the world's electricity demand. Solar fuel, in the form of biomass, accounts for approximately 11% of world fuel use, but the majority of that is harvested unsustainably. Solar heat provides 0.3% of the energy used for heating space and water. It is anticipated that by the year 2030 the world demand for electricity will double and the demands for fuel and heat will increase by 60%. The utilization gap between solar energy's potential and our use of it can be overcome by raising the efficiency of the conversion processes, which are all well below their theoretical limits.

Physics Today (2007)

G. W. Crabtree and N. S. Lewis

Photovoltaic Conversion Efficiencies & Novel Conducting Polymers

Photovoltaic conversion efficiencies

	Laboratory best*	Thermodynamic limit
Single junction		31%
Silicon (crystalline)	25%	
Silicon (nanocrystalline)	10%	
Gallium arsenide	25%	
Dye sensitized	10%	
Organic	3%	
Multijunction	32%	66%
Concentrated sunlight (single junction)	28%	41%
Carrier multiplication		42%

*As verified by the National Renewable Energy Laboratory. Organic cell efficiencies of up to 5% have been reported in the literature.

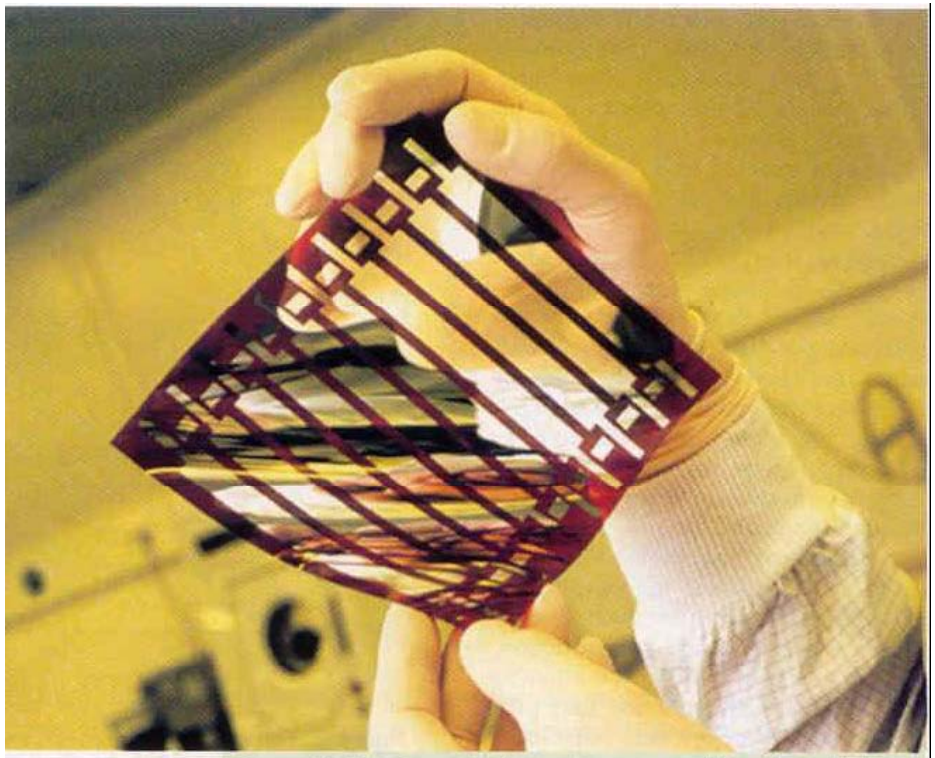

Figure 2. Novel conducting polymers enable solar cells that are flexible, inexpensive, and versatile. The new materials can be coated or printed onto flexible or rigid surfaces. (Image courtesy of Konarka Technologies.)

Physics Today (2007)

Illustration of the Energy Landscape

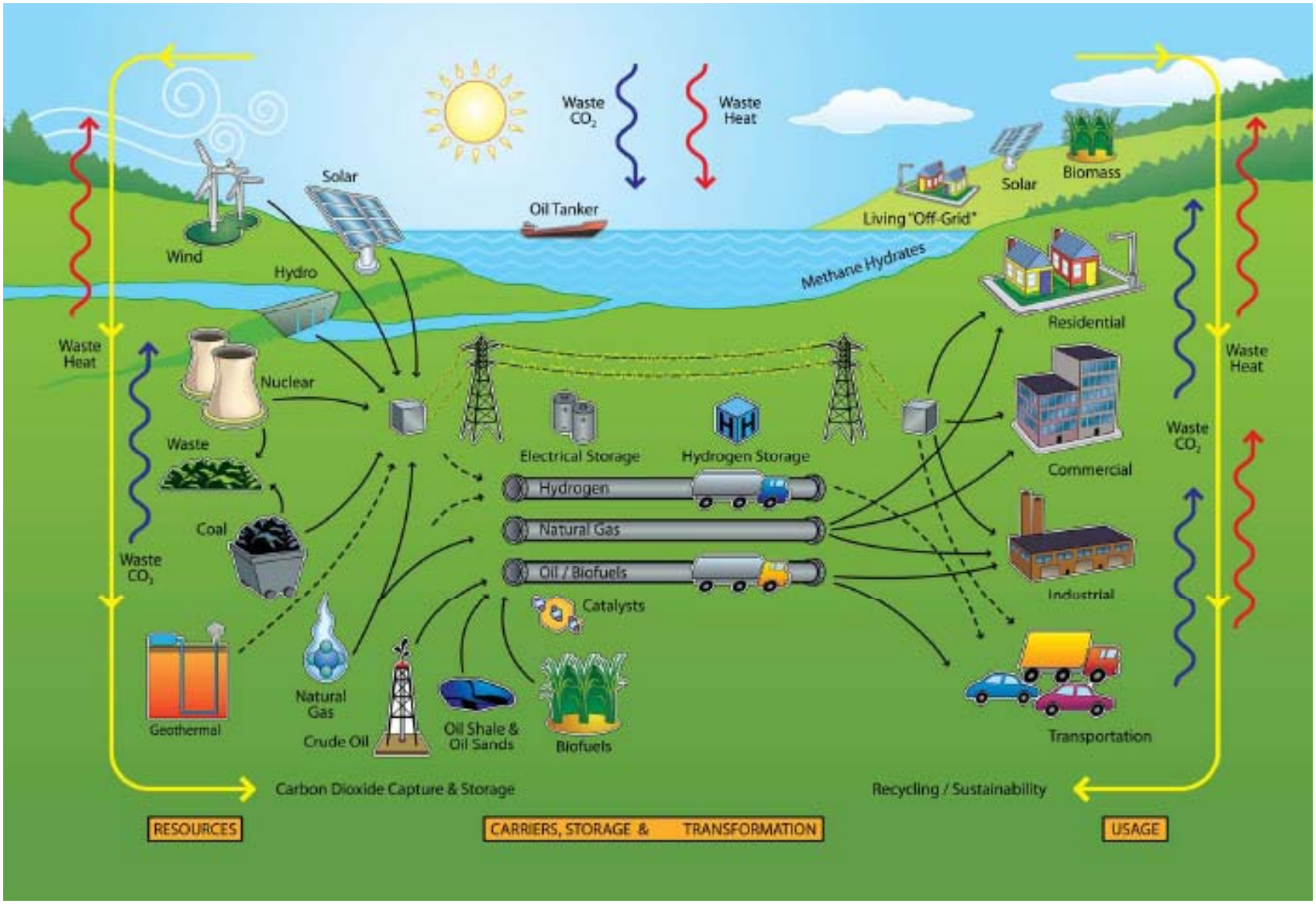

MRS Bulletin (2008).

The Global Energy Landscape and Materials Innovation

V.S. Arunachalam (Center for Study of Science, Technology & Policy, India)
E.L. Fleischer (Materials Research Society, USA)

Abstract

Availability of affordable energy has enabled spectacular growth of industrialization and human development in all parts of the world. With growth now accelerating in developing countries, demands on energy sources and infrastructure are being stretched to new limits. Additional energy issues include the push for renewable resources with reduced greenhouse gas emissions and energy security affected by the uneven distribution of energy resources around the globe. Together, these issues present a field of opportunity for innovations to address energy challenges throughout the world and all along the energy flow. These energy challenges form the backdrop for this special expanded issue of *MRS Bulletin* on Harnessing Materials for Energy. This article introduces the global landscape of materials issues associated with energy. It examines the complex web of energy availability, production, storage, transmission, distribution, use, and efficiency. It focuses on the materials challenges that lie at the core of these areas and discusses how revolutionary concepts can address them. Cross-cutting topics are introduced and interrelationships between topics explored. Article topics are set in the context of the grand energy challenges that face the world into the middle of this century.

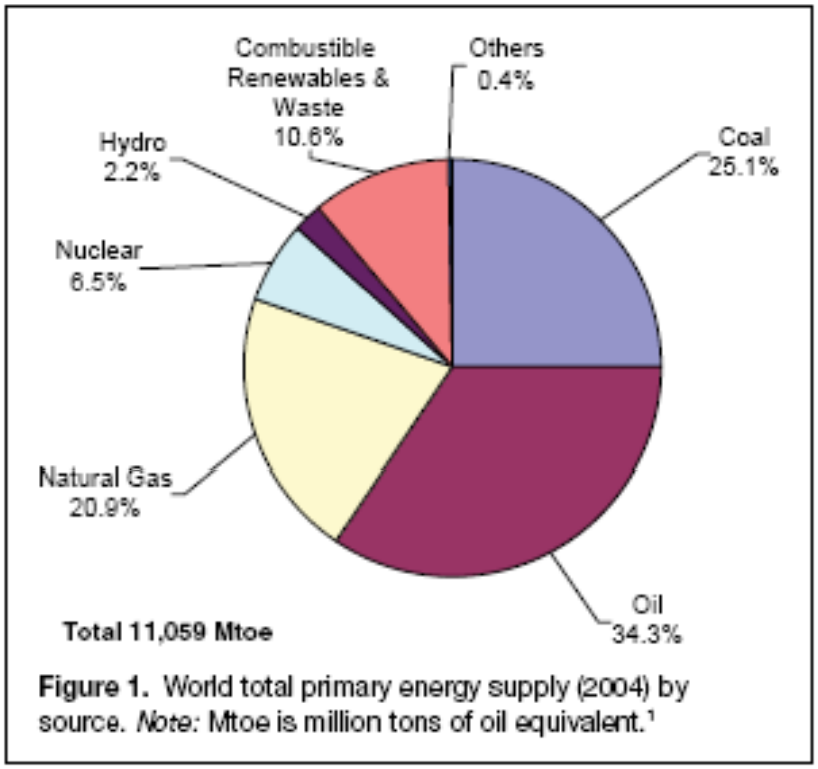

Figure 1. World total primary energy supply (2004) by source. *Note:* Mtoe is million tons of oil equivalent.[1]

V. S. Arunachalam (Center for Study of Science, India) and E. L. Fleischer (MRS)
MRS Bulletin (2008).

Energy Flow Diagram for the U.S.A. (2006)

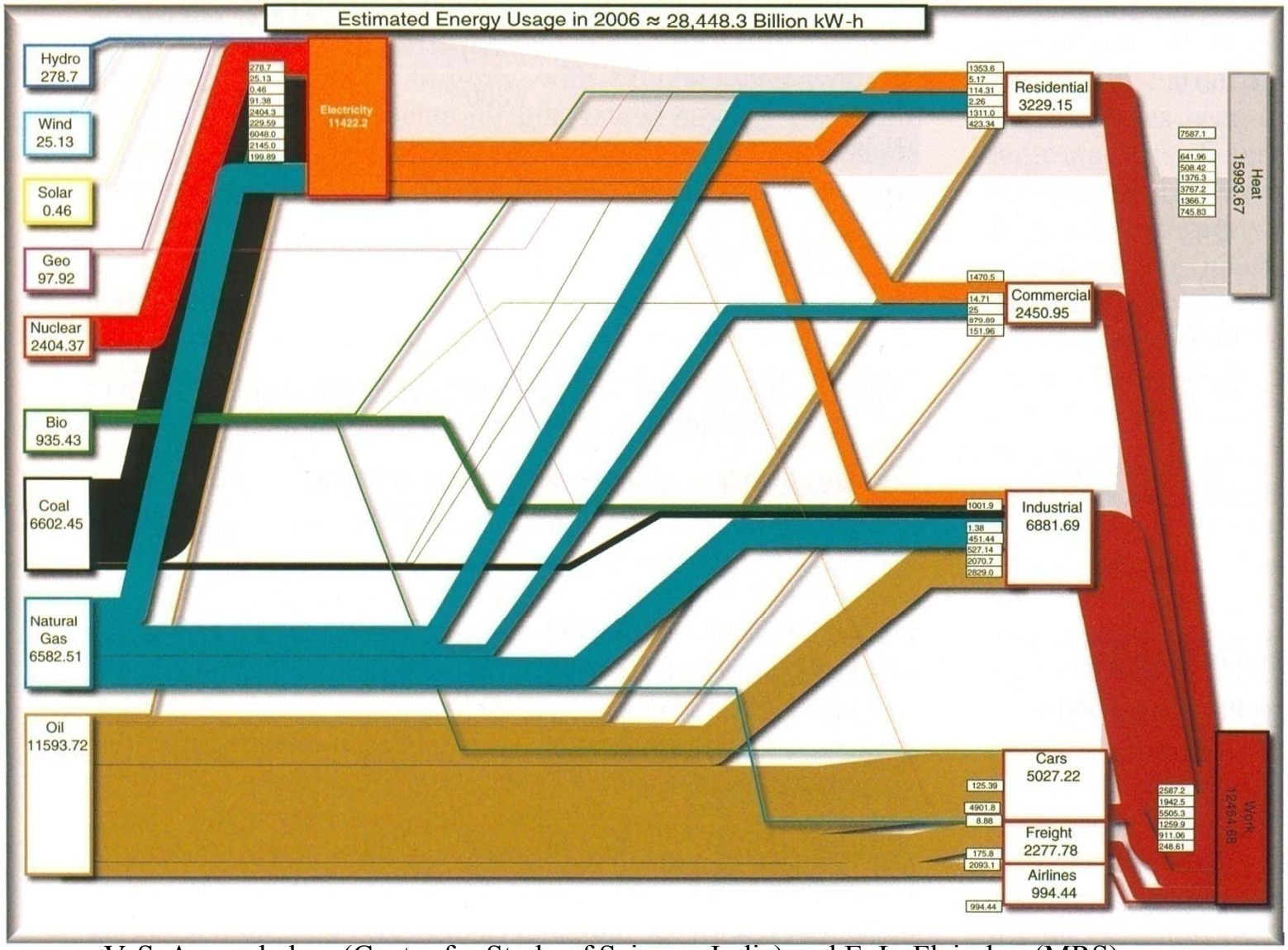

V. S. Arunachalam (Center for Study of Science, India) and E. L. Fleischer (MRS)
MRS Bulletin (2008).

Solar Energy Conversion Toward 1 Terawatt

David Ginley (National Renewable Energy Laboratory, USA)
Martin A. Green (University of New South Wales, Australia)
Reuben Collins (Colorado School of Mines, USA)

Abstract

The direct conversion of solar energy to electricity by photovoltaic cells or thermal energy in concentrated solar power systems is emerging as a leading contender for next-generation green power production. The photovoltaics (PV) area is rapidly evolving based on new materials and deposition approaches. At present, PV is predominately based on crystalline and polycrystalline Si and is growing at >40% per year with production rapidly approaching 3 gigawatts/year with PV installations supplying <1% of energy used in the world. Increased cell efficiency and reduced manufacturing expenses are critical in achieving reasonable costs for PV and solarthermal. CdTe thin-film solar cells have reported a manufactured cost of $1.25/watt. There is also the promise of increased efficiency by use of multijunction cells or hybrid devices organized at the nanoscale. This could lead to conversion efficiencies of greater than 50%. Solar energy conversion increasingly represents one of the largest new businesses currently emerging in any sector of the economy.

David Ginley (NREL), Matin A. Green (University of New South Wales), and Reuben Collins (Colorado School of Mines) *MRS Bulletin* (2008).

World Photovoltaic Module Production

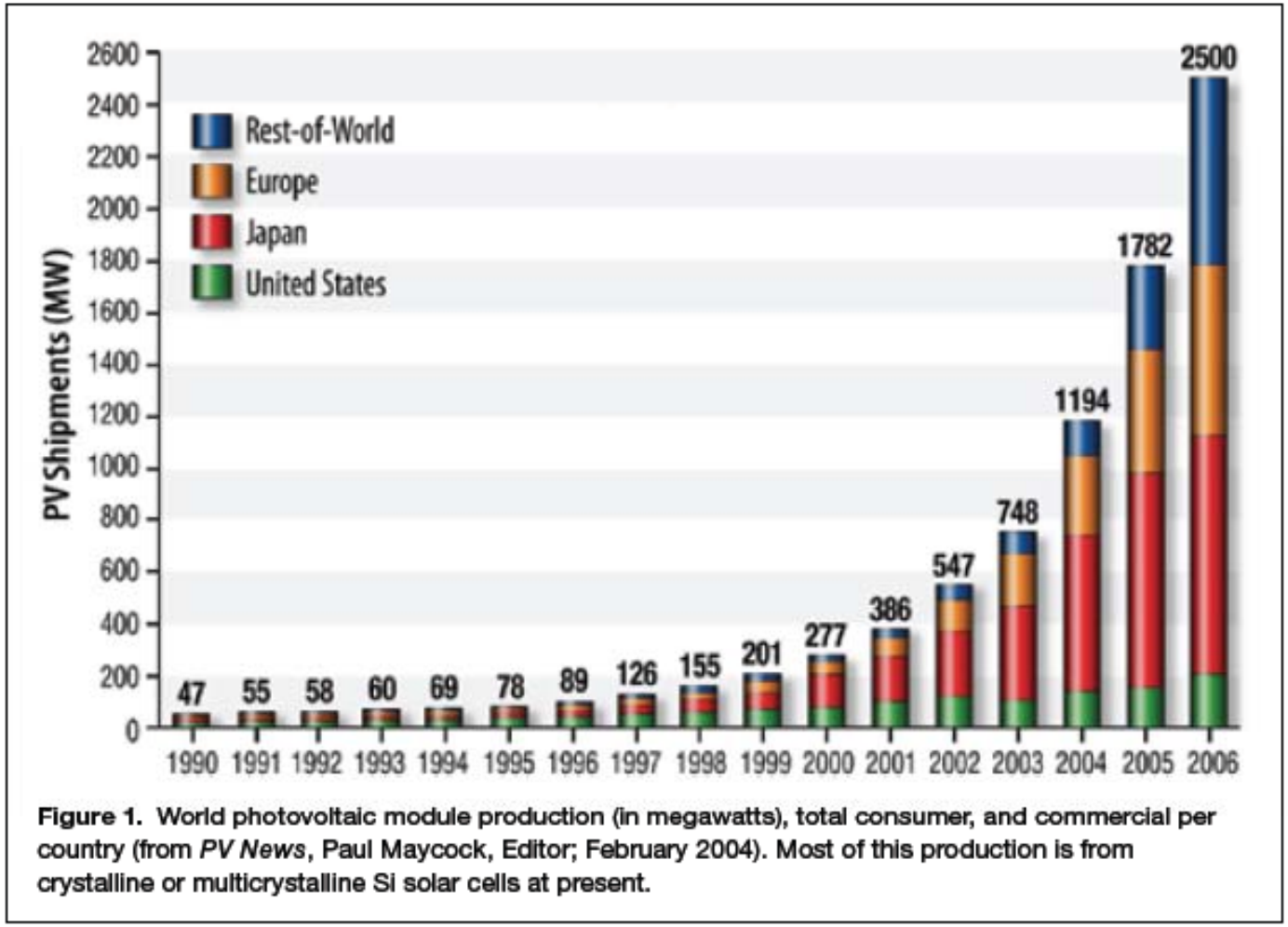

Figure 1. World photovoltaic module production (in megawatts), total consumer, and commercial per country (from *PV News*, Paul Maycock, Editor; February 2004). Most of this production is from crystalline or multicrystalline Si solar cells at present.

David Ginley (NREL), Matin A. Green (University of New South Wales), and Reuben Collins (Colorado School of Mines) *MRS Bulletin* (2008).

Solar Cell Basics

History

- 1839, Becquerel
  - Finding Photovoltaic Effect
- 1876, The same effect was demonstrated in selenium
- 1883, Se Solar Cells
- 1930, Cu_2O/Cu Solar Cells
- 1941, First silicon based solar cell demonstrated
- 1954, Beginning of modern solar cell research (Bell Lab, 4% Efficiency)
- 1958, Using as Assistant Power in the Spaceship (Vanguard I); 5 mW
- 1980, CdTe, CIS, TiO_2 Solar Cells
- 1991, Dye Sensitized Solar Cell (M. Gratzel *et al*, *Nature*)

U.S. Department of Energy
Energy Efficiency and Renewable Energy
http://www1.eere.energy.gov/solar

Solar Cell Structure

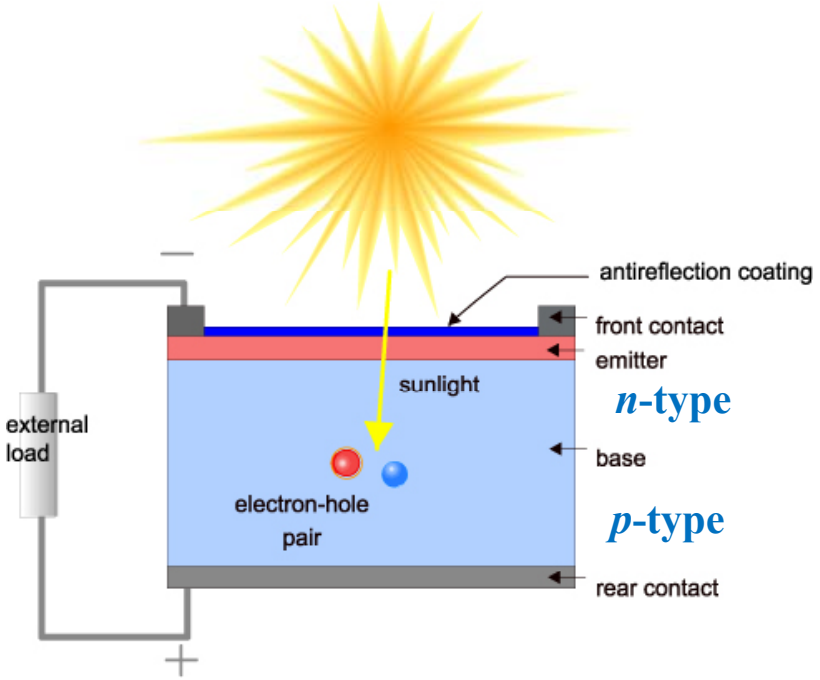

The basic steps in the operation of a solar cell:

1. Generation of light-generated carriers.
2. Collection of the light-generated carries to generate a current.
3. Generation of a large voltage across the solar cell.
4. Dissipation of power in the load and in parasitic resistances.

http://pvcdrom.pveducation.org/

LED vs. Photovoltaic

- Light-emitting diode (LED)
  - Converts electrical input to light output: electron in → photon out
  - Light source with long life, low power, compact design.
  - Applications: traffic and car lights, large displays, solid-state lighting.

- Photovoltaic (PV)
  - Converts light input to electrical output: photon in → electron out (generated electrons are "swept away" by *E* field of *p*-*n* junction).
  - Renewable energy source.

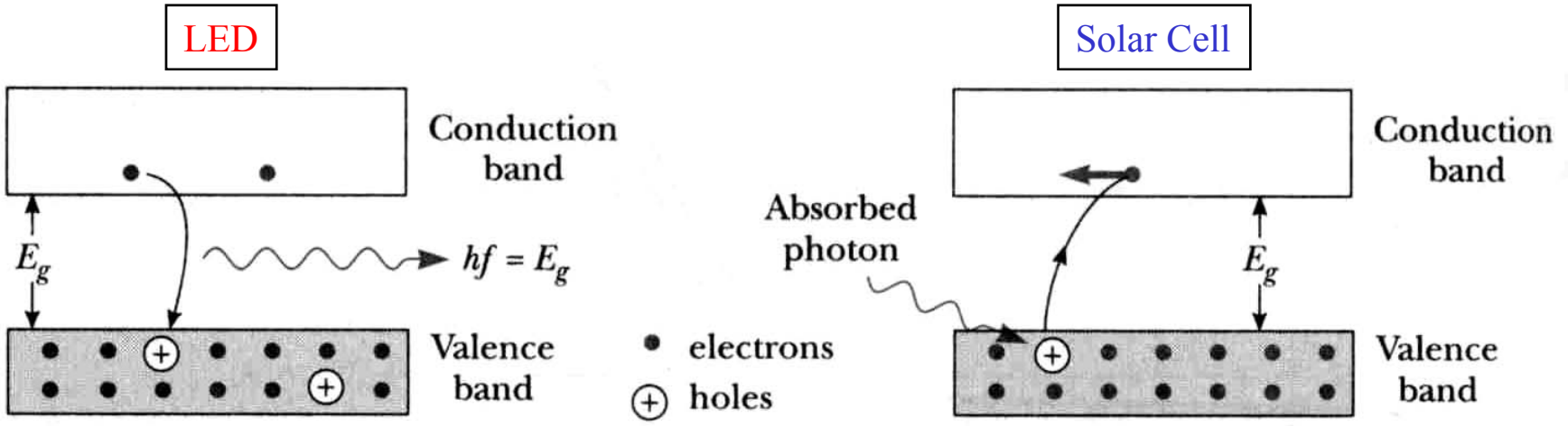

J. Nelson, *The Physics of Solar Cells*
London: Imperial College Press, 2003

Basic Structure of Si Solar Cells

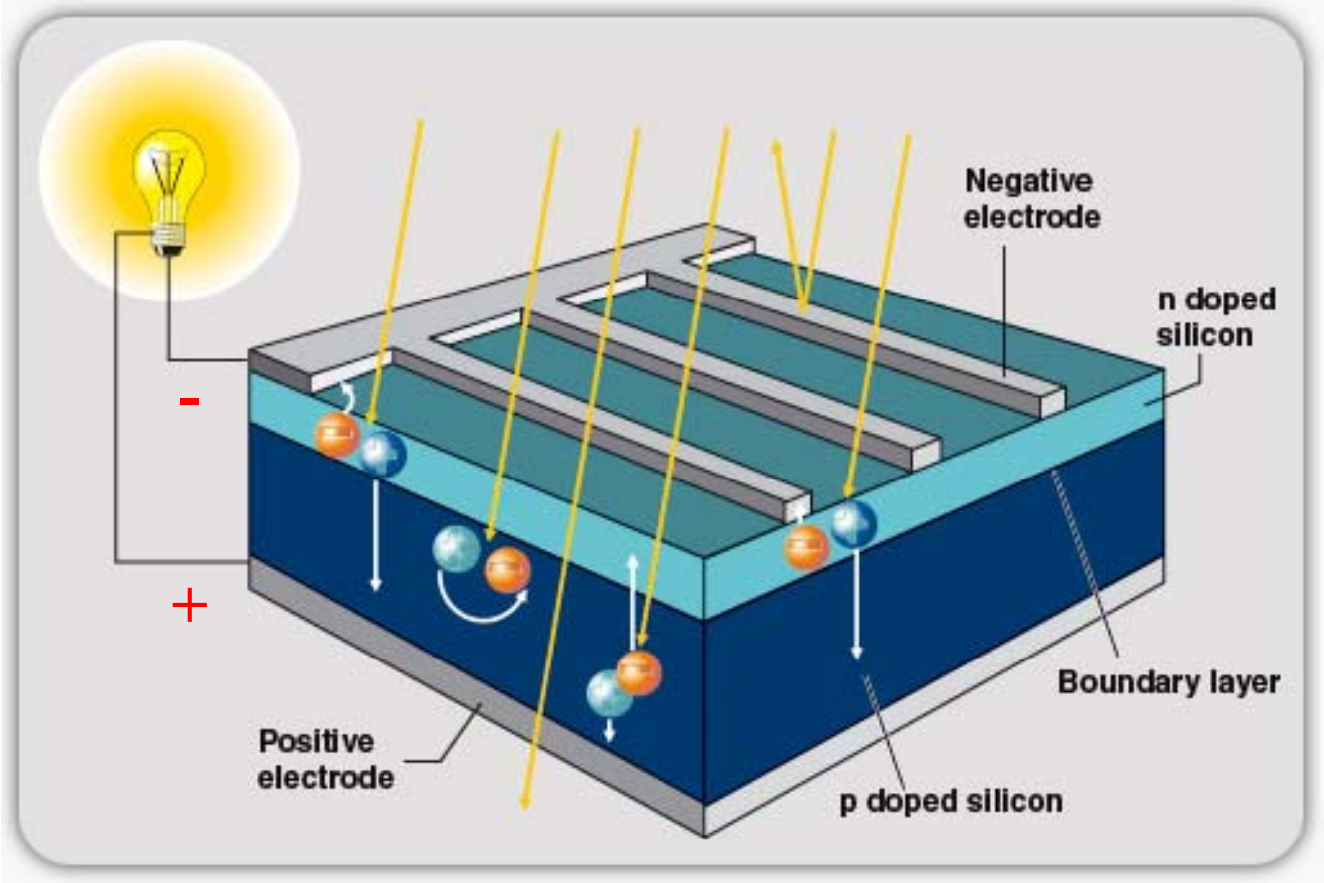

Solar-is-Future.com Homepage
http://www.solar-is-future.com

Band Structure for *c*-Si

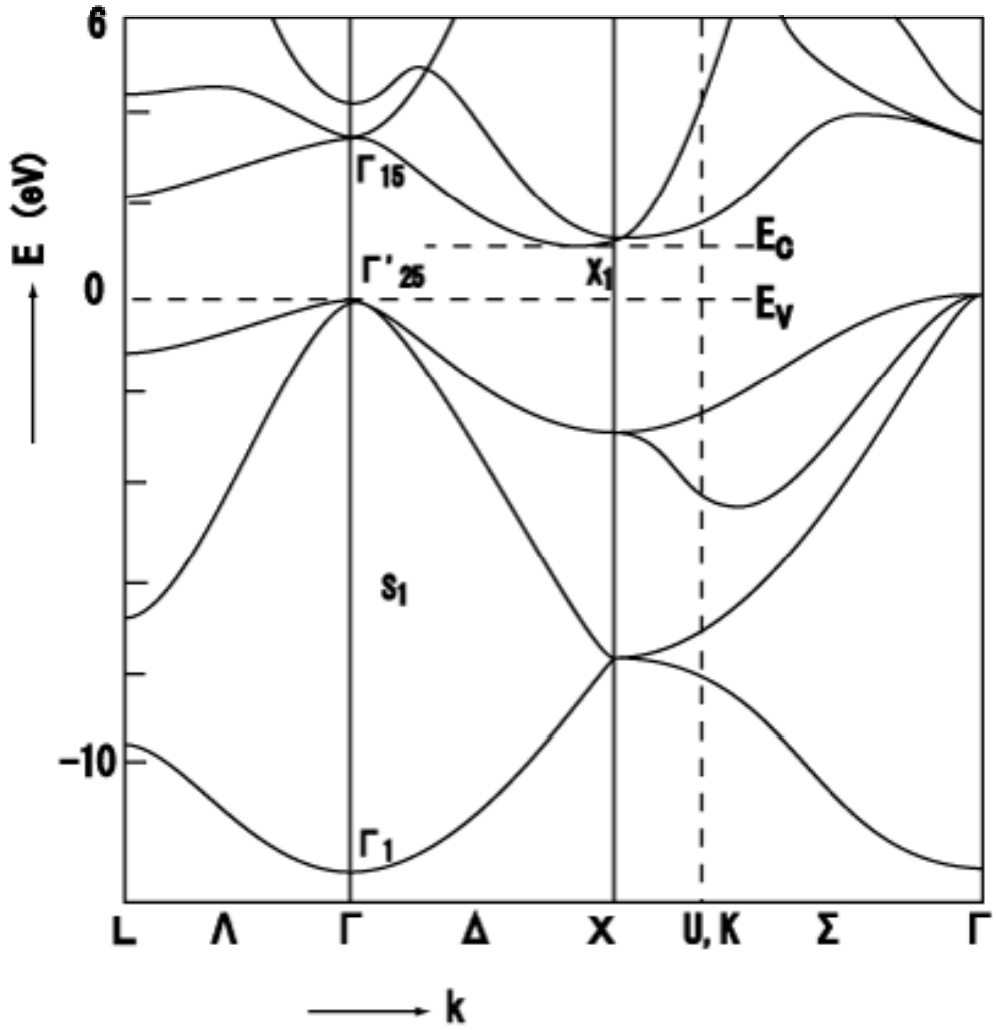

J. R. Chelikowsky (UC Berkeley) and M. L. Cohen (Lawrence Berkeley Lab.)
Phys. Rev. B **10** 5095 (1974)

PHYSICAL REVIEW B VOLUME 10, NUMBER 12 15 DECEMBER 1974

Electronic structure of silicon*

James R. Chelikowsky and Marvin L. Cohen
Department of Physics, University of California, Berkeley, California 94720
and Inorganic Materials Research Division, Lawrence Berkeley Laboratory, Berkeley, California 94720
(Received 1 July 1974)

It is shown that a purely local-pseudopotential calculation is able to accurately reproduce the major optical gaps and cyclotron masses. However, deviations from the experimental results become manifest in photoemission and x-ray charge-density results as we extend our calculations to the lower valence bands. These deviations indicate the necessity of an energy-dependent nonlocal *s*-well potential, a conclusion which is also supported by an analysis of the Heine-Abarenkov pseudopotential scheme. A detailed comparison is made between experimental results obtained from optical, photoemission, x-ray, and cyclotron-resonance measurements, and the results of both the local calculation and an energy-dependent nonlocal calculation. Yang and Coppens's recent determination of the valence charge density in silicon makes it possible to assess the accuracy of the pseudocharge densities for the first time.

p-n Junction: Band Diagram

- In equilibrium, Fermi levels must equalize.
- Hence, electrons move from *n* to *p*-side (diffusion process).
- Depletion zone occurs at junction where immobile charged ion cores remain.
- Results in a built-in electric field (10^3 to 10^5 V/cm), which opposes further diffusion.

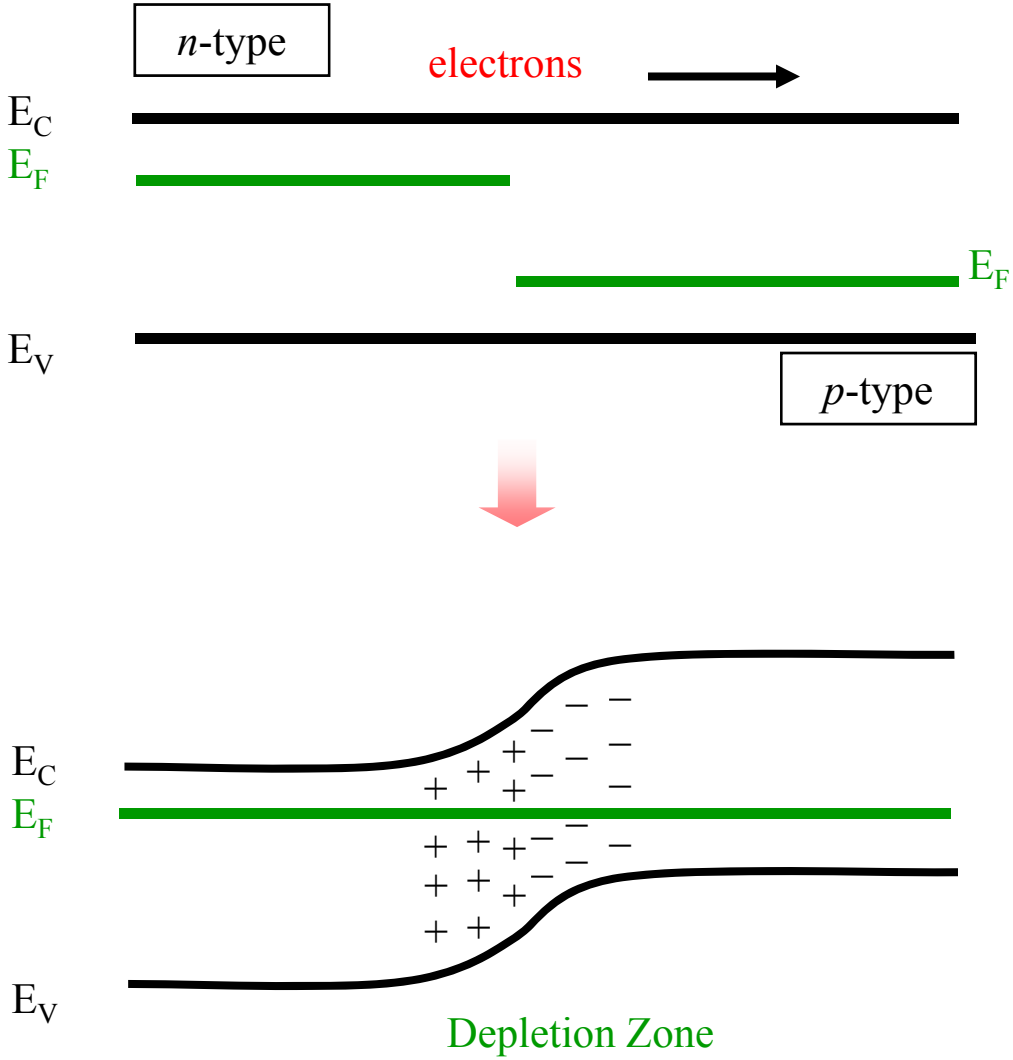

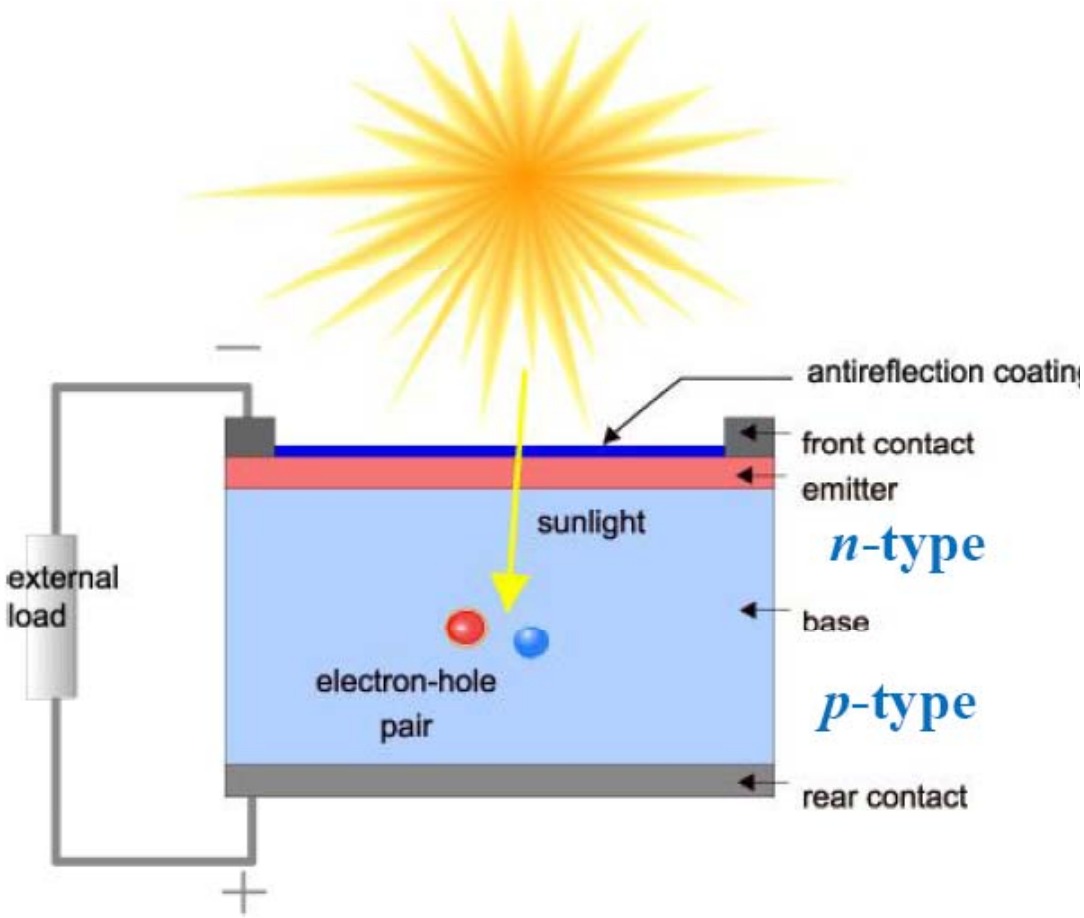
antireflection coating
front contact
emitter
sunlight
n-type
external load
base
electron-hole pair
p-type
rear contact

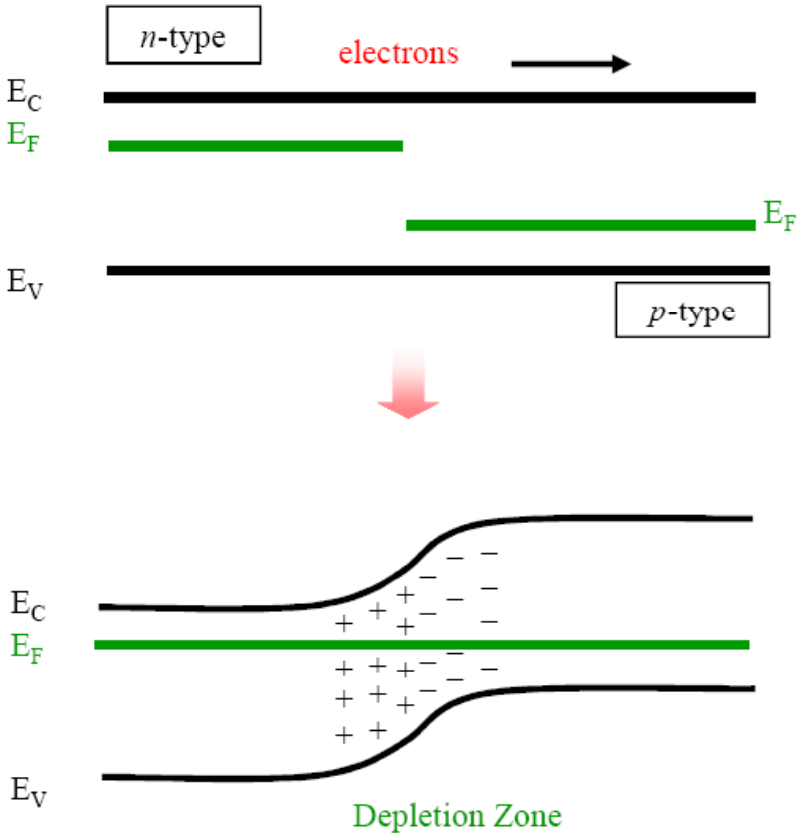
n-type
electrons
E_C
E_F
E_F
E_V
p-type
E_C
E_F
E_V
Depletion Zone

Issues

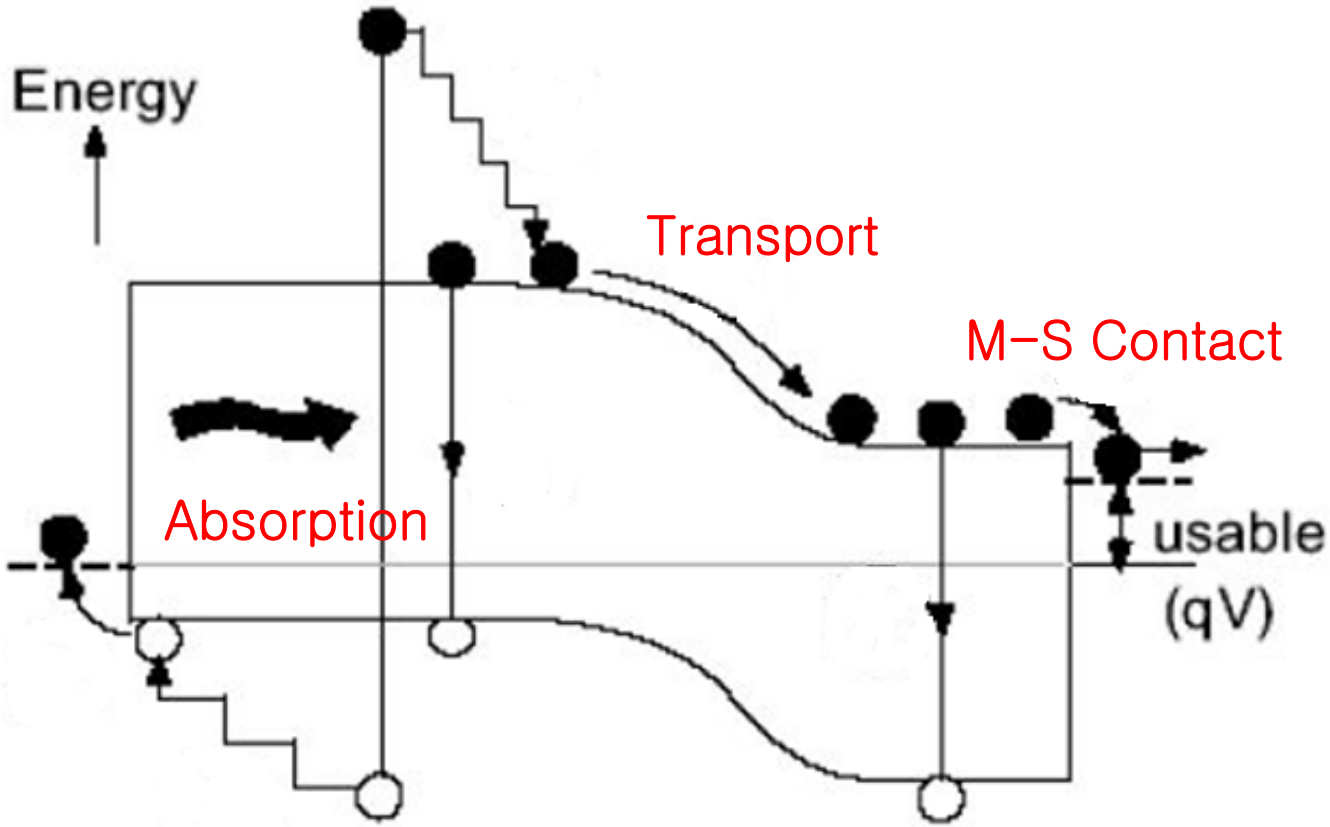

p-n Junction: Essential for Solar Cell

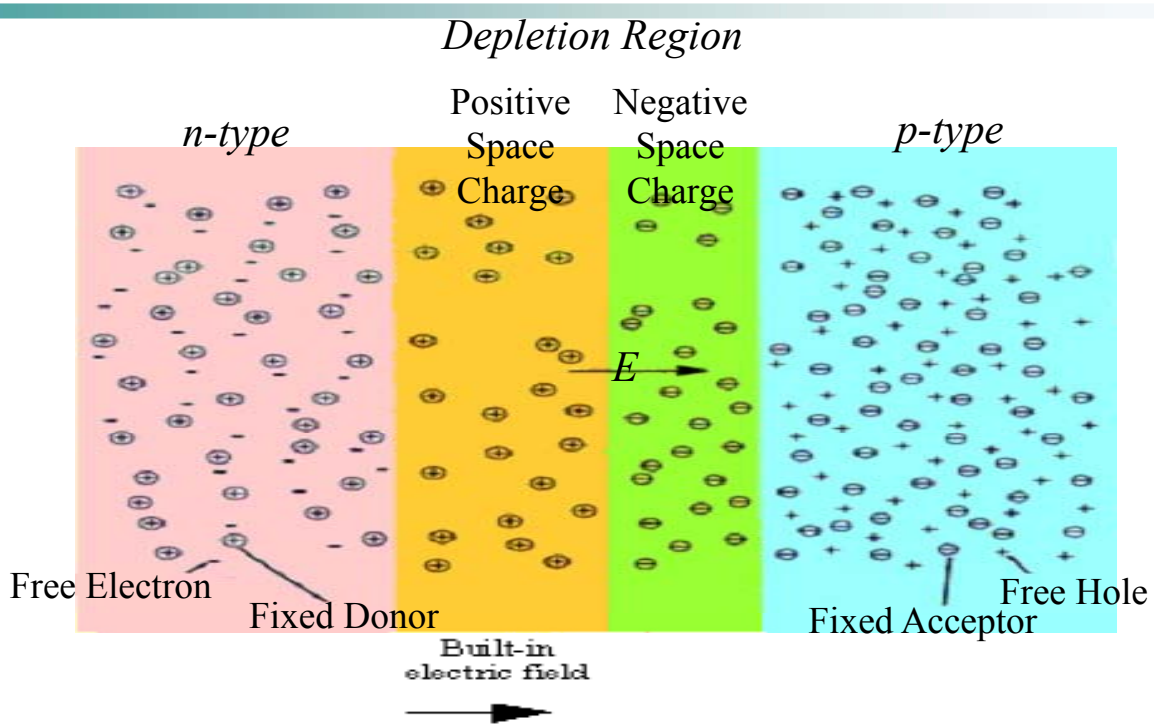

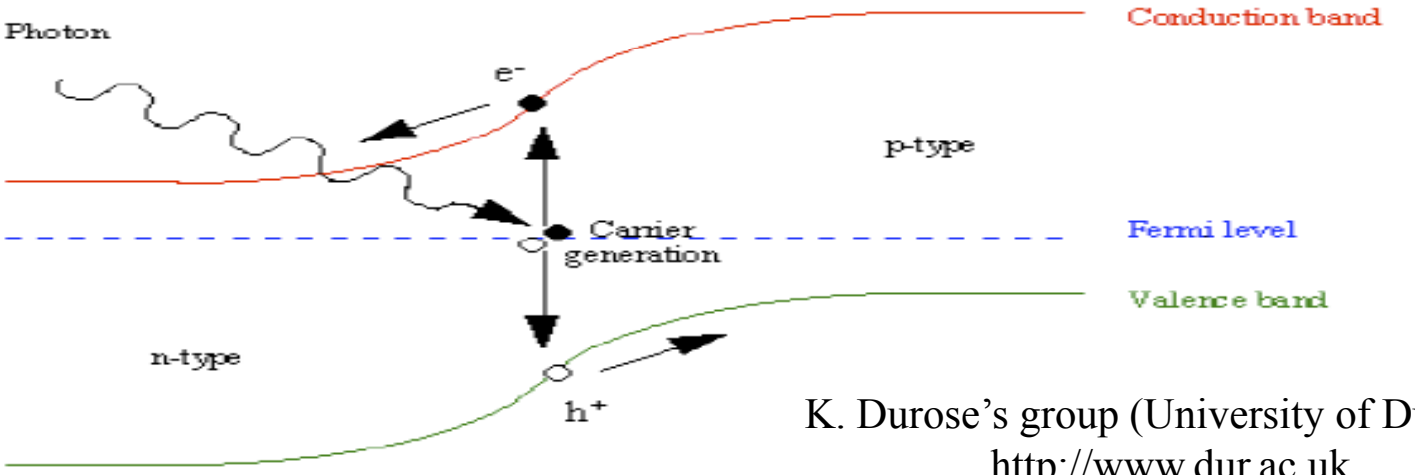

K. Durose's group (University of Durham)
http://www.dur.ac.uk

Energy Band of *p-n* Junction Solar Cell

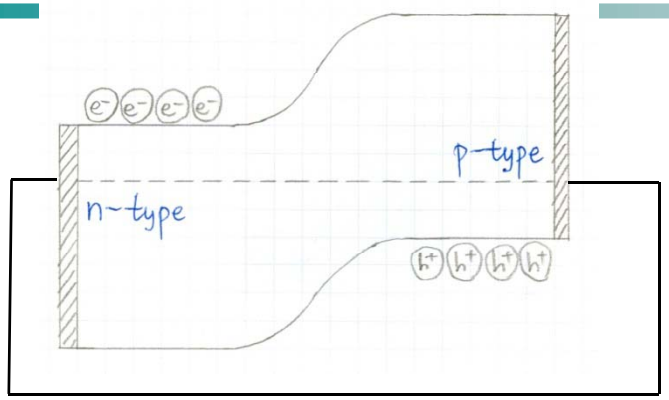

Dark flux & 0 V

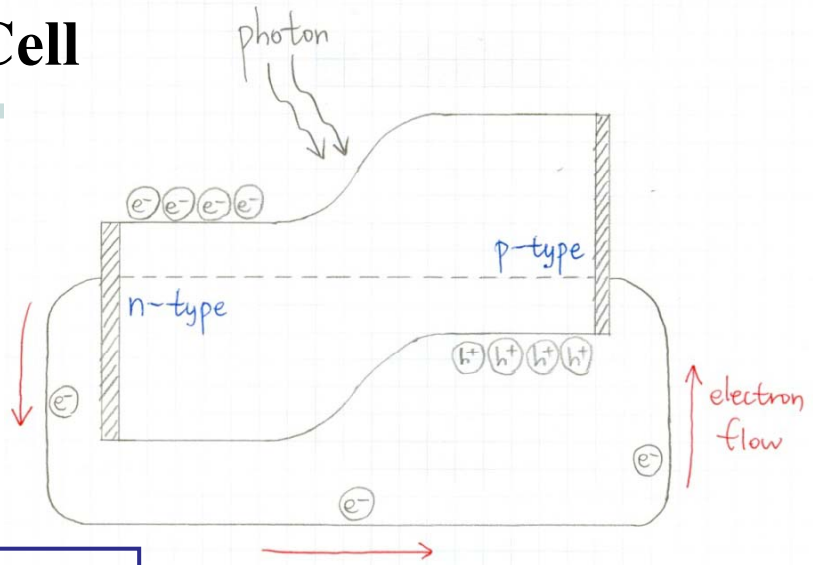

Short Circuit Current (J_{sc})

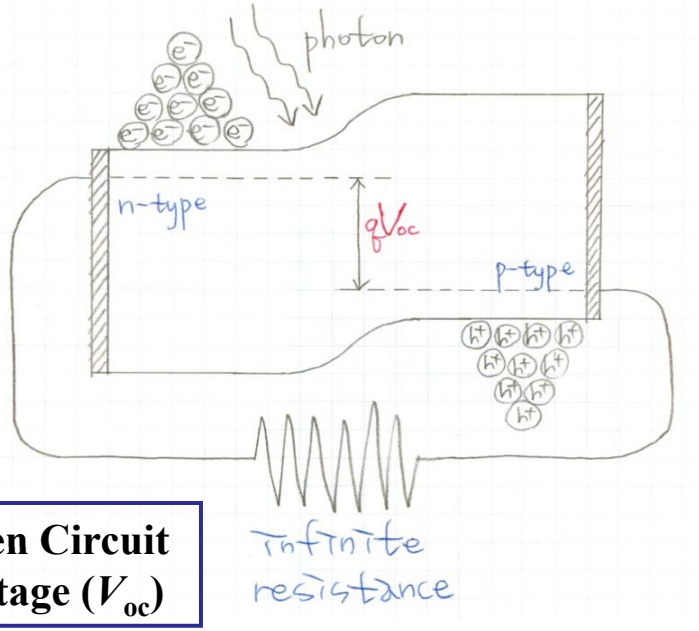

Open Circuit Voltage (V_{oc})

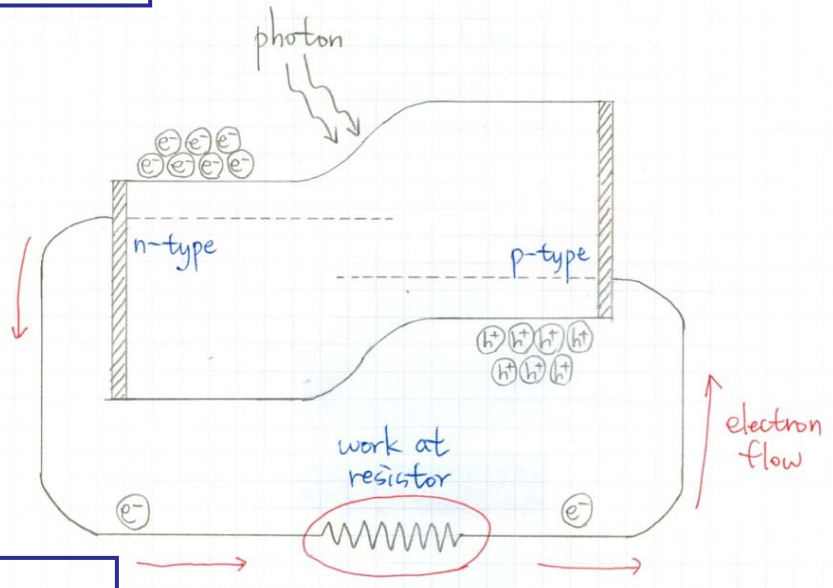

Maximum Power (P_{max})

J-V Curve

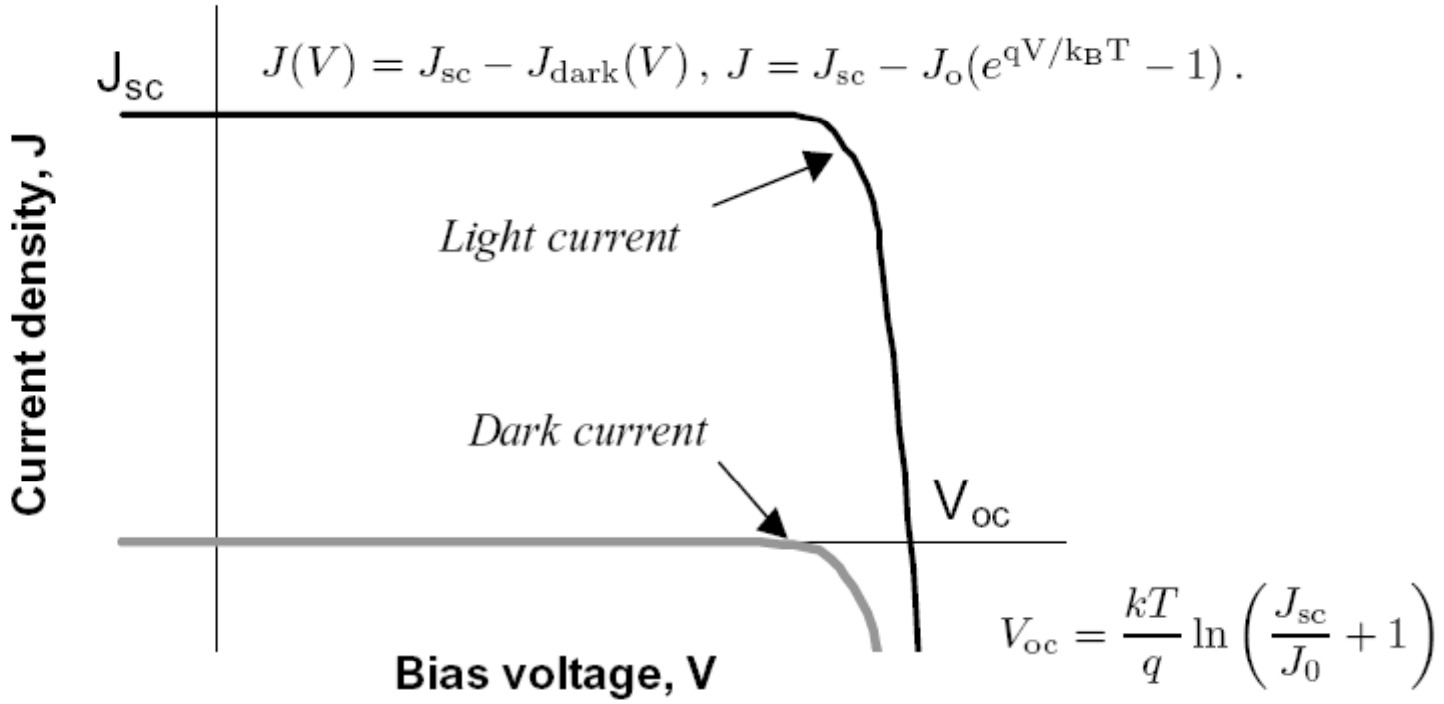

Fig. 1.6. Current–voltage characteristic of ideal diode in the light and the dark. To a first approximation, the net current is obtained by shifting the bias dependent dark current up by a constant amount, equal to the short circuit photocurrent. The sign convention is such that the short circuit photocurrent is positive.

p-type Contact Metal

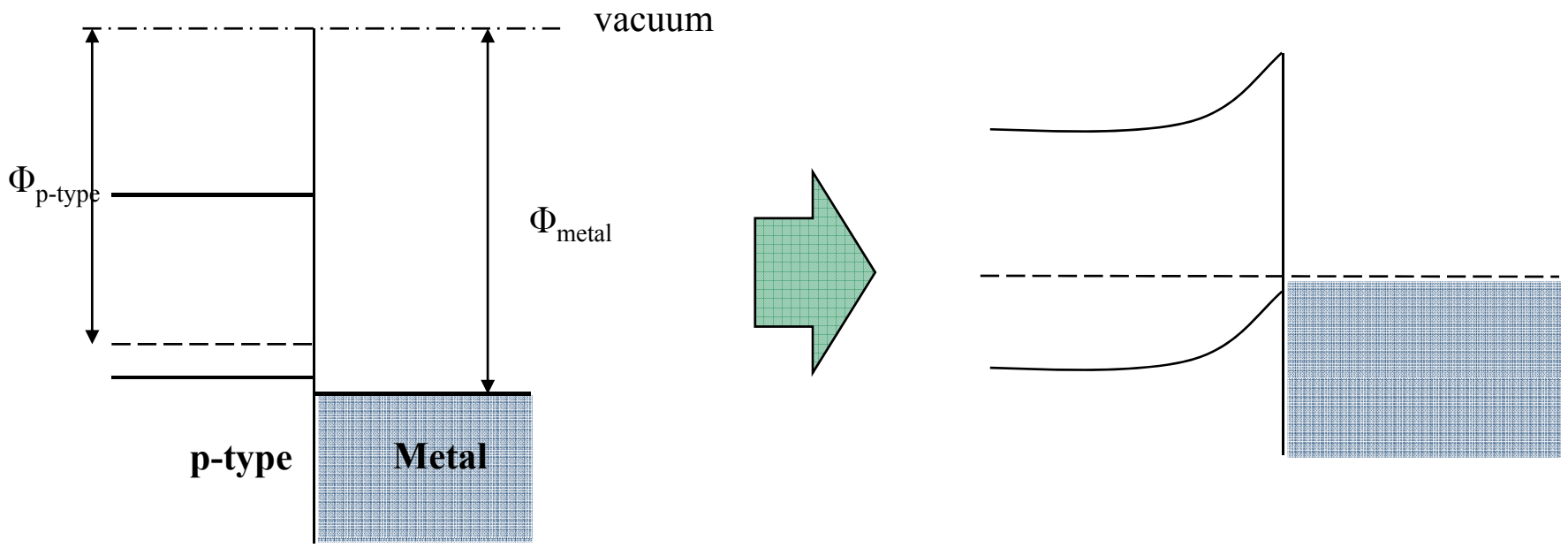

$\Phi_{p\text{-type}} < \Phi_{metal}$ for recombination

n-type Contact Metal

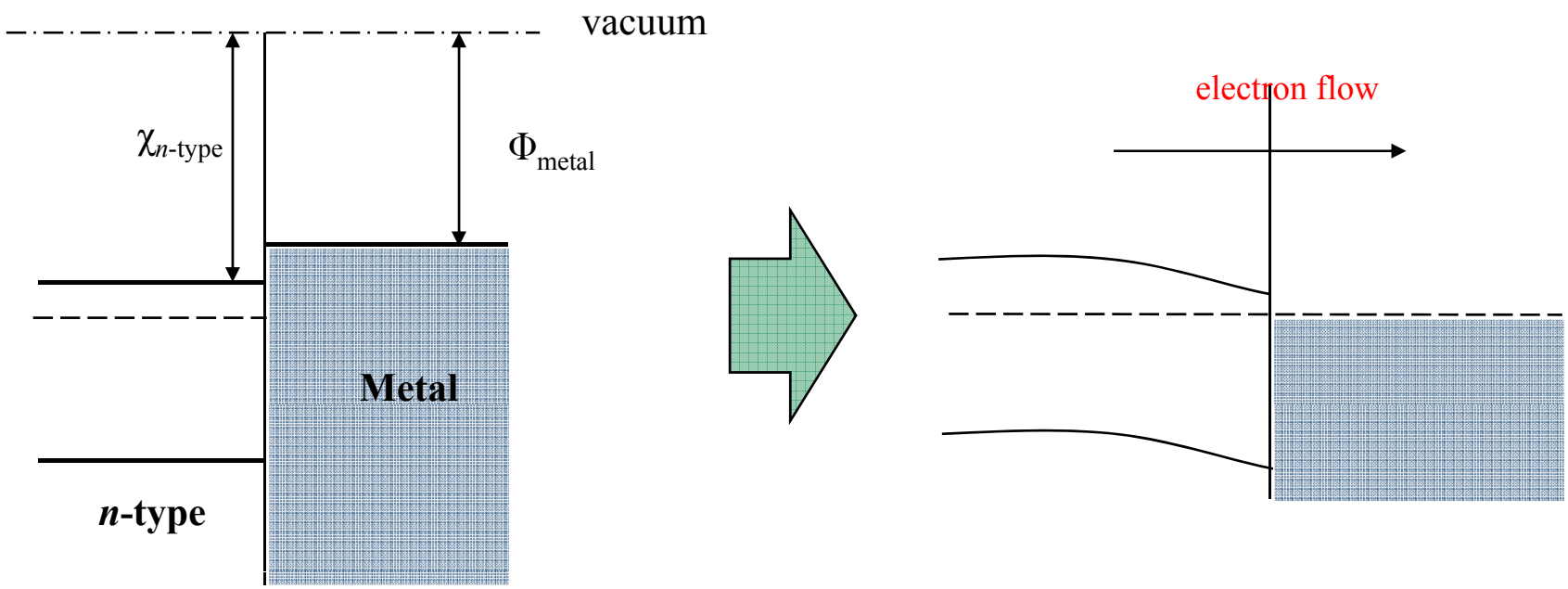

$\Phi_{n\text{-type}} > \Phi_{metal}$ for electron flow

Requirements for Solar Cells

- **Bandgap Energy (between 1.1 and 1.7 eV)**
- **Consisting of Readily Available, Non-Toxic Materials**
- **Easy, Reproducible Deposition Techniques**
- **Suitable for Large Area Production**
- **Good Photovoltaic Conversion Efficiency**
- **Long-Term Stability**

Quantum Efficiency

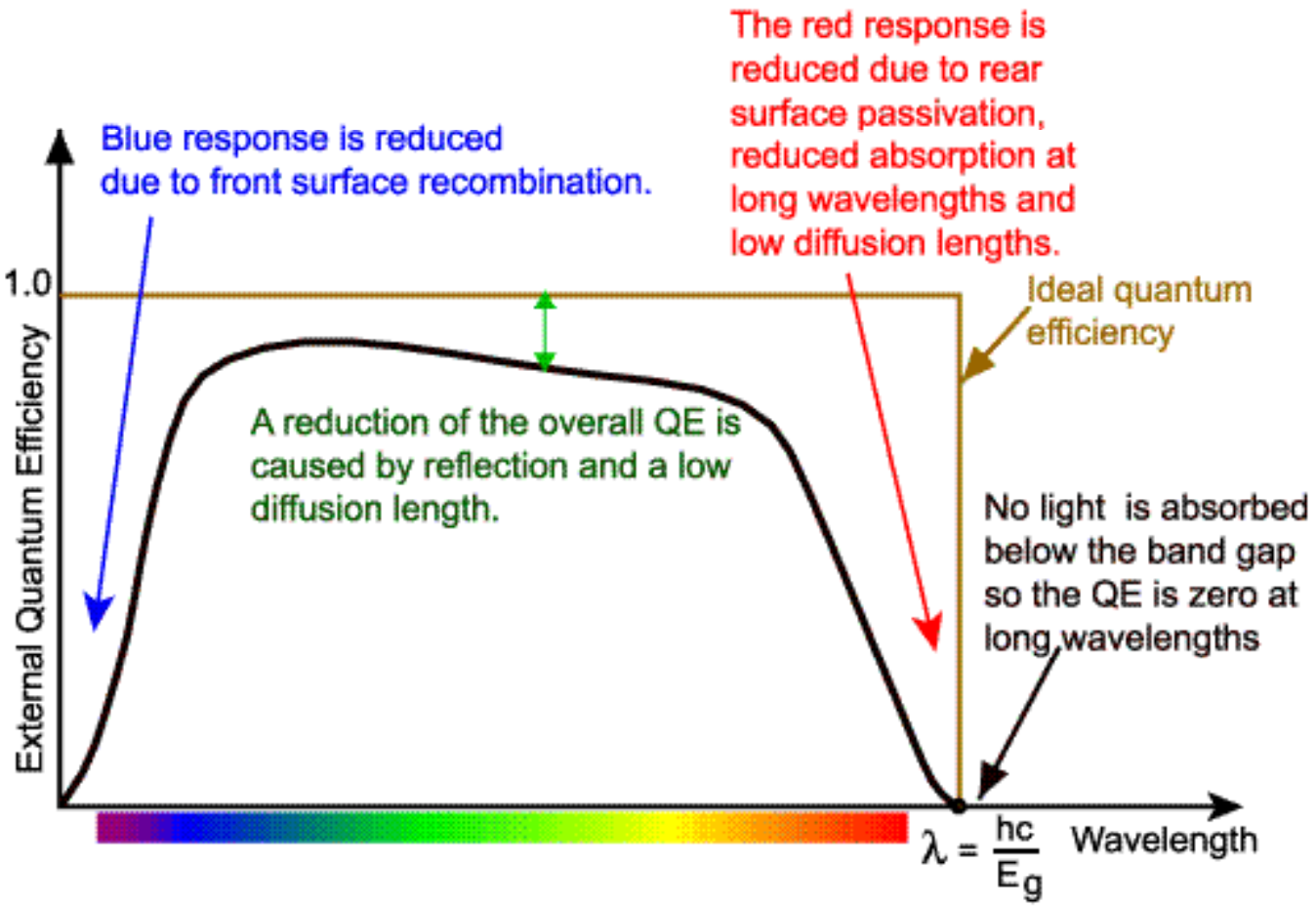

Photovoltaic CD ROM
http://pvcdrom.pveducation.org/
(the most instructional and kind web site for basic study for solar cell)

Quantum Efficiency

$$\text{Quantum efficiency (QE)} = \frac{\text{the number of charge carriers collected by the solar cell}}{\text{the number of photons of a given energy on the solar cell}}$$

$$= \text{IPCE}$$

(incident photon to current conversion efficiency)

$$= 1240\ \frac{J_{sc}}{\lambda P_i}$$

We can derive J_{sc} from the QE as follows:

$$J_{sc} = q\int_0^{\infty} \text{QE}(E) b_s(E) dE.$$

Where $b_s(E)$ represents the spectral photon flux.

J_{sc} is the short circuit current, which is the sum of the total charge of QE at the each spectra.

Quantum Efficiency

IPCE (Incident Photon to electron Conversion Efficiency)

Short circuit 상태에서 (작은 문제점) 측정 파장 별로 photon이 electron으로 변환되는 효율

$$IPCE(\lambda) = \frac{\#\text{ of electrons obtained from a solar cell}}{\#\text{ of incident photons to a solar cell}}$$

EQE (External Quantum Efficiency)

Short circuit 상태에서 전체 photon이 electron으로 변환되는 효율

IQE (Internal Quantum Efficiency)

Short circuit 상태에서 흡수된 photon이 electron으로 변환되는 효율

PCE (Power Conversion Efficiency) or ECE (Energy Conversion Efficiency)

- 전체 태양 에너지 중 파워로 변환되는 효율, 파워 맥시멈 지점에서 측정.
- 약자로는 잘 쓰이지 않는 듯 합니다.

The photocurrent quantum efficiency dependence on the applied voltage in organic solar cells

Jędrzej Szmytkowski[1]

Institut für Angewandte Physik, Universität Karlsruhe (TH), Wolfgang-Gaede-Str. 1, 76131 Karlsruhe, Germany

E-mail: jedrek@mif.pg.gda.pl

Received 29 May 2007
Published 15 November 2007
Online at stacks.iop.org/SST/22/1329

Abstract

We demonstrate that our recently reported model (Szmytkowski 2007 *J. Phys. D: Appl. Phys.* **40** 3352) of the photocurrent quantum efficiency in organic semiconductors explains the external quantum efficiency dependence on the electric field in organic solar cells. This effect can be explained by taking into account that the photogeneration of charge carriers occurs via the electron–hole pair dissociation and the space charge effects and recombination of charge influence the loss of photocurrent.

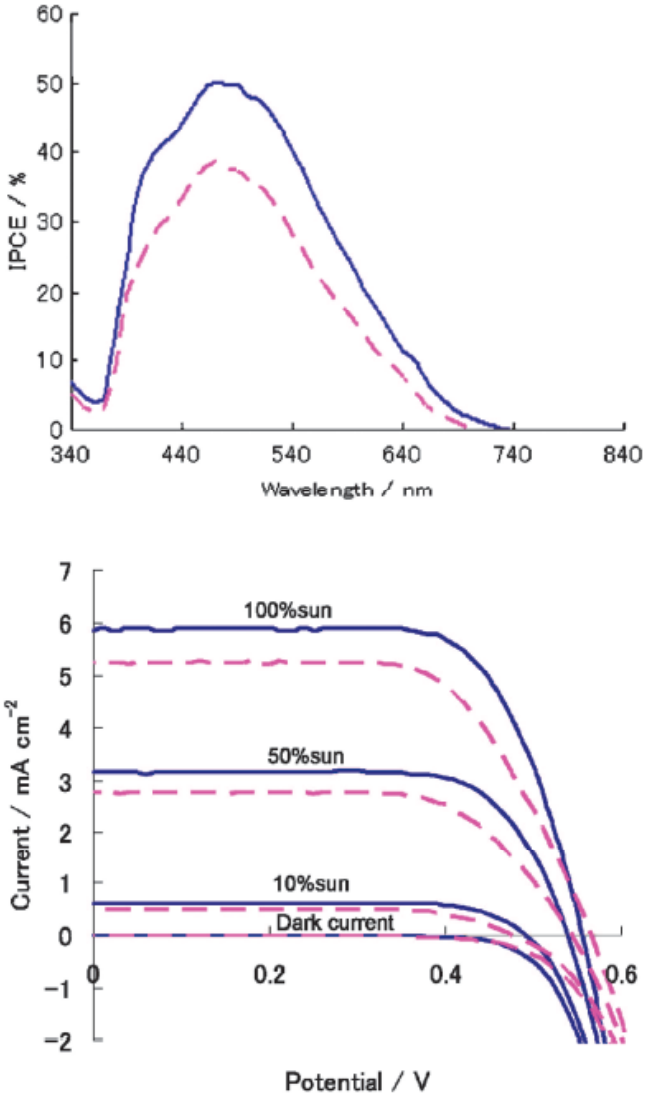

Fig. 3 IPCE (top) and *I–V* (bottom) curves for DSSCs prepared with copper(I) complexes of **1** (--) and **2** (—) at light intensity of 100%, 50% and 10% sun, respectively.

J. Szmytkowski, Universit¨at Karlsruhe (Poland)
Semicond. Sci. Technol. **22** 1329–1331 (2007).

Representative IPCE and *I-V* Curve

Key Aims for High Power

(1) Generating a large short circuit current, J_{sc}
→ Generation and Collection of Carriers

(2) Generate a large open-circuit voltage, V_{oc}
→ Moderate Diffusion Length, Low Surface Recombination, Thin Devices, and (incompatible with each other or with high J_{sc}, so need trade-offs)

(3) Minimize parasitic power loss mechanisms.

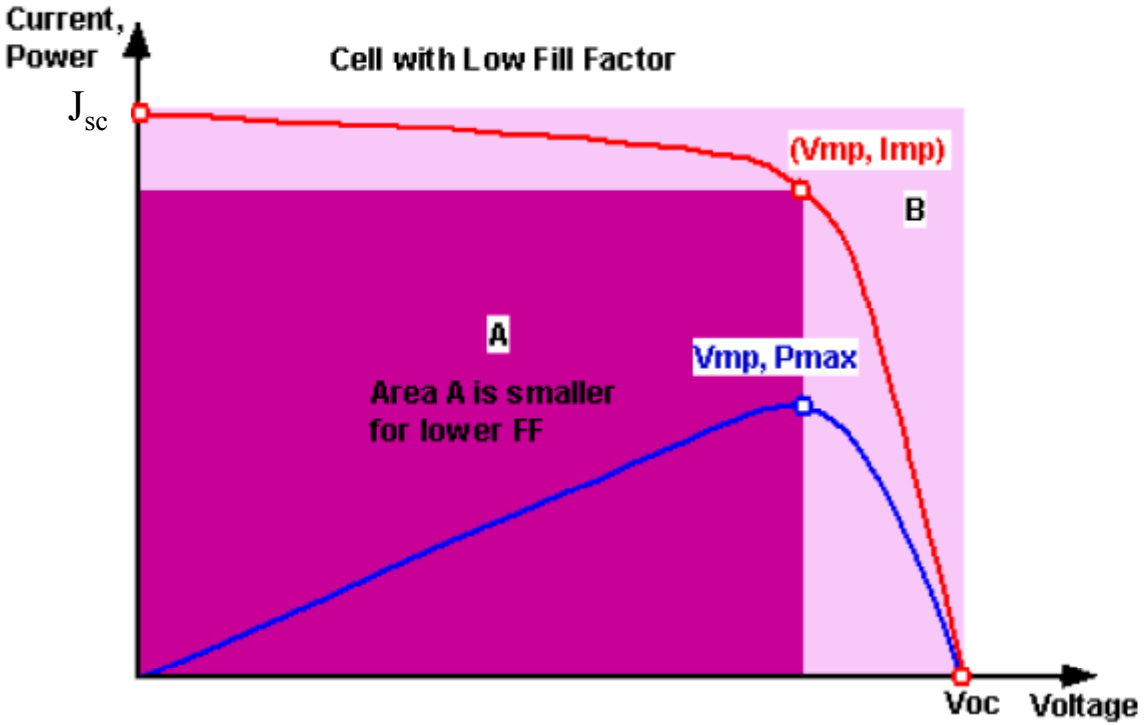

$$\eta = \frac{V_{oc} J_{sc} FF}{P_{in}}$$

(power conversion efficiency)

J. Nelson, *The Physics of Solar Cells*
London: Imperial College Press, 2003

Efficiency Loss

Efficiency Losses in Solar Cell

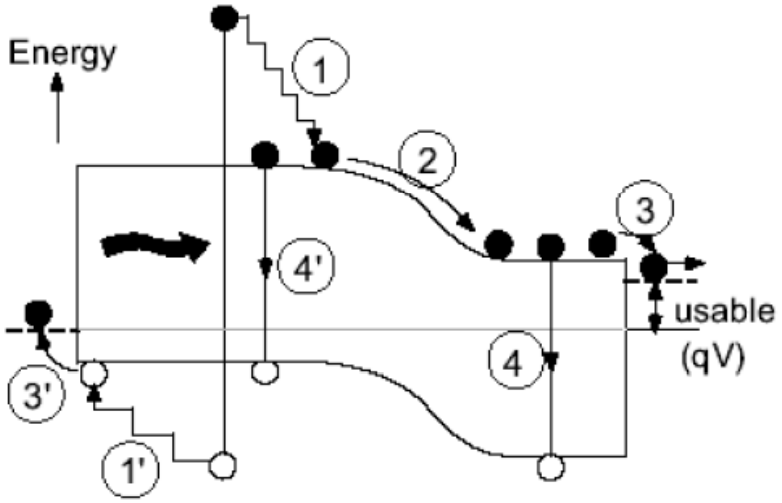

1 = Thermalization loss

2 and 3 = Junction and contact voltage loss

4 = Recombination loss

The Solid State Lighting and Display Center @ UC Santa Barbara
http://ssldc.ucsb.edu

World Market for Solar Cells

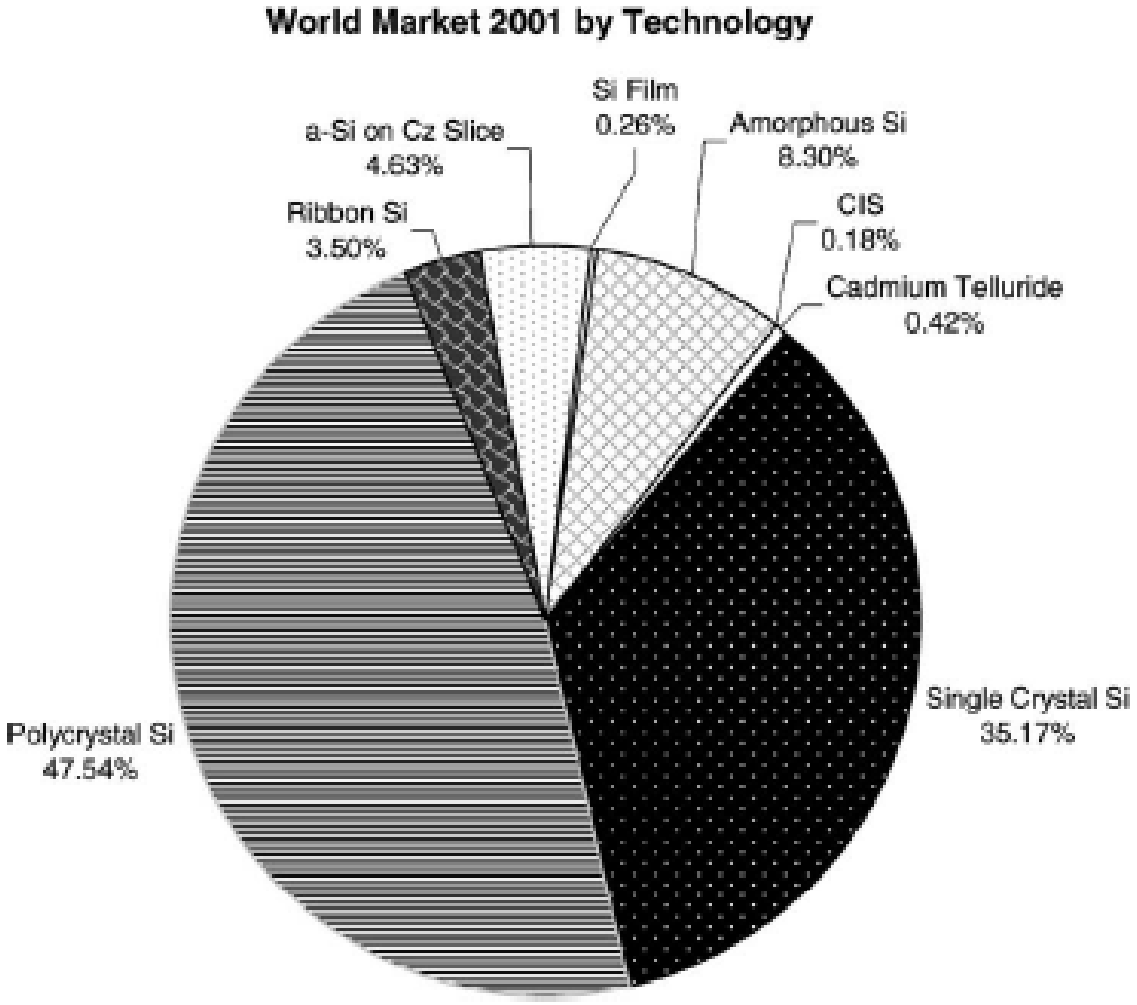

Fig. 3. Market shares of different photovoltaic materials.

A. Goetzberger *et al.*, *Materials Science and Engineering R*, **40**, 1-46 (2003)

Si Solar Cells

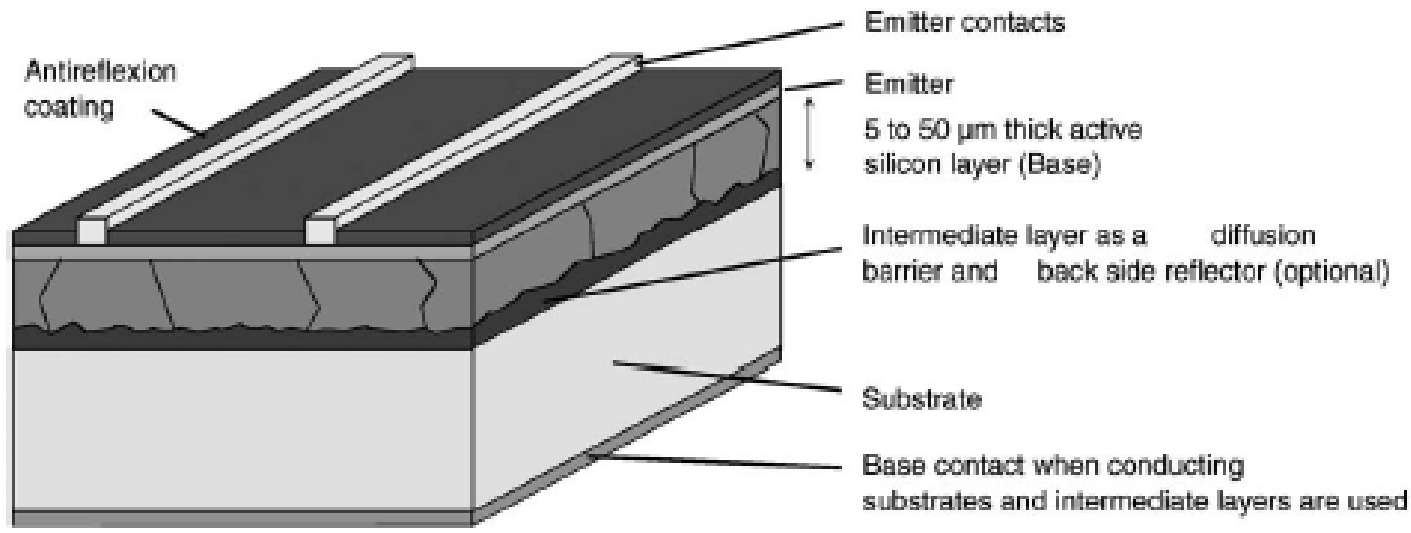

Fig. 17. The basic components of a crystalline silicon solar cell.

A. Goetzberger *et al.*, *Materials Science and Engineering R*, **40**, 1-46 (2003)

CIS/CdTe Solar Cells

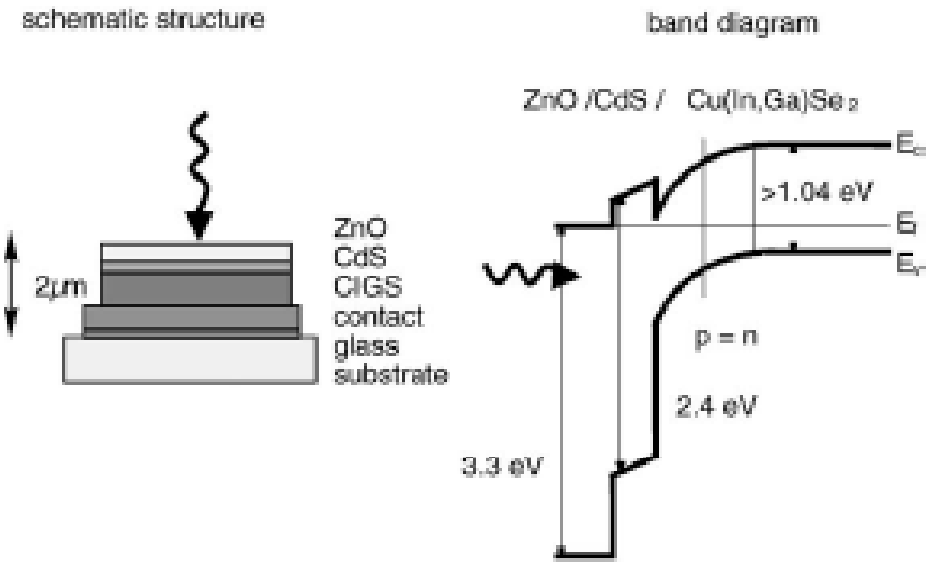

Fig. 26. Schematic structure of a CIGS-based solar cell.

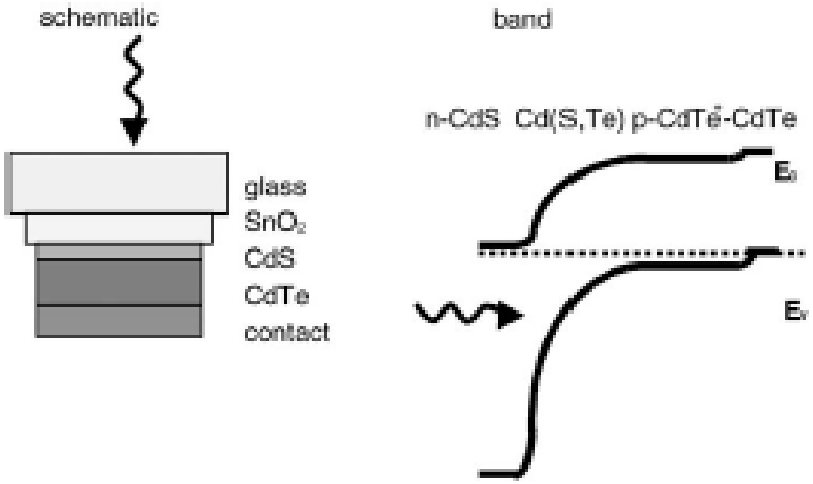

Fig. 28. Schematic structure of a CdTe-based superstrate solar cell.

A. Goetzberger *et al.*, *Materials Science and Engineering R*, **40**, 1-46 (2003)

A. Goetzberger *et al.*
Materials Science and Engineering R **40**, 1-46 (2003)

Photovoltaic materials, history, status and outlook

Adolf Goetzberger[a,*], Christopher Hebling[a], Hans-Werner Schock[b]
[a]*Fraunhofer Institute for Solar Energy Systems, Oltmannsstr. 5, D-79100 Freiburg, Germany*
[b]*Institute for Physical Electronics, Universität Stuttgart, Pfaffenwaldring 47, D-70569 Stuttgart, Germany*

Accepted 20 August 2002

Abstract

This paper reviews the history, the present status and possible future developments of photovoltaic (PV) materials for terrestrial applications. After a brief history and introduction of the photovoltaic effect theoretical requirements for the optimal performance of materials for pn-junction solar cells are discussed. Most important are efficiency, long-term stability and, not to be neglected, lowest possible cost. Today the market is dominated by crystalline silicon in its multicrystalline and monocrystalline form. The physical and technical limitations of this material are discussed. Although crystalline silicon is not the optimal material from a solid state physics point of view it dominates the market and will continue to do this for the next 5–10 years. Because of its importance a considerable part of this review deals with materials aspects of crystalline silicon. For reasons of cost only multicrystalline silicon and monocrystalline Czochralski (Cz) crystals are used in practical cells. Light induced instability in this Cz-material has recently been investigated and ways to eliminate this effect have been devised. For future large scale production of crystalline silicon solar cells development of a special solar grade silicon appears necessary. Ribbon growth is a possibility to avoid the costly sawing process. A very vivid R&D area is thin-film crystalline silicon (about 5–30 μm active layer thickness) which would avoid the crystal growing and sawing processes. The problems arising for this material are: assuring adequate light absorption, assuring good crystal quality and purity of the films, and finding a substrate that fulfills all requirements. Three approaches have emerged: high-temperature, low-temperature and transfer technique. Genuine thin-film materials are characterized by a direct band structure which gives them very high light absorption. Therefore, these materials have a thickness of only one micron or less. The oldest such material is amorphous silicon which is the second most important material today. It is mainly used in consumer products but is on the verge to also penetrate the power market. Other strong contenders are chalcogenides like copper indium diselenide (CIS) and cadmium telluride. The interest has expanded from $CuInSe_2$, to $CuGaSe_2$, $CuInS_2$ and their multinary alloys $Cu(In,Ga)(S,Se)_2$. The two deposition techniques are either separate deposition of the components followed by annealing on one hand or coevaporation. Laboratory efficiencies for small area devices are approaching 19% and large area modules have reached 12%. Pilot production of CIS-modules has started in the US and Germany. Cadmium telluride solar cells also offer great promise. They have only slightly lower efficiency and are also at the start of production. In the future other materials and concepts can be expected to come into play. Some of these are: dye sensitized cells, organic solar cells and various concentrating systems including III/V-tandem cells. Theoretical materials that have not yet been realized are Auger generation material and intermediate metallic band material.

Solar Cell Efficiency

Efficiencies of different Photovoltaic Cells throughout history.

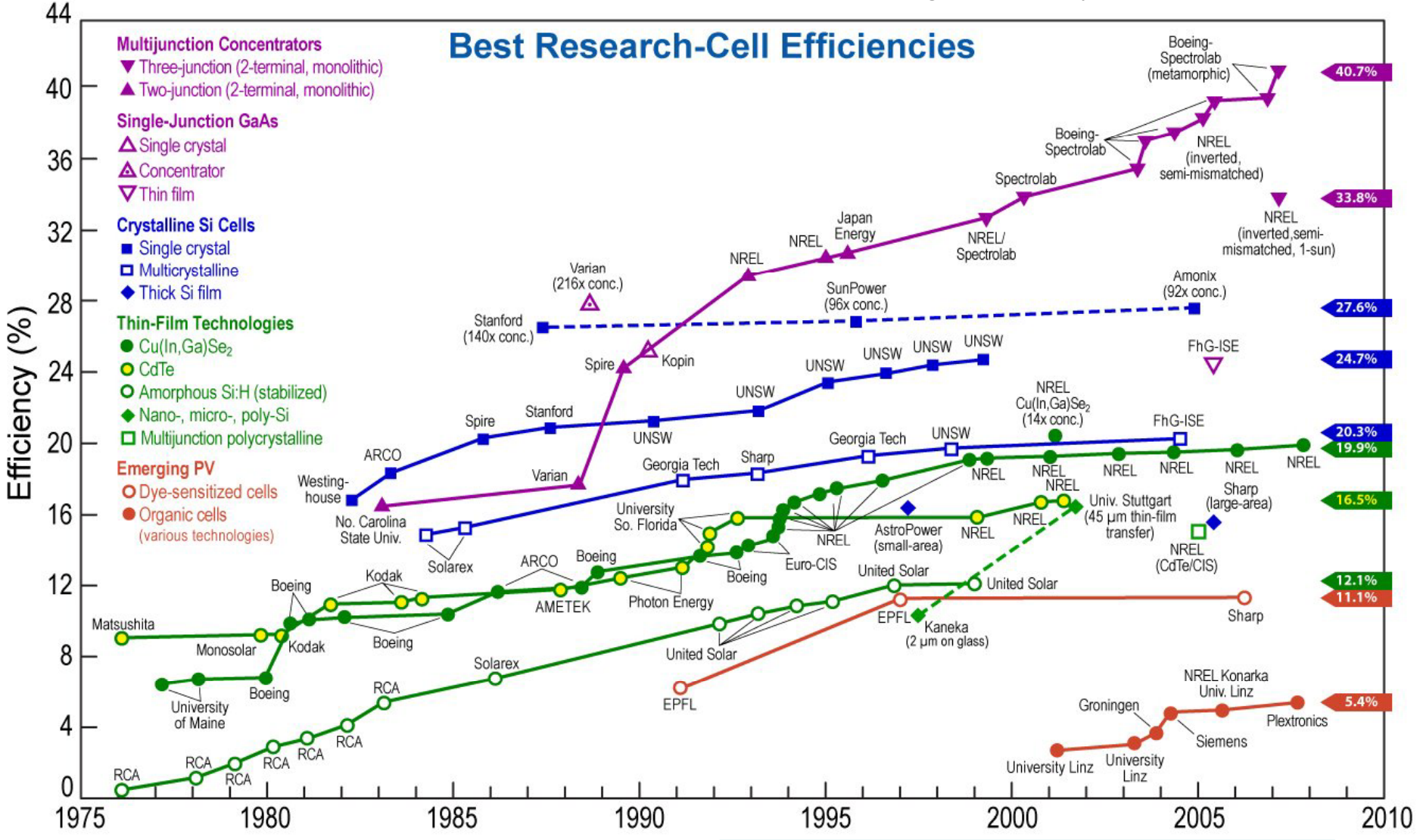

Solar Radiation

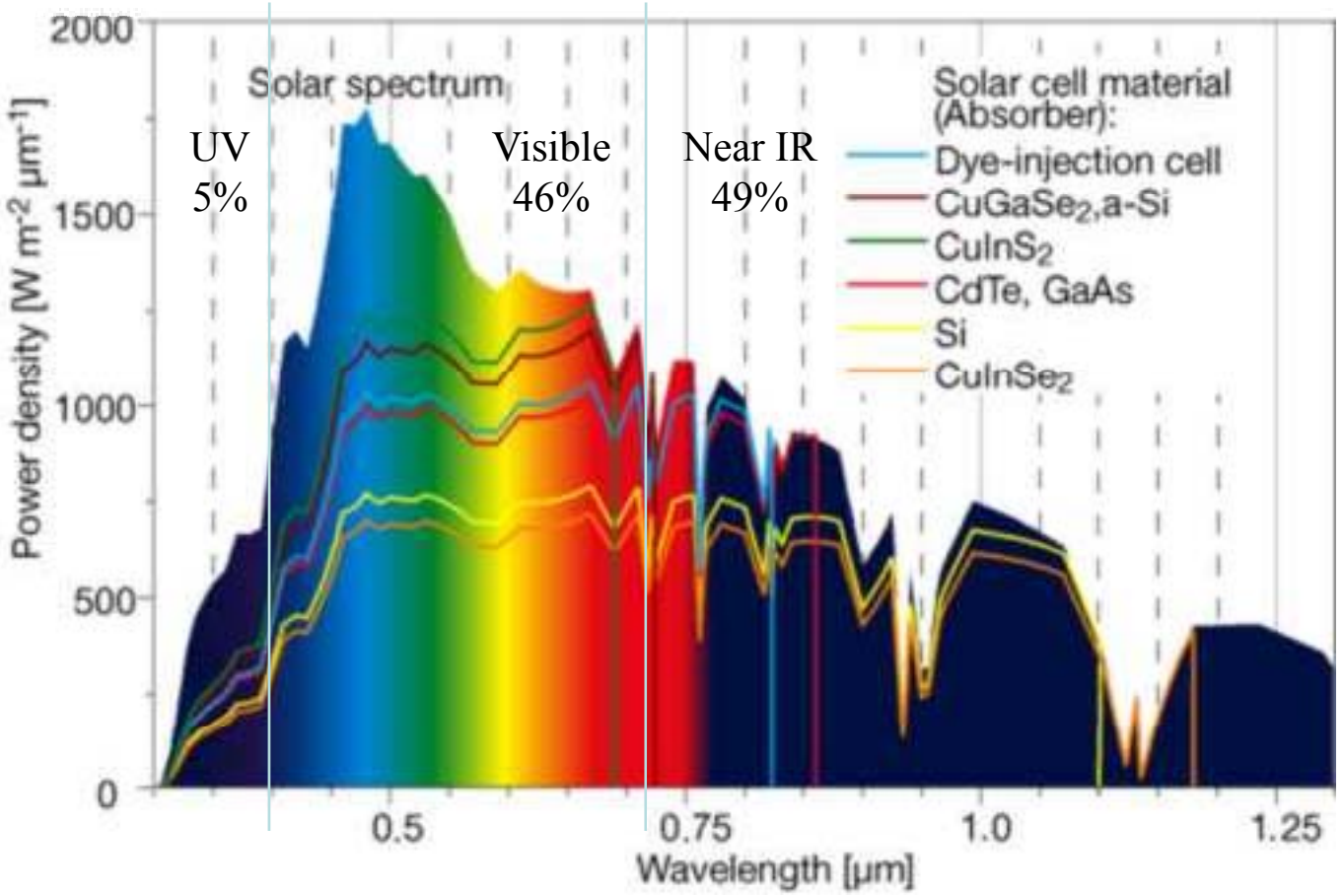

Power reaching earth: 1.37 kW/m^2

Photovoltaic Applications and Technologies
http://www.pvresources.com

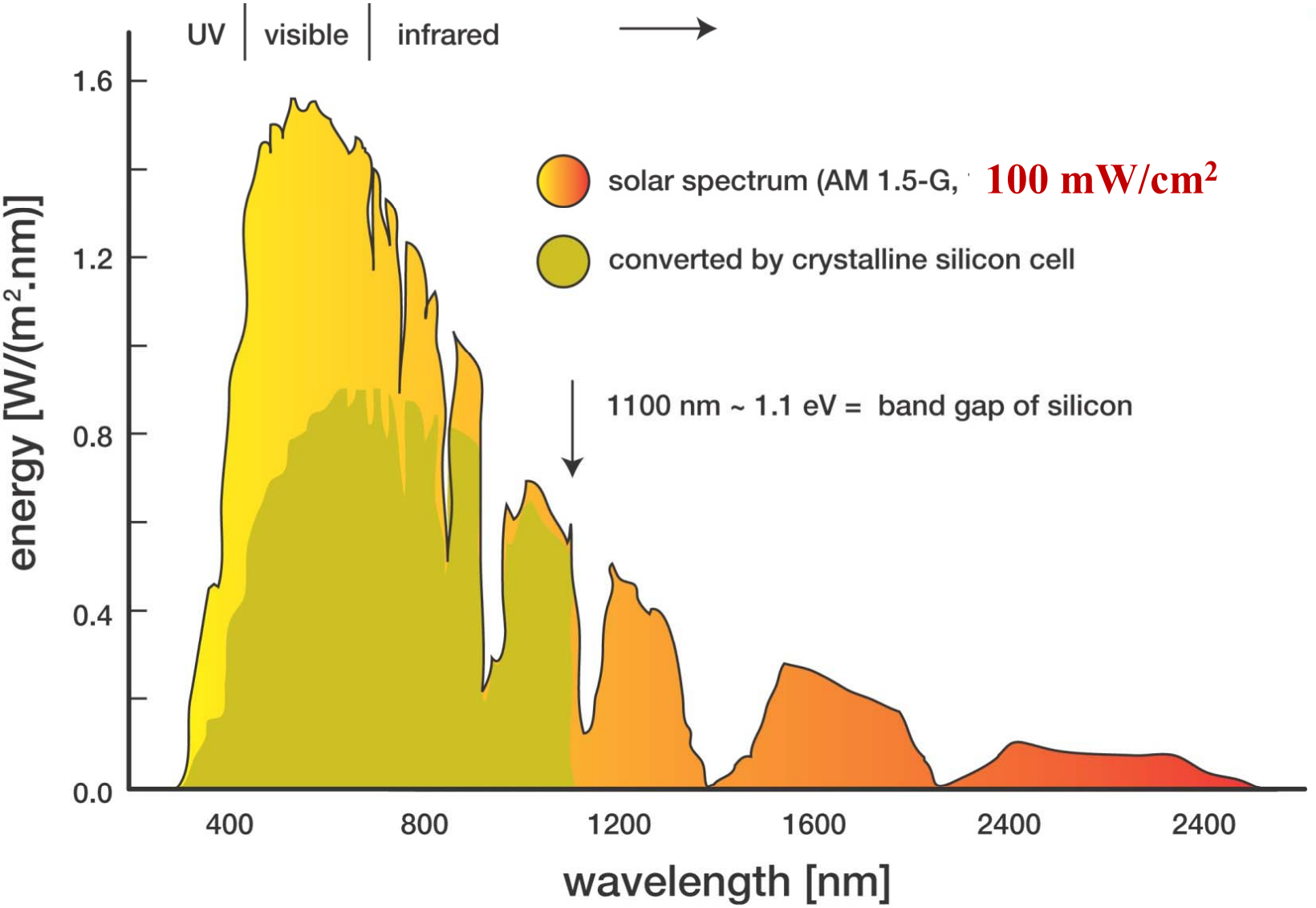
UV
visible
infrared
energy [W/(m².nm)]
1.6
1.2
0.8
0.4
0.0
solar spectrum (AM 1.5-G, 100 mW/cm²
converted by crystalline silicon cell
1100 nm ~ 1.1 eV = band gap of silicon
400
800
1200
1600
2400
2400
wavelength [nm]

Solar Spectrum

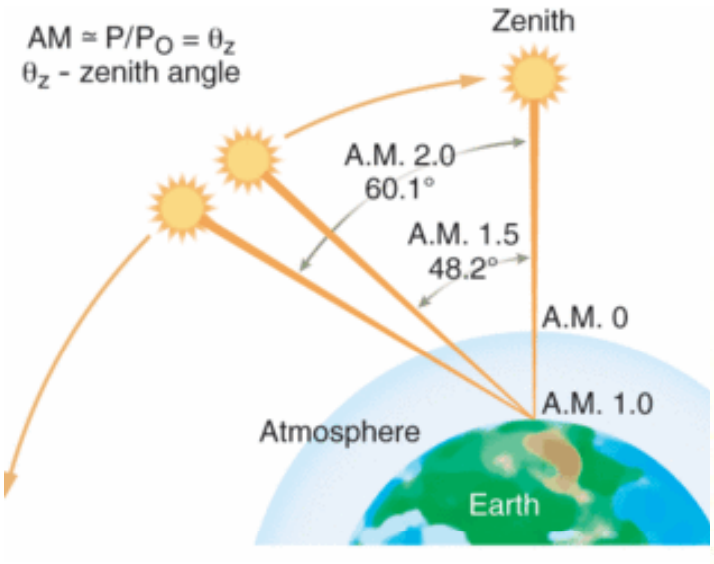

The solar spectrum and irradiance is established by the air mass. Air mass (AM) refers to the amount of air a beam of sunlight must go through before reaching the solar converter. It is determined by the angle, θ, that the sun makes with a vertical line perpendicular to the horizontal plane (see Appendix, Fig. A.1). It is given by

$$\text{AM (number)} = \frac{1}{\cos\theta} \quad . \qquad (2.2)$$

The solar spectrum outside the atmosphere, AM0, is close to a 5743 K (Planck) blackbody-radiation spectrum and has an irradiance of 1365 W/m^2. The shape of this blackbody spectrum is shown in Fig. 2.1. Air mass 1.0 refers to the thickness of the atmosphere sunlight passes through if the beam is directly overhead. An AM1 atmosphere reduces the direct flux by a factor 0.7. On a clear day, and when the sun is directly overhead, nearly 70% of the solar radiation incident to Earth's atmosphere reaches its surface undisturbed. About another 7% reaches the ground in an approximately isotropic manner after scattering from atmospheric molecules and particles. The rest is absorbed or scattered back into space. Both the direct and scattered fluxes vary with time and location because the amounts of dust and water vapor in the atmosphere are not constant even on clear days. For purposes of standard solar cell measurements, an average solar spectrum at AM1.5 is used (θ = 48.19 deg). It should be noted that the total irradiance used for AM1.5 was 844 W/m^2 in earlier work, but is often normalized to 1000 W/m^2 in more recent work (ASTM E 892, IEC 60904-3). It is therefore best to specify the AM and the irradiance when reporting measurement conditions. Figure 2.1 shows the spectral irradiance for the sun when viewed as a blackbody, but is scaled (diluted) such that the total power is approximately 1000 W/m^2.

Solar Spectrum

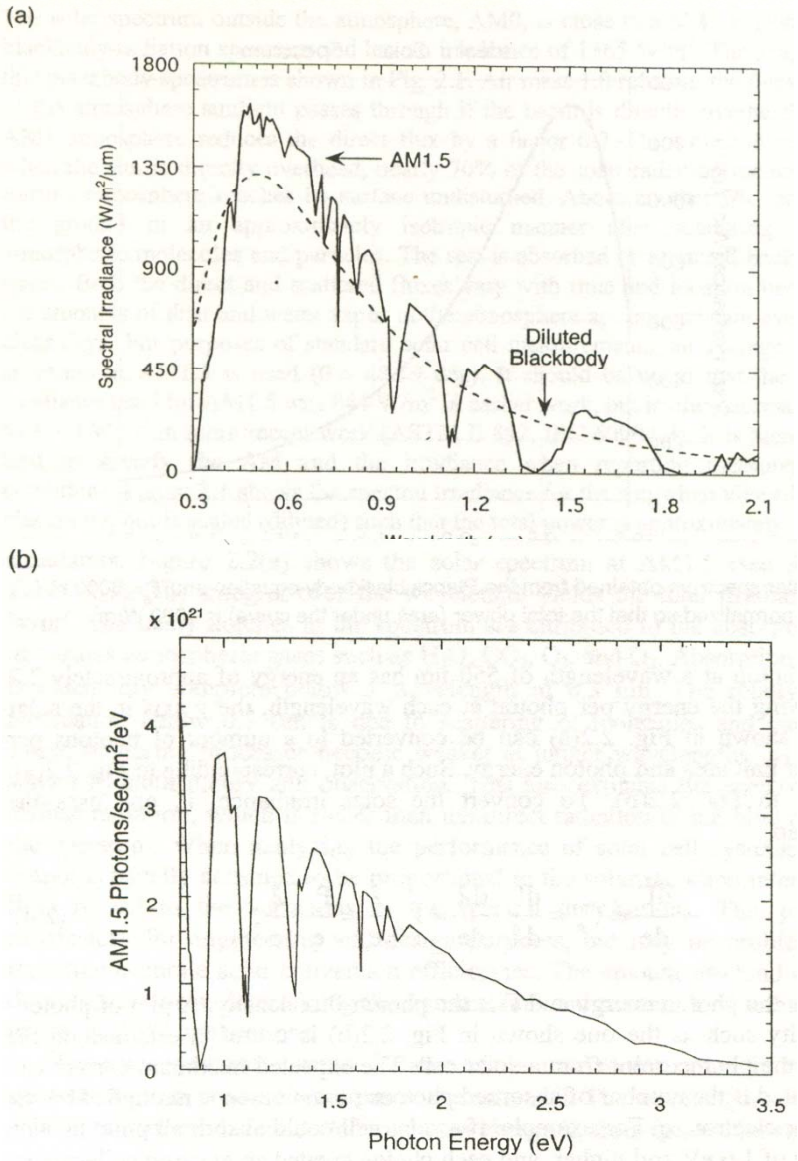

An attempt to replicate the AM1.5 spectrum is made in standardized solar simulators. Figure 2.2(a) shows the solar spectrum at AM1.5 (see Appendix, Table A.1). The integral over the wavelength yields the total irradiance, 1000 W/m^2. The many notches in the spectrum are attributed to the absorption bands of various atmospheric gases such as H_2O, CO_2, O_3, and O_2. Absorption by ozone is essentially complete below a wavelength of 0.3 μm. The relatively large attenuation below 0.8 μm is due to scattering of molecules and particulates. These scattering processes become weaker at longer wavelengths, as has been shown by both theory and observation. This also explains the spectrum of the diffuse radiation, which is richer than the direct radiation in the blue portion of the spectrum. When analyzing the performance of solar cell systems, the cell output is usually assumed to be proportional to the solar radiation intensity with little regard to the variations in the spectral distributions. This practice is satisfactory for engineering and design purposes, but may be problematic for reporting accurate solar conversion efficiencies. The amount of cloud cover is a dominant factor in determining the transmission and scattering of solar radiation in practical PV applications.

The solar spectrum discussed above can be used to determine the number of photons that can produce electrons in the solar cell. The wavelength scale on the solar spectrum can be converted to photon energy, e, from the relationship

$$\text{Photon Energy} \equiv e = \frac{hc}{\lambda} \cong \frac{1.239}{\lambda(\mu m)} \text{ [in eV]}. \qquad (2.3)$$

Fig. 2.2 The solar spectrum at AM1.5, 1000 W/m^2 conditions for (a) Irradiance normal to the beam, and (b) corresponding photon flux (number of photons). For the AM1.5 data, see the Appendix, Table A.1.

Relations between Optical Parameters

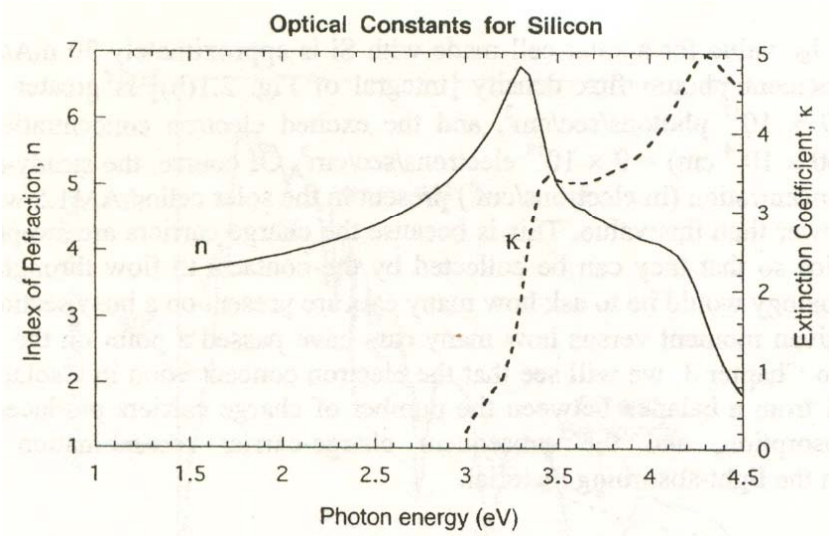

Fig. 2.3 Optical constants n and κ for silicon as real and imaginary components of the index of refraction. At photon energies smaller than 3 eV, the extinction coefficient of Si is below 0.006, and the index of refraction, n, is approximately 3.5.

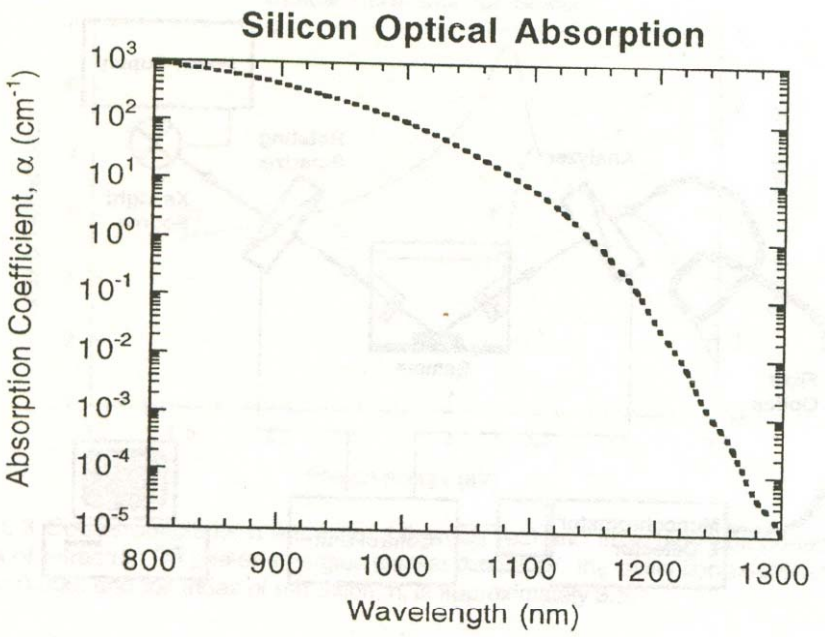

Fig. 2.5 Silicon optical absorption coefficient, α.

The optical properties of a material depend on the complex index of refraction, n_c, given by the relationship

$$n_c = n - i\kappa, \qquad (2.5)$$

where the imaginary part of n_c is the extinction coefficient, κ. The real part of n_c is the index of refraction, n, familiar in optical design of lenses and geometrical optics. Note that the symbol "n" is used in most texts for both electron concentration, to be discussed later, and index of refraction. Figure 2.3 shows the n and κ values for silicon.

The absorption coefficient describes the decrease in light intensity as a beam of light propagates through a material (e.g., a solar cell). If the number of photons per unit time per unit area is Γ, then the change in this "photon-flux density" as a function of position is given by

$$\frac{d\Gamma}{\Gamma} = -\alpha\, dx, \qquad [2.7(a)]$$

where x is the position in the absorbing material along the beam. Here, reflection is neglected, and only the light that has already entered the light-absorbing material is considered. By integrating the above equation, one obtains the number of unabsorbed photons. This is given by

$$\Gamma = \Gamma_0 \exp(-\alpha t), \qquad [2.7(b)]$$

where t is the thickness of the material, and Γ_0 is the number of photons that initially entered the material.

Relations between Optical Parameters

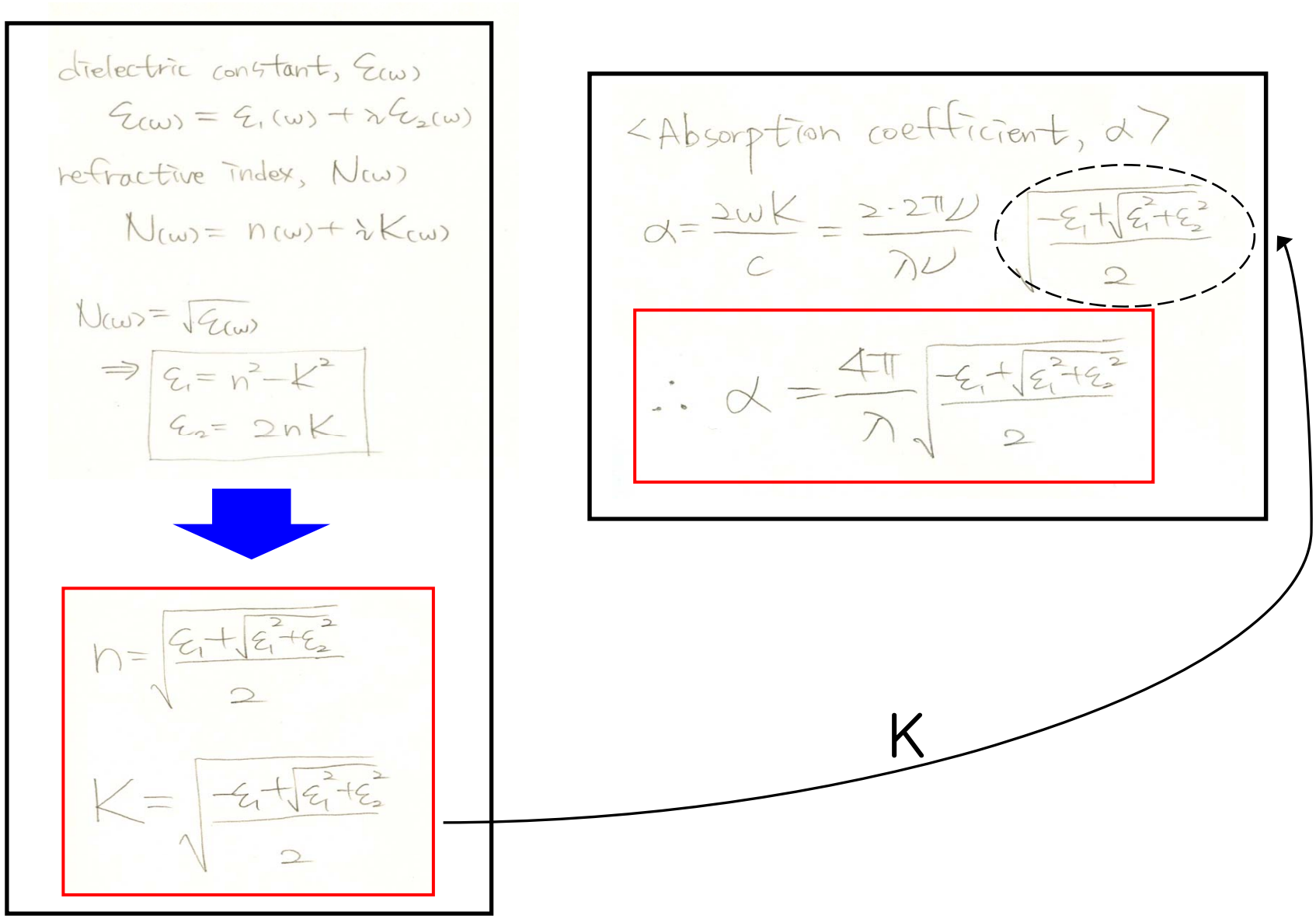

Dye-Sensitized Solar Cell (DSSC)

Photoelectrochemical Cells (Solar Cell and Water Cleavage)

M. Grätzel, *Nature (2001)*

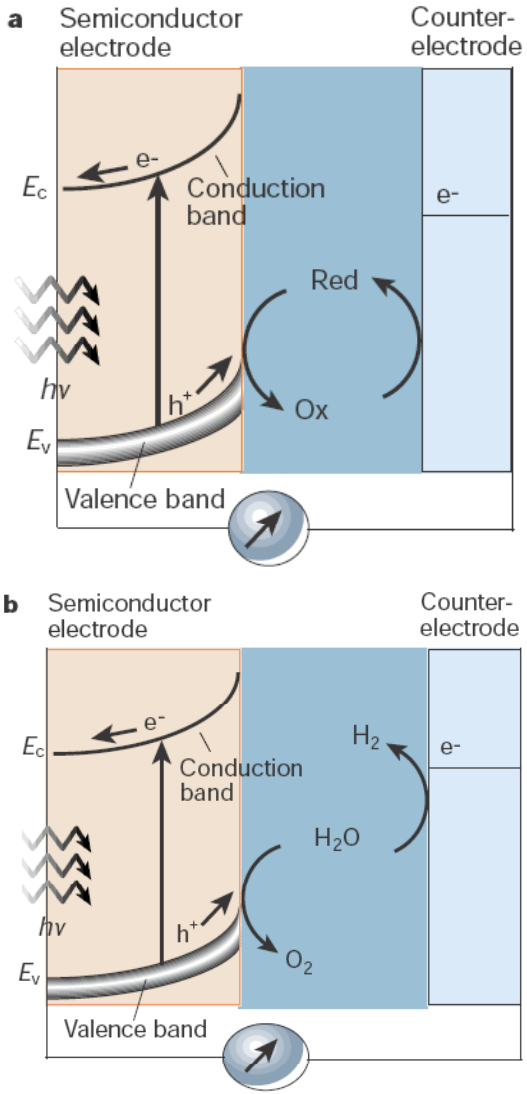

Table 1 Performance of photovoltaic and photoelectrochemical solar cells

Type of cell	Efficiency (%)* Cell	Module	Research and technology needs
Crystalline silicon	24	10–15	Higher production yields, lowering of cost and energy content
Multicrystalline silicon	18	9–12	Lower manufacturing cost and complexity
Amorphous silicon	13	7	Lower production costs, increase production volume and stability
$CuInSe_2$	19	12	Replace indium (too expensive and limited supply), replace CdS window layer, scale up production
Dye-sensitized nanostructured materials	10–11	7	Improve efficiency and high-temperature stability, scale up production
Bipolar AlGaAs/Si photoelectrochemical cells	19–20	—	Reduce materials cost, scale up
Organic solar cells	2–3	—	Improve stability and efficiency

*Efficiency defined as conversion efficiency from solar to electrical power.

Figure 1 Principle of operation of photoelectrochemical cells based on *n*-type semiconductors. **a**, Regenerative-type cell producing electric current from sunlight; **b**, a cell that generates a chemical fuel, hydrogen, through the photo-cleavage of water.

Electrode potential (E^0) vs. Vacuum potential (eV)

Figure 2 Band positions of several semiconductors in contact with aqueous electrolyte at pH 1. The lower edge of the conduction band (red colour) and upper edge of the valence band (green colour) are presented along with the band gap in electron volts. The energy scale is indicated in electron volts using either the normal hydrogen electrode (NHE) or the vacuum level as a reference. Note that the ordinate presents internal and not free energy. The free energy of an electron–hole pair is smaller than the band gap energy due to the translational entropy of the electrons and holes in the conduction and valence band, respectively. On the right side the standard potentials of several redox couples are presented against the standard hydrogen electrode potential.

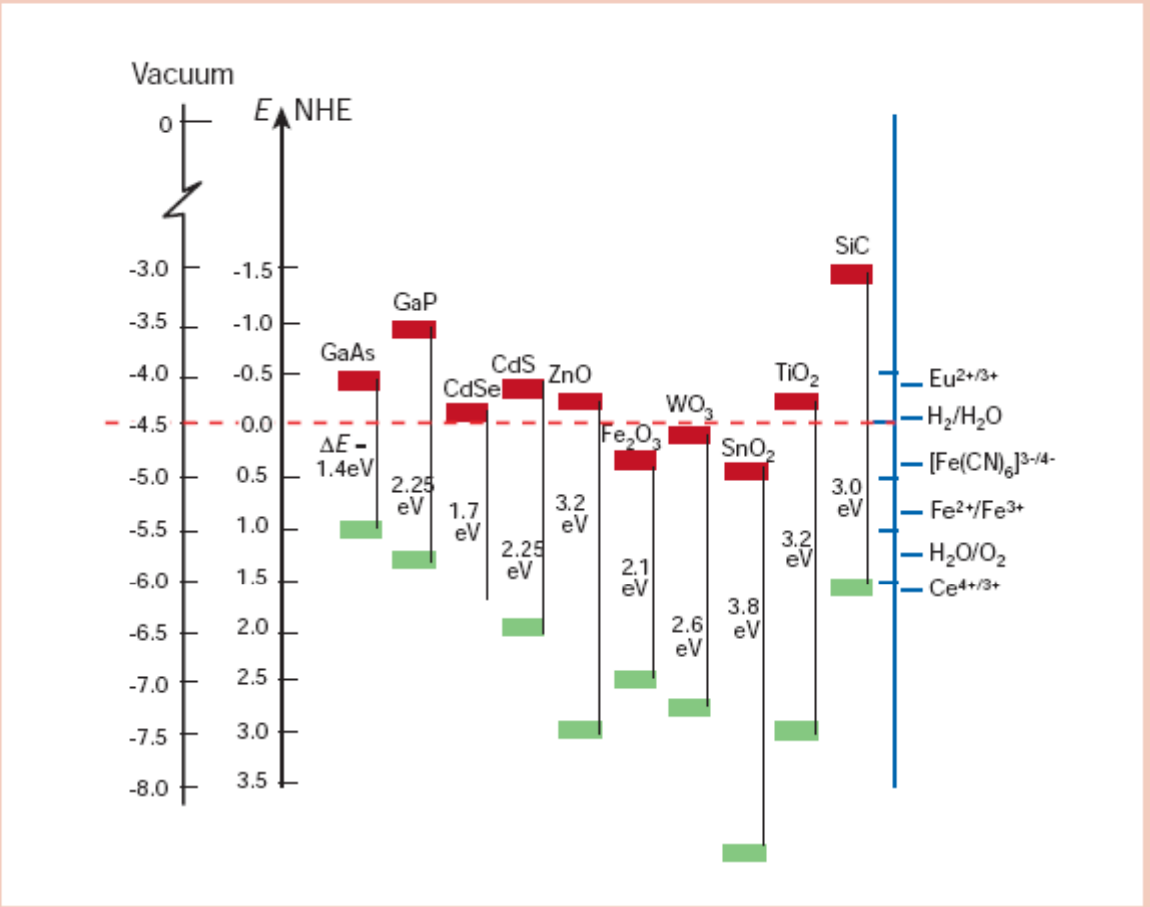

M. Grätzel, ***Nature (2001)***

Until now, photovoltaics — the conversion of sunlight to electrical power — has been dominated by solid-state junction devices, often made of silicon. But this dominance is now being challenged by the emergence of a new generation of photovoltaic cells, based, for example, on nanocrystalline materials and conducting polymer films. These offer the prospect of cheap fabrication together with other attractive features, such as flexibility. The phenomenal recent progress in fabricating and characterizing nanocrystalline materials has opened up whole new vistas of opportunity. Contrary to expectation, some of the new devices have strikingly high conversion efficiencies, which compete with those of conventional devices. Here I look into the historical background, and present status and development prospects for this new generation of photoelectrochemical cells.

Dye-Sensitized Solar Cells (DSSCs)

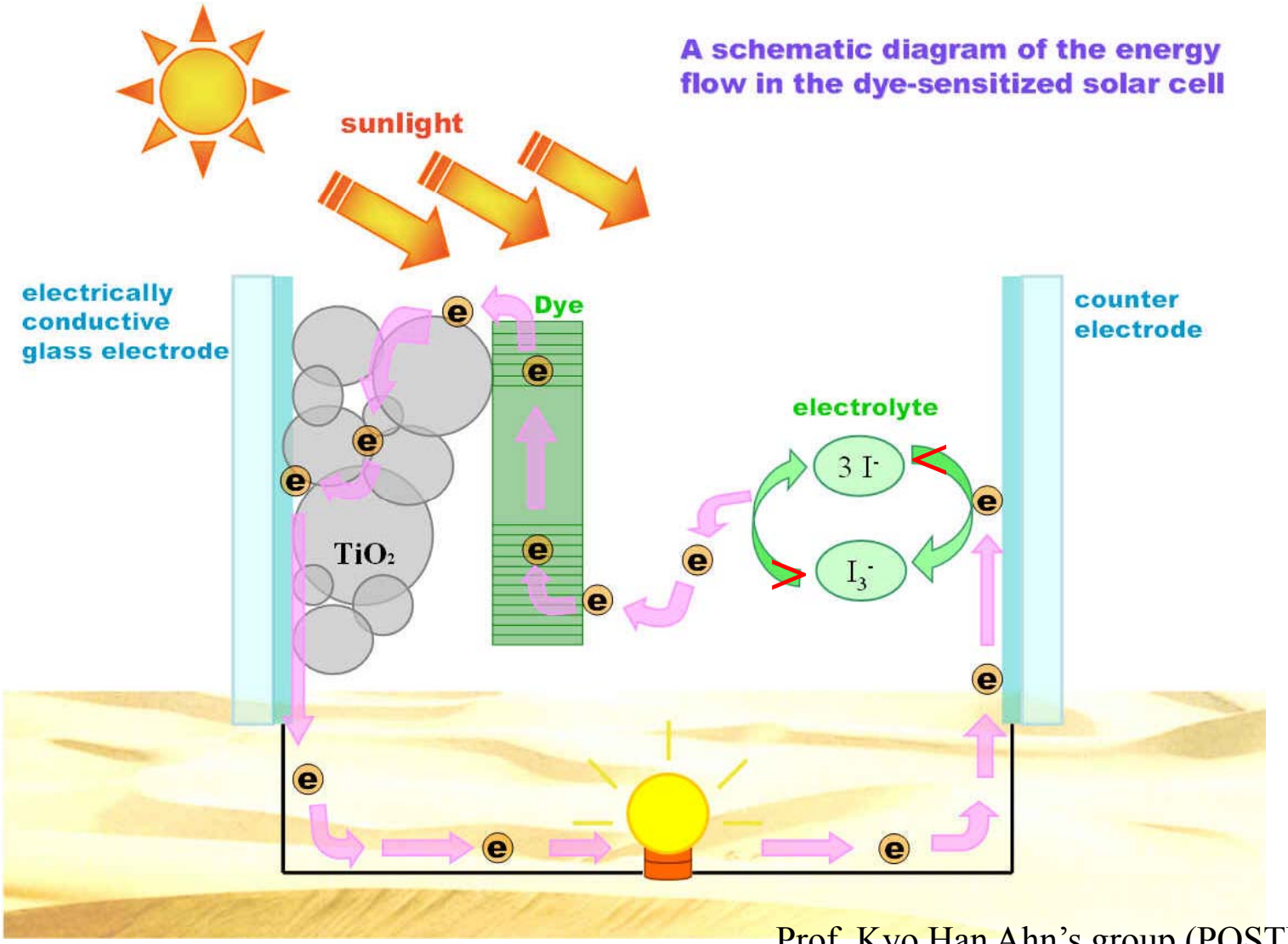

Prof. Kyo Han Ahn's group (POSTECH)
http://www.postech.ac.kr/chem/mras

Dye-Sensitized Solar Cell

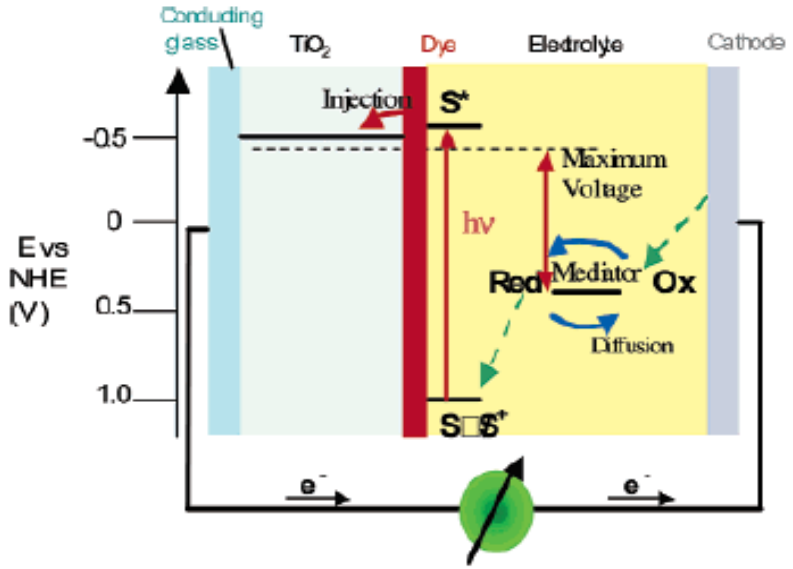

Michael Grätzel (Ecole Polytechnique)
Inorg. Chem. **44,** 6841 (2005)

1. Dye electrons are excited by solar energy absorption.
2. They are injected into the conduction band of TiO_2.
3. Get to counter-electrode (cathode) through the external circuit.
4. $I_3^- + 2e^- \rightarrow 3I^-$: Redox regeneration at the counter-electrode (reduction).
5. $3I^- \rightarrow I_3^- + 2e^-$: Dye regeneration reaction (oxidation).
6. Potential used for external work: $\Delta V_{ext} = E_F - \Delta V_{redox}$

Dye-Sensitized Solar Cell

< Introduction >

- Dye-sensitized solar cells (DSSC) were invented by Michael Grätzel and Brian O'Regan [*Nature*, **353**, 737 (1991)] .

- The DSSC is formed by a combination of organic and inorganic components that could be produced at a low cost.
- The DSSC offers the prospect of a cheap and versatile technology for large scale production of solar cells.

- The basic element of a DSSC is a nanostructured material, an assembly of TiO_2 nanoparticles about 20 nm diameter, well connected to their neighbors.
- TiO_2 is the preferred material since its surface induces highly effective electron transfer.
- However, TiO_2 only absorbs a small fraction of the solar photons (those in the UV).
- Molecular sensitizers (dye molecules) attached to the semiconductor surface, are used to harvest a great portion of the solar light.
- The main dye molecules consist on one Ru metal atom and a large organic structure that provides the required properties (wide absorption range, fast electron injection, and stability).

Dye-Sensitized Solar Cell

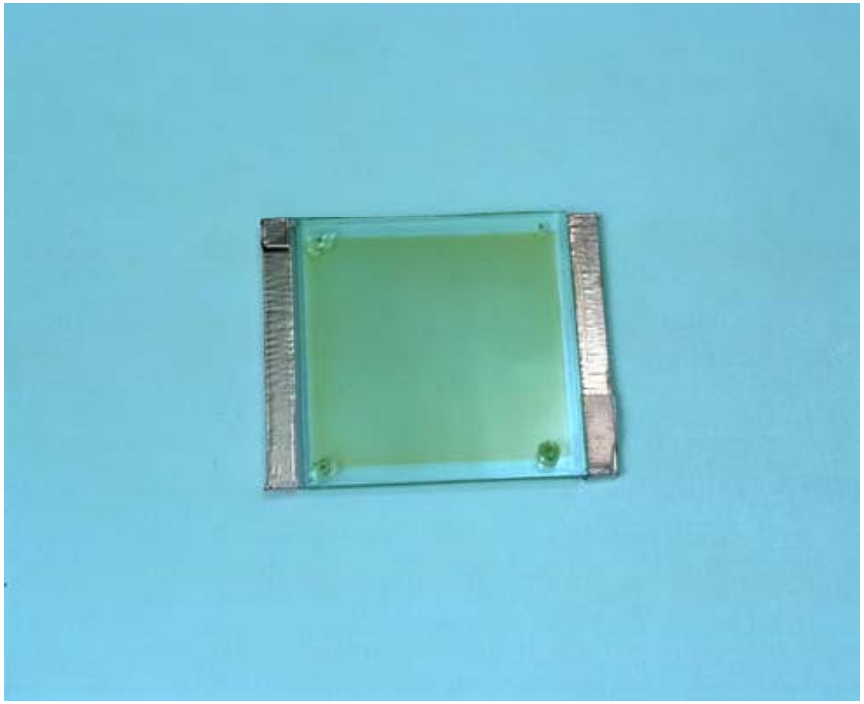

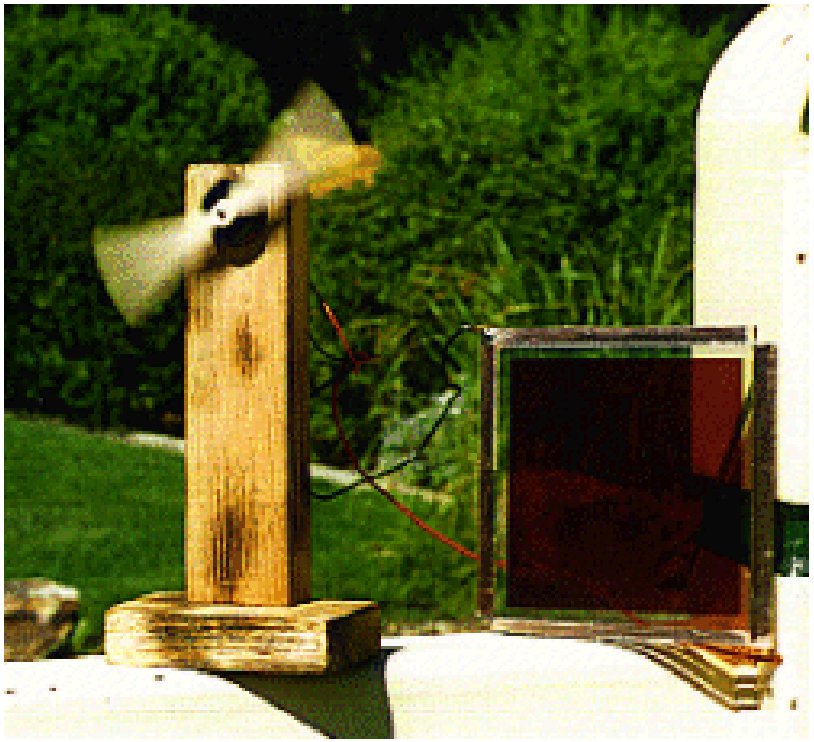

Homepage in Grätzel's group

The Benefits of DSSC

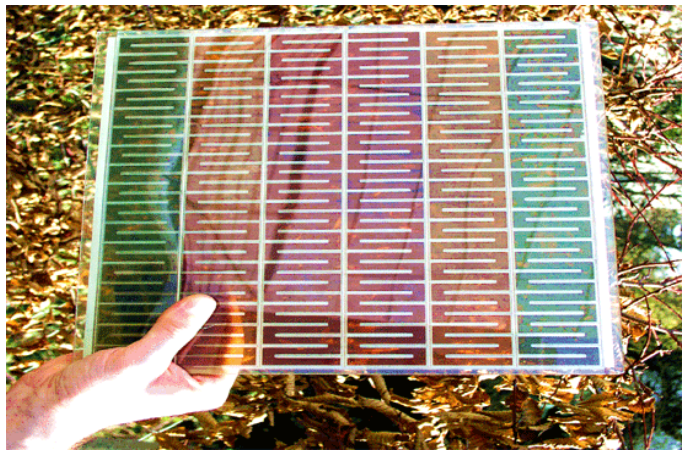

Silicon Solar Cell	Dye Sensitized Solar Cell
- Costly fabrication process - Expensive raw materials	- Easy to be fabricated - Low cost
- Toxic gases	- Friendly to the environment

Dye-Sensitized Solar Cell (DSSC)

THE large-scale use of photovoltaic devices for electricity generation is prohibitively expensive at present: generation from existing commercial devices costs about ten times more than conventional methods[1]. Here we describe a photovoltaic cell, created from low- to medium-purity materials through low-cost processes, which exhibits a commercially realistic energy-conversion efficiency. The device is based on a 10-μm-thick, optically transparent film of titanium dioxide particles a few nanometres in size, coated with a monolayer of a charge-transfer dye to sensitize the film for light harvesting. Because of the high surface area of the semiconductor film and the ideal spectral characteristics of the dye, the device harvests a high proportion of the incident solar energy flux (46%) and shows exceptionally high efficiencies for the conversion of incident photons to electrical current (more than 80%). The overall light-to-electric energy conversion yield is 7.1–7.9% in simulated solar light and 12% in diffuse daylight. The large current densities (greater than 12 mA cm^{-2}) and exceptional stability (sustaining at least five million turnovers without decomposition), as well as the low cost, make practical applications feasible.

M. Grätzel's group, ***Nature (1991)***

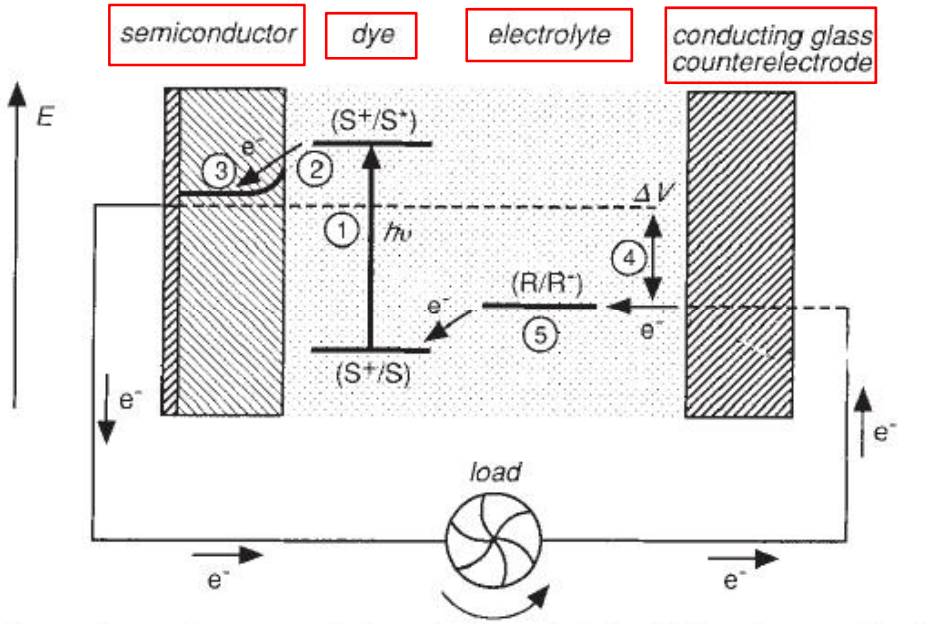

FIG. 1 Schematic representation of the principle of the dye-sensitized photovoltaic cell to indicate the electron energy level in the different phases. The cell voltage observed under illumination corresponds to the difference, ΔV, between the quasi-Fermi level of TiO_2 under illumination and the electrochemical potential of the electrolyte. The latter is equal to the Nernst potential of the redox couple (R/R^-) used to mediate charge transfer between the electrodes. S, sensitizer; S*, electronically excited sensitizer; S^+, oxidized sensitizer.

TiO_2 Nanoparticles for DSSC

(1) Colloidal Synthesis

Typical synthesis of the TiO_2 nanoparticles can be described as follows. A quantity (125 mL) of titanium isopropoxide (97%, Aldrich Chemical Co., Milwaukee, WI) is added, dropwise and at room temperature, to 750 mL of a 0.1*M* nitric acid solution under vigorous stirring. A white precipitate forms instantaneously. Immediately after the hydrolysis, the slurry is heated to 80°C and stirred vigorously for 8 h, to achieve peptization (i.e., destruction of the agglomerates and redispersion into primary particles). The solution is then filtered on a glass frit to remove nonpeptized agglomerates. Water is added to the filtrate to adjust the final solids concentration to ~5 wt%.

The growth of these particles, up to 10–25 nm, is achieved under hydrothermal conditions in a titanium autoclave that is heated for 12 h in the temperature range of 200°–250°C; the temperature is dependent on the desired particle size. Sedimentation occurs during the autoclaving, and the particles are redispersed using a titanium ultrasonic horn (400 W, 15 × 2 s pulses). After two sonications, the colloidal suspension is introduced in a rotary evaporator and evaporated (35°C, 30 mbar (3 MPa)) to a final TiO_2 concentration of 11 wt%.

M. Grätzel's group,
***J. Am. Ceram. Soc.* (1997)**

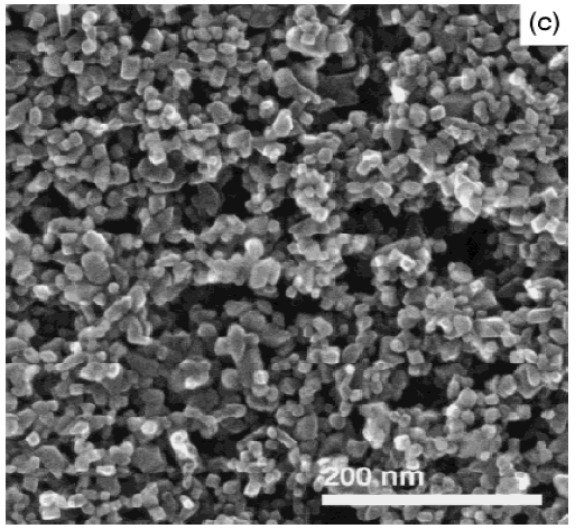

Fig. 2. SEM micrographs of films synthesized from colloids autoclaved at (a) 210°, (b) 230°, and (c) 250°C.

· hydrothermal method

· ~20 nm size, anatase phase

· ~10 μm thickness for efficient photon absorption

TiO_2 Phase Dependency for DSSC

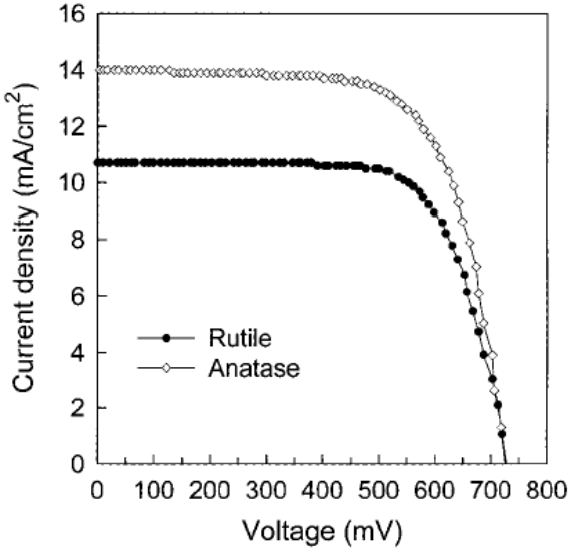

Figure 5. Comparison of the $J-V$ characteristics of dye-sensitized rutile- and anatase films of the same thickness (11.5 μm) at one-sun illumination.

Rutile phase도 DSSC에 사용되었을 때 효율을 나타내지만, anatase phase를 사용했을 때보다 낮은 효율을 나타낸다고 많은 논문에서 보고되고 있습니다. 하지만 그 구체적인 원인에 대해서는 정확하게 규명되지 않았습니다.

Rutile phase의 nanoparticle을 합성하면 20 nm × 80 nm 정도 크기의 rod형태가 만들어지고, spherical anatase nanoparticle은 20 nm 정도의 크기를 가집니다. 따라서 rutile nanoparticle은 anatase nanoparticle에 비해 표면적이 작아 달라붙는 dye의 양이 적고, photocurrent가 적게 발생해 효율이 떨어지는 것이라고 아래 논문에서 주장하고 있습니다.

N.-G. Park *et al.*,
J. Phys. Chem. B (2000)

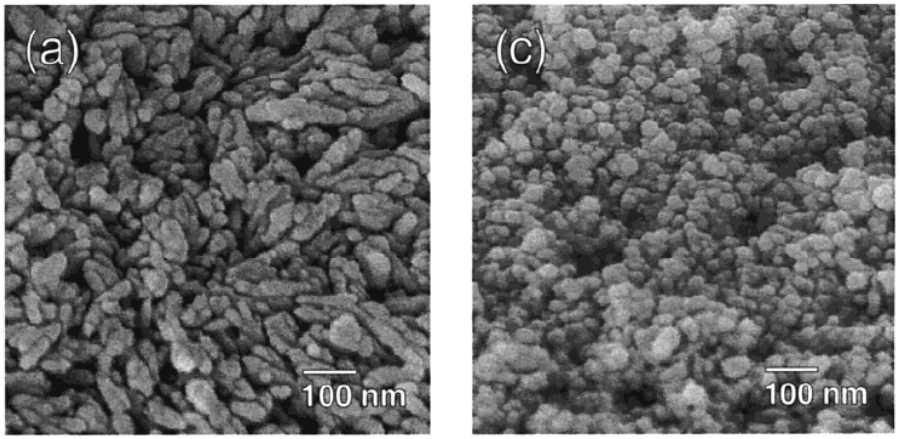

Figure 6. Surface and cross sectional SEM micrographs of a rutile (a, b) and an anatase (c, d) film coated on conducting glass and annealed at 500 °C for 1 h.

Dyes for DSSC

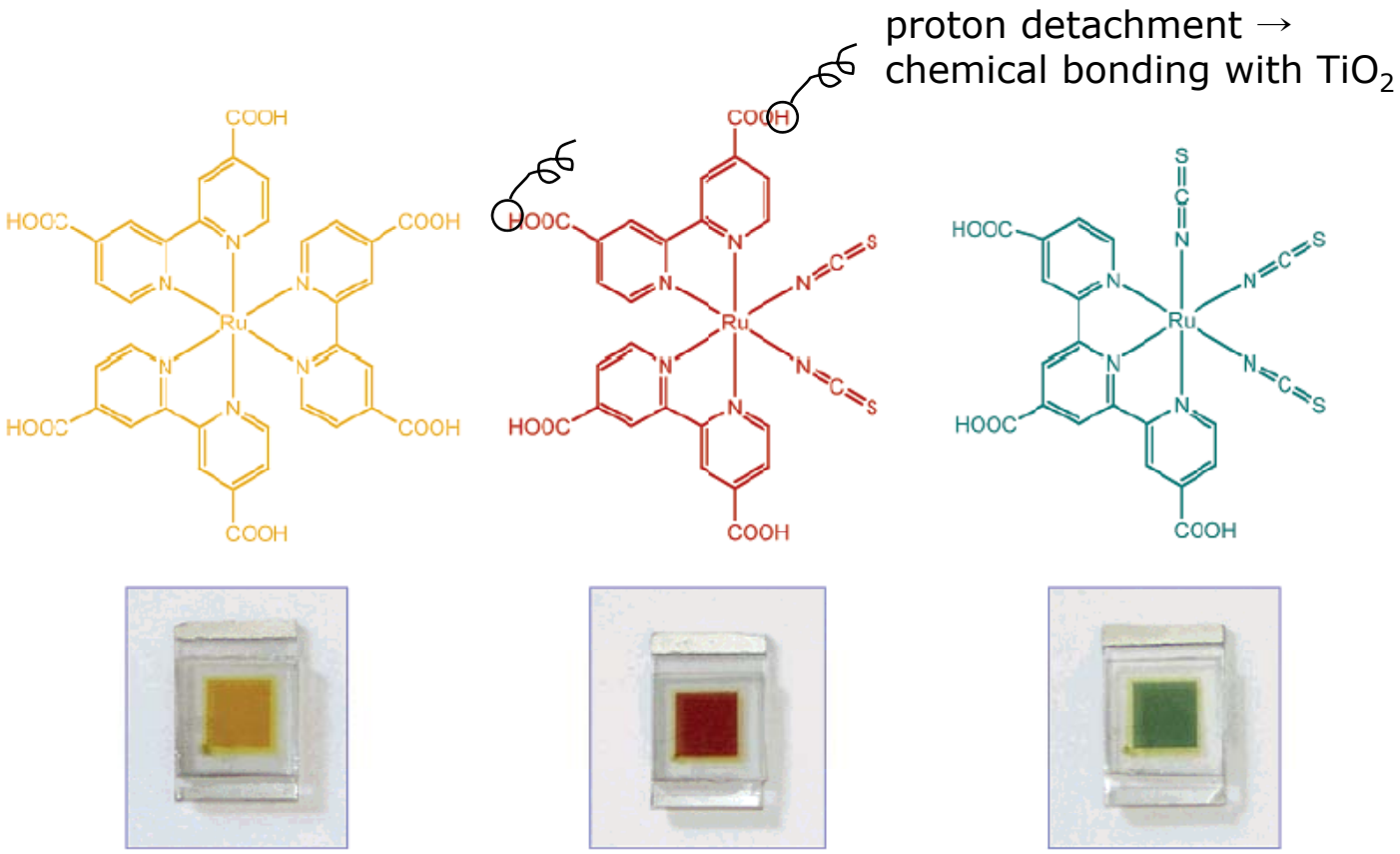

Figure 5. Structure of the ruthenium sensitizers RuL_3 (yellow) *cis*-$RuL_2(NCS)_2$ (red) and $RuL'(NCS)_3$ (green) where L = 2,2′-bipyridyl-4,4′-dicarboxylic acid and L′ = 2,2′,2″-terpyridyl-4,4′,4″-tricarboxylic acid. The lower part of the picture shows nanocrystalline TiO_2 films loaded with a monolayer of the respective sensitizer. The film thickness is 5 μm.

M. Grätzel, ***Inorganic Chemistry (2005)***

Dyes for DSSC (N719)

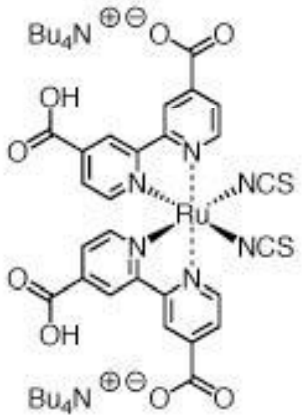

Chemical Structure of N719 dye

Specifications

Product designation:	**Ruthenium 535 bis-TBA** (also known as "N719" or "dye salt")
Chemical Name:	*cis*-bis(isothiocyanato)bis(2,2'-bipyridyl-4,4'-dicarboxylato)-ruthenium(II) bis-tetrabutylammonium
Short Formula:	$RuL_2(NCS)_2$: 2 TBA (L = 2,2'-bipyridyl-4,4'-dicarboxylic acid ; TBA = tetrabutylammonium)
Molecular Formula:	$C_{58}H_{86}O_8N_8S_2Ru$
Formula Weight:	1187.7 g/mol
Aspect:	Dark purple powder
Caution:	Substance not fully tested

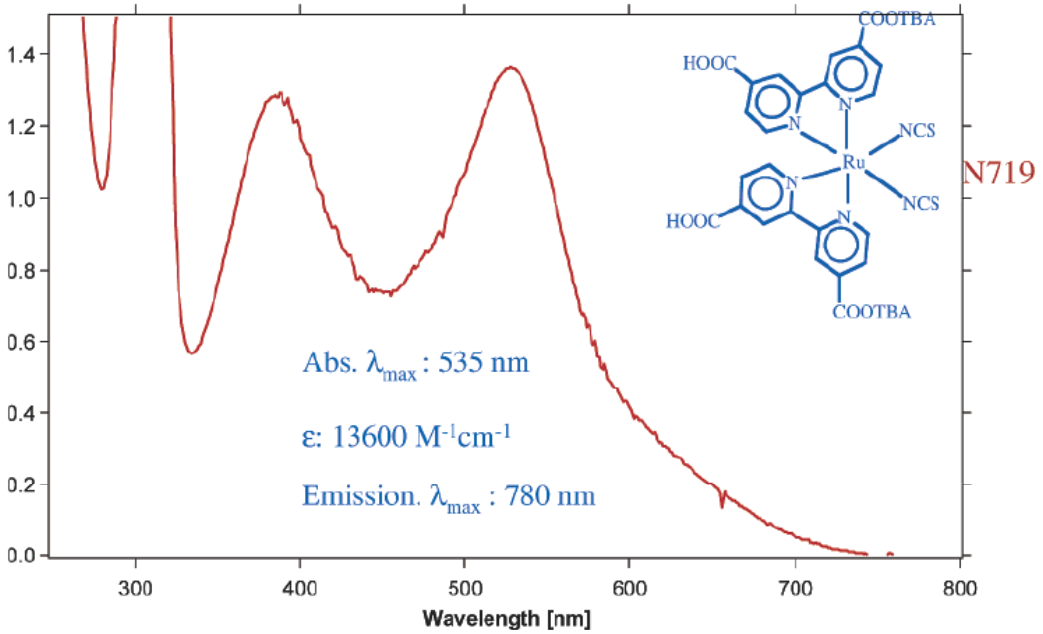

Figure 13. Absorption spectrum of the N-719 dye in ethanol featuring two MLCT bands.

M. Grätzel, ***Inorganic Chemistry (2005)***

Dyes for DSSC (N719)

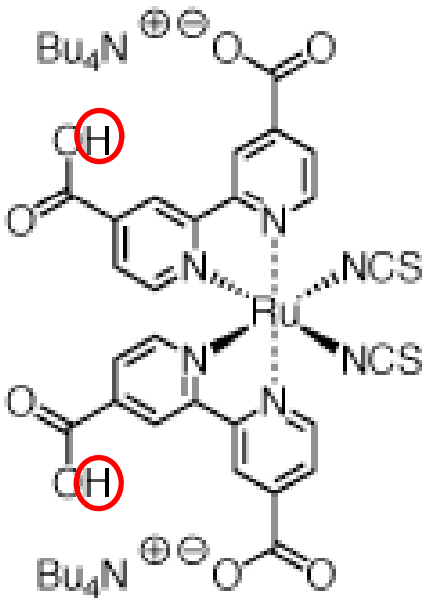

Chemical Structure of N719 dye

Bu$_4$N: tetrabutylammonium

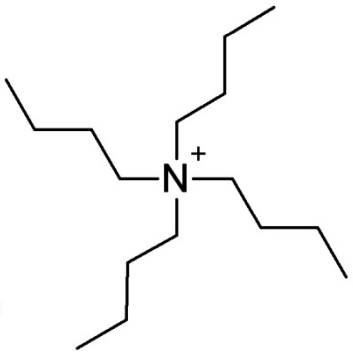

○ 부분이 떨어져나가면서 아래 그림과 같이 Ti와 bonding을 형성하게 됩니다. → dye adsorption to TiO_2

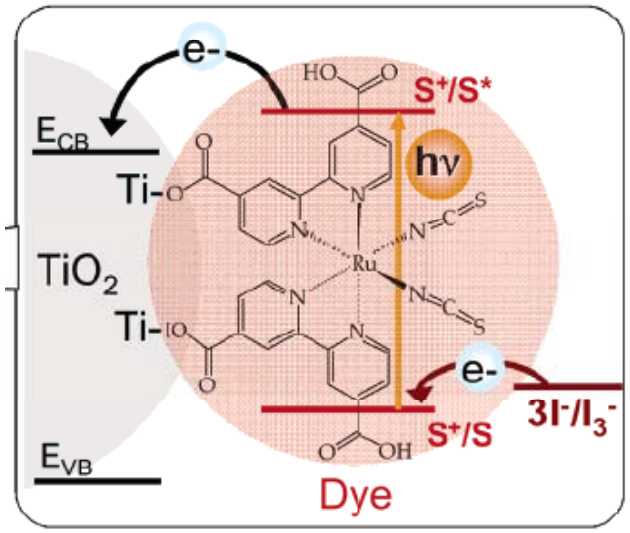

cf) Chemical Structure of N3 dye

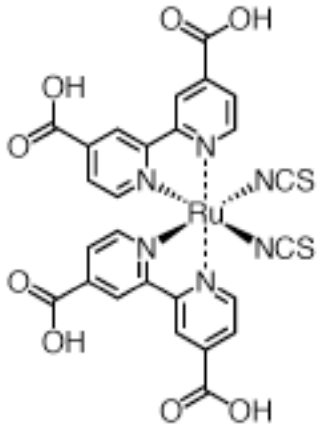

Optimizing Dyes for DSSC

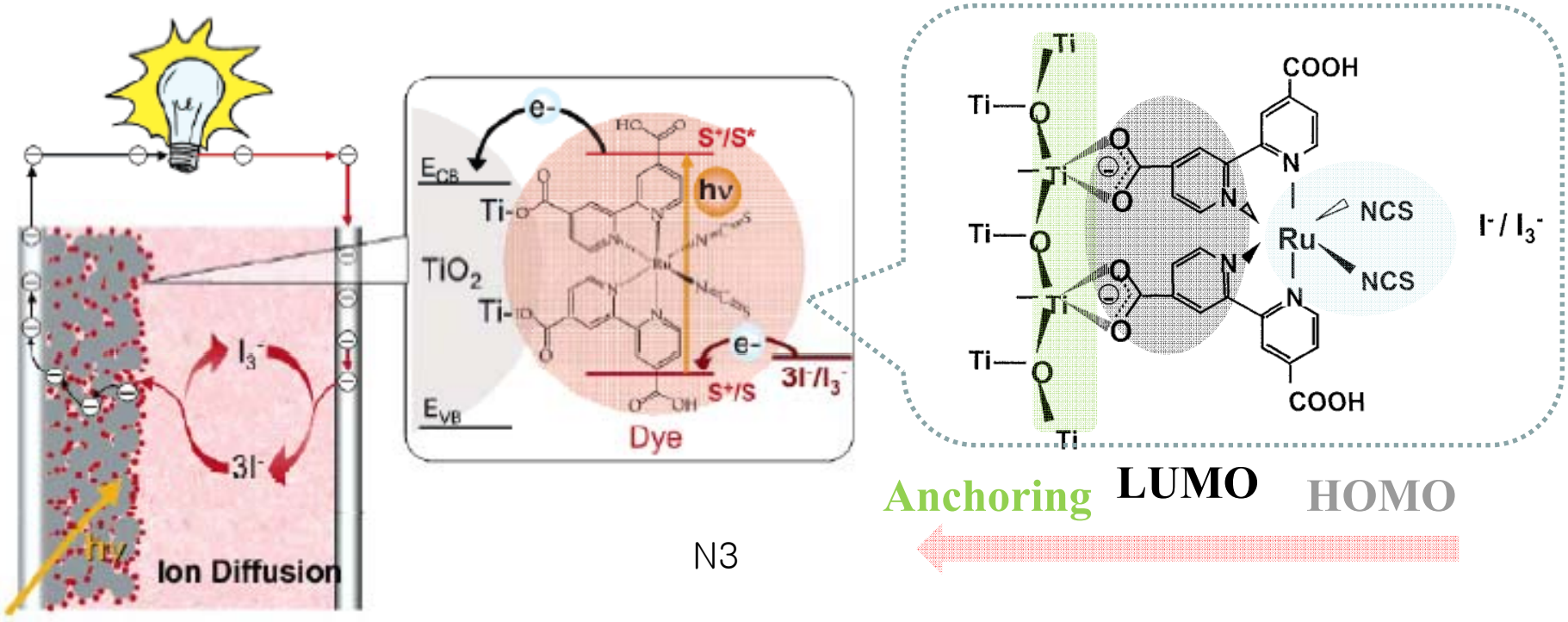

Organometallic dye: charge separation

anatase (001)

anatase (101)

→ the most stable plane

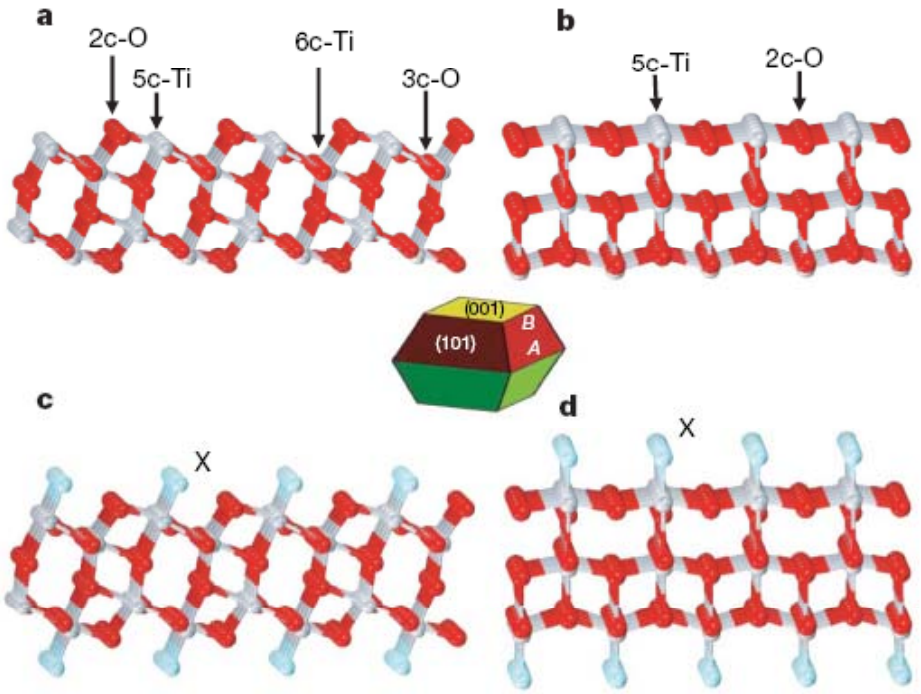

H. G. Yang *et al.*,
Nature **453**, 638 (2008)

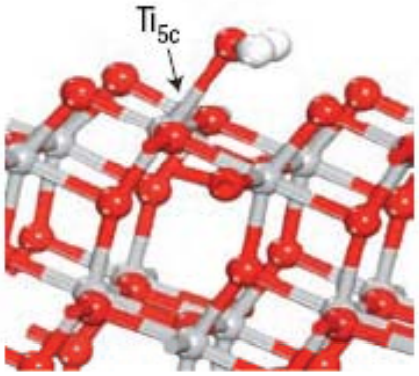

Water on TiO_2(101):
molecular adsorption

A. Selloni,
Nat. Mater. **7**, 613 (2008)

Anatase TiO_2 표면에서 chemical adsorption이 발생할 경우, 표면에서 더 불안정한 Ti 와 bonding을 형성한다고 알려져 있습니다.

anatase (101)

dye

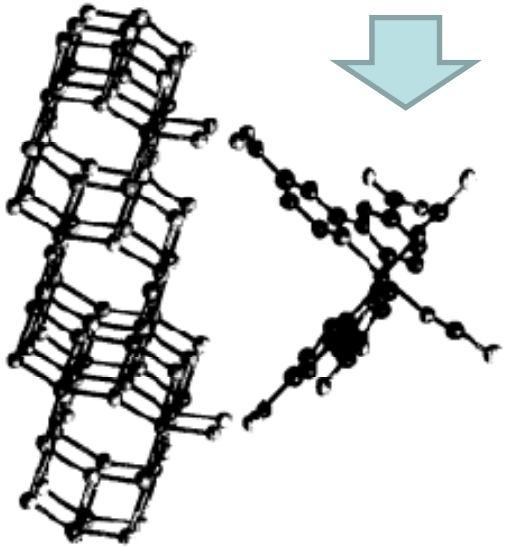

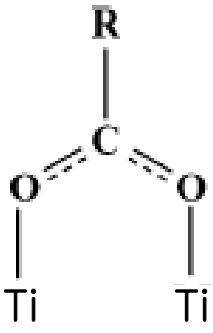

Bridging bidentate

N719 dye

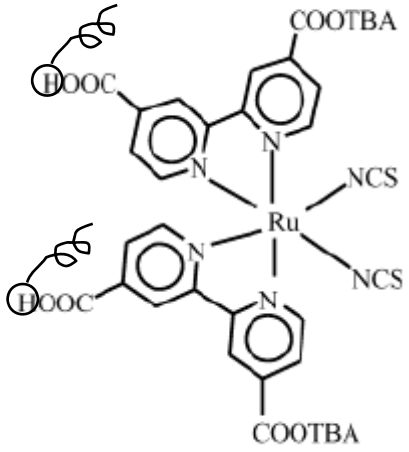

M. Graetzel's group,
JPCB (2003)

이 논문에서는, dye-coated TiO_2 film의 FT-IR 분석을 통해, TiO_2 표면의 Ti와 dye 사이의 chemical bonding 형성을 분석했습니다.

Dyes for DSSC (N719)

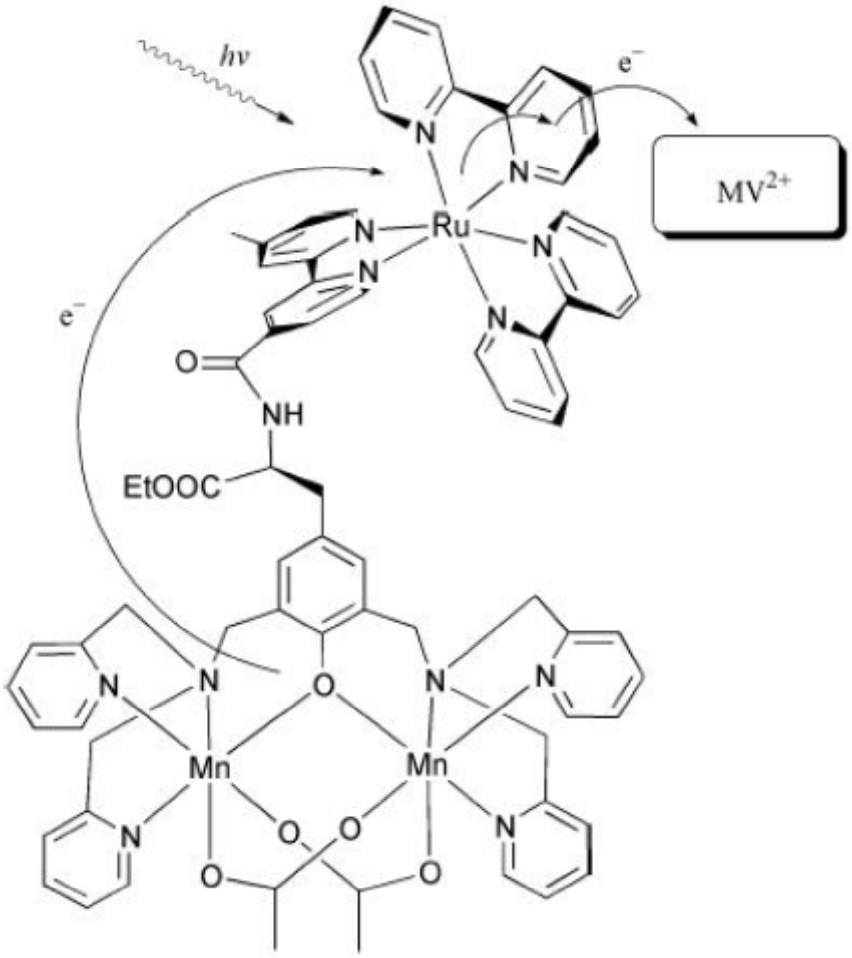

3-D Structure of Ru complex

Operation of DSSC

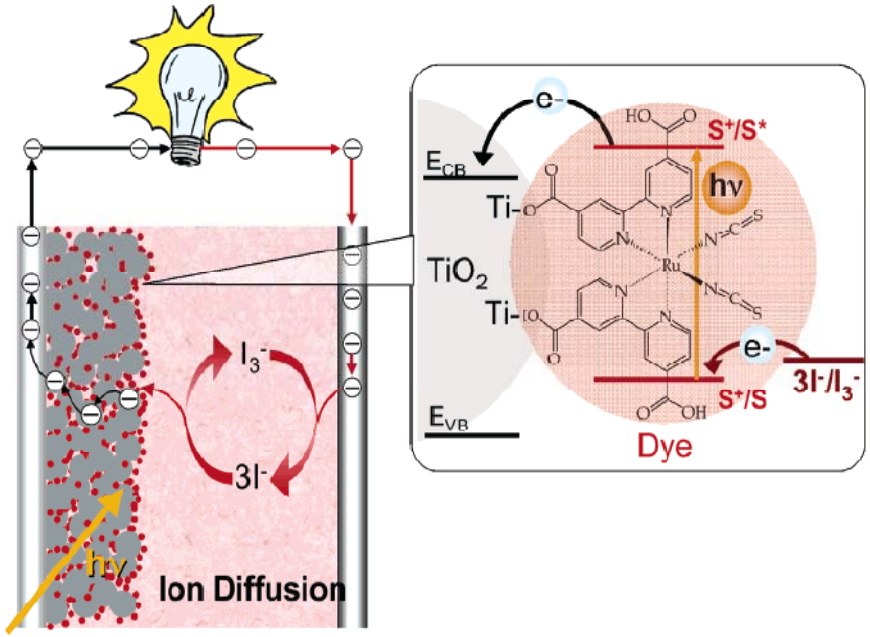

M. Grätzel, ***Inorganic Chemistry (2005)***

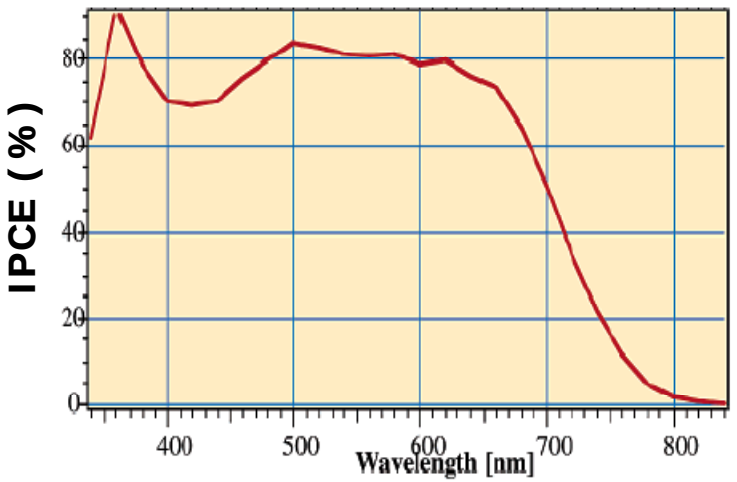

Figure 12. Conversion of light to electric current by mesoscopic solar cells sensitized with the ruthenium dye N-719. The IPCE is plotted as a function of the excitation wavelength. The electrolyte contains alkyl-imidazolium iodide and triiodide as the redox system.

Dynamic Competition

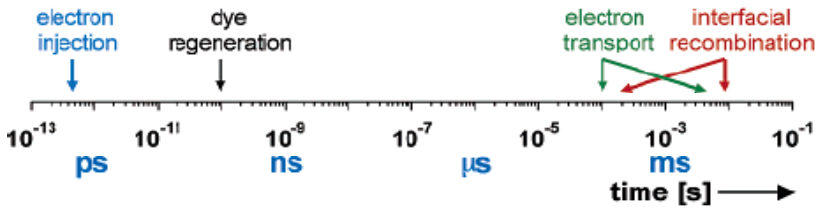

good photon absorption,
good charge separation

IPCE: Incident Photon to Current Conversion Efficiency

Dye-Sensitized Photovoltaic Cells

M. Grätzel, ***Inorganic Chemistry (2005)***

Forum

Solar Energy Conversion by Dye-Sensitized Photovoltaic Cells

Michael Grätzel*

Laboratory for Photonics and Interfaces, Swiss Federal Institute of Technology, CH-1015 Lausanne, Switzerland

Received May 24, 2005

The quality of human life depends to a large degree on the availability of energy. This is threatened unless renewable energy resources can be developed in the near future. Chemistry is expected to make important contributions to identify environmentally friendly solutions of the energy problem. One attractive strategy discussed in this Forum Article is the development of solar cells that are based on the sensitization of mesoscopic oxide films by dyes or quantum dots. These systems have already reached conversion efficiencies exceeding 11%. The underlying fundamental processes of light harvesting by the sensitizer, heterogeneous electron transfer from the electronically excited chromophore into the conduction band of the semiconductor oxide, and percolative migration of the injected electrons through the mesoporous film to the collector electrode will be described below in detail. A number of research topics will also be discussed, and the examples for the first outdoor application of such solar cells will be provided.

TiO_2 Nanotubes for DSSC

C. A. Grimes's group,
Nano Letters (2006)

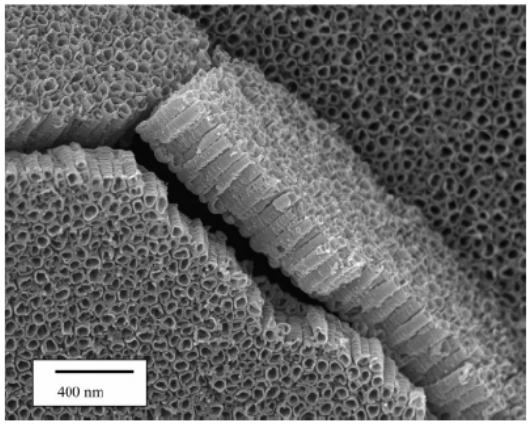

Figure 2. Top and lateral view FESEM images of titanium nanotubes grown from a 500-nm-thick Ti thin film (sputtered onto SnO_2:F coated glass at 500 °C) anodized using a 0.5% HF electrolyte concentration at a potential of 12 V.

Ti deposition by sputtering (500 nm)

Anodizing Ti film at constant potential, 12 V. (HF condition)

Pore diameter: 46 nm
Wall thickness: 17 nm
Length: 360 nm

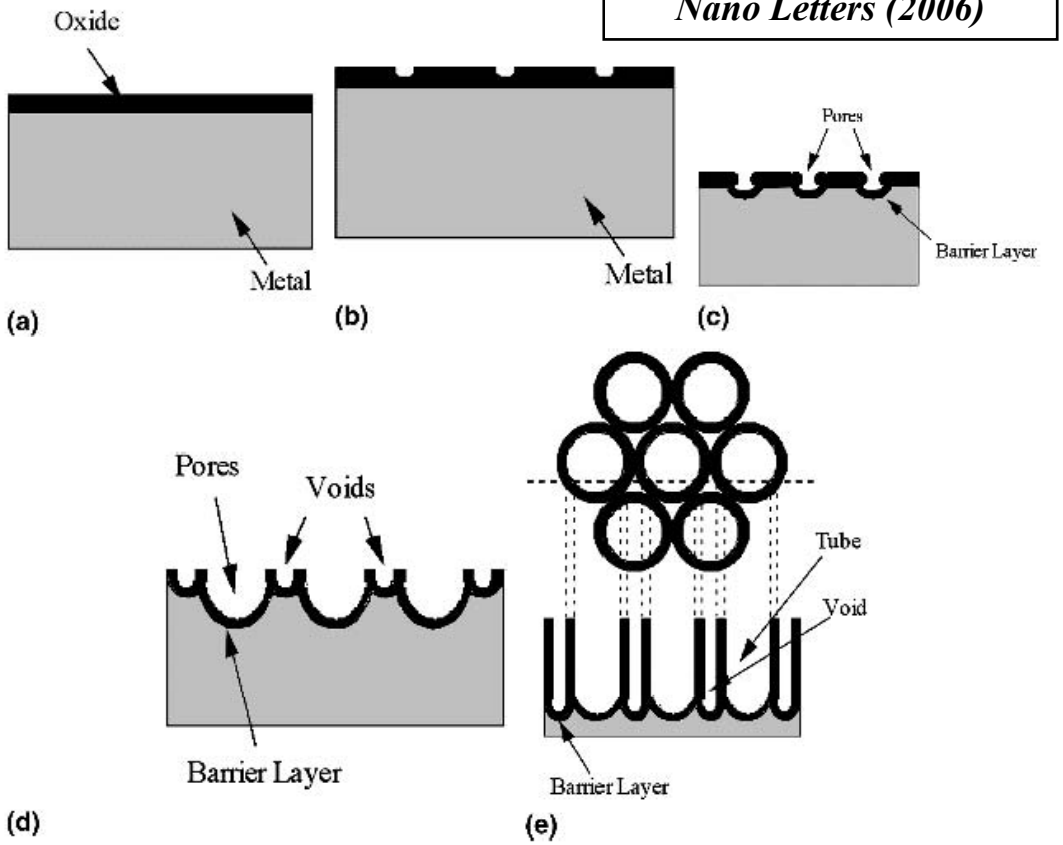

FIG. 5. Schematic diagram of the evolution of straight nanotubes at a constant anodization voltage, as follows: (a) oxide layer formation; (b) pit formation on the oxide layer; (c) growth of the pit into scallop-shaped pores; (d) the metallic part between the pores undergoes oxidation and field-assisted dissolution; and (e) fully developed nanotubes with a corresponding top view.

TiO_2 Nanotubes for DSSC

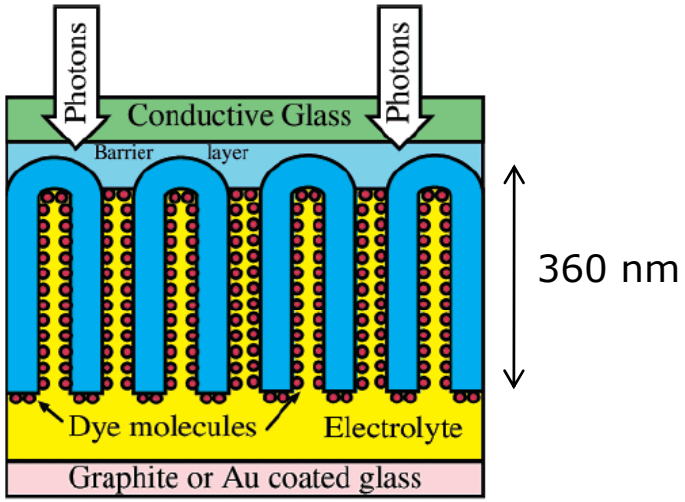

Figure 3. Integration of transparent nanotube array architecture into dye solar cell structure.

C. A. Grimes's group,
Nano Letters (2006)

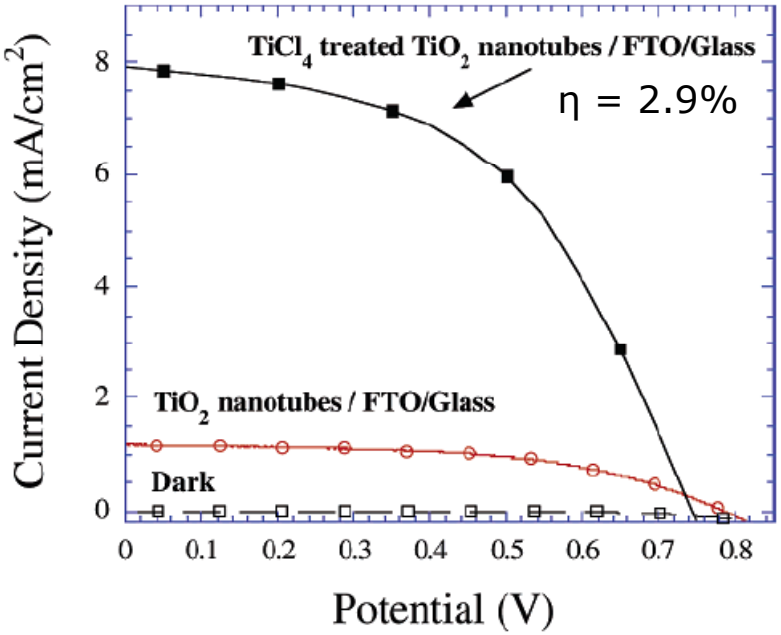

Figure 4. Photocurrent–photovoltage characteristics of a transparent nanotube array DSC under 100% AM-1.5 illumination.

ABSTRACT

We describe the use of highly ordered transparent TiO_2 nanotube arrays in dye-sensitized solar cells (DSCs). Highly ordered nanotube arrays of 46-nm pore diameter, 17-nm wall thickness, and 360-nm length were grown perpendicular to a fluorine-doped tin oxide-coated glass substrate by anodic oxidation of a titanium thin film. After crystallization by an oxygen anneal, the nanotube arrays are treated with $TiCl_4$ to enhance the photogenerated current and then integrated into the DSC structure using a commercially available ruthenium-based dye. Although the negative electrode is only 360-nm-thick, under AM 1.5 illumination the generated photocurrent is 7.87 mA/cm^2, with a photocurrent efficiency of 2.9%. Voltage-decay measurements indicate that the highly ordered TiO_2 nanotube arrays, in comparison to nanoparticulate systems, have superior electron lifetimes and provide excellent pathways for electron percolation. Our results indicate that remarkable photoconversion efficiencies may be obtained, possibly to the ideal limit of ~31% for a single photosystem scheme, with an increase of the nanotube-array length to several micrometers.

Electrode/Electrolyte Interface Problem

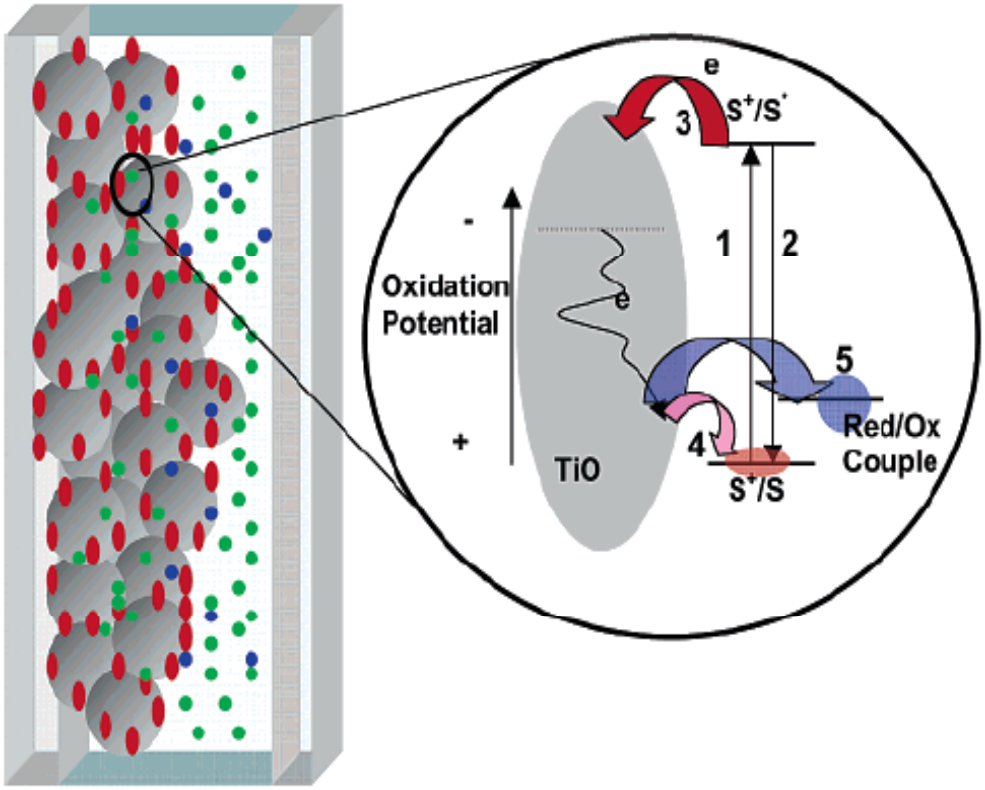

Solutions

· Core-shell Structure

→ wide bandgap materials

· Surface Treatment

→ Ar or O_2 plasma, $TiCl_4$ treatment

· Nanoscale Coating on the TCO

$CaCO_3$-Coated TiO_2 Nanoparticles

·$CaCO_3$-coated TiO_2 nanoparticle (core-shell)

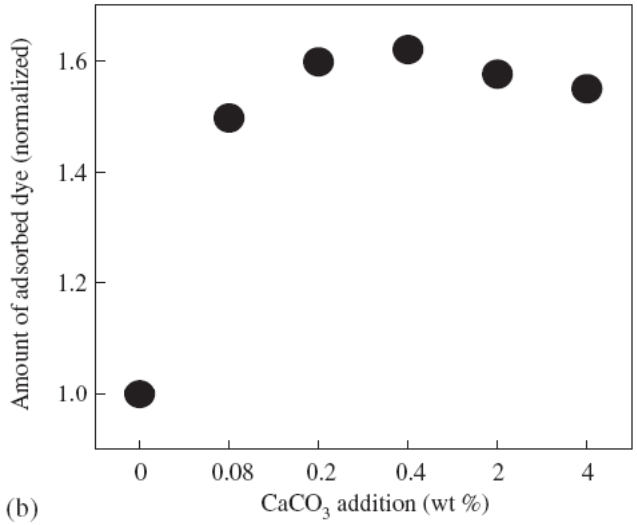

$CaCO_3$: basic than TiO_2 → carboxyl group of dye can adsorb more easily

$CaCO_3$ is insulator (band gap: 6 eV) → thick shell of $CaCO_3$ block electron transfer from dye to TiO_2

K. Hong's group,

Sol. Energy Mater. Sol. Cells (2006)

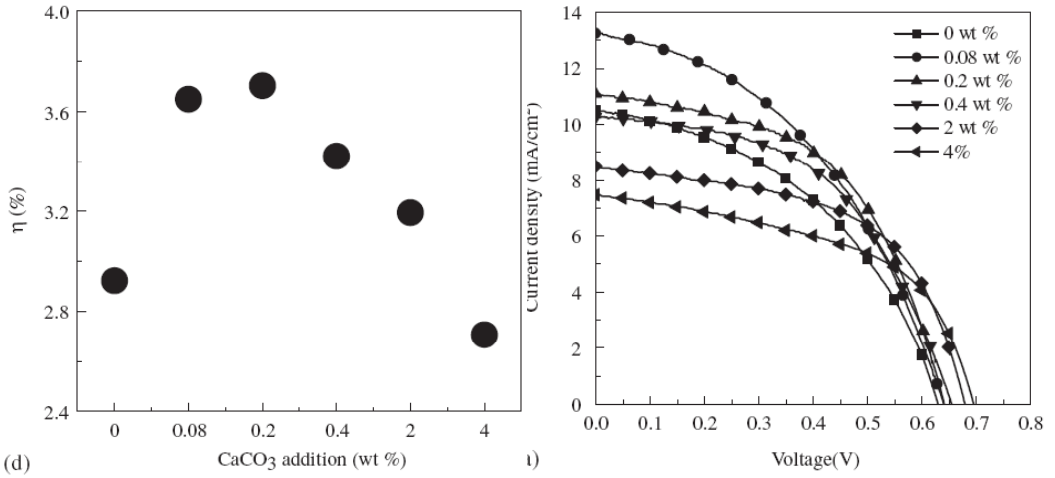

Fig. 3. E(a) Photocurrent–voltage characteristics of dye-sensitized TiO_2 and $CaCO_3$-coated TiO_2 electrodes, (b) short circuit current density (J_{sc}), (c) open circuit voltage (V_{oc}), and (d) cell efficiency (η) as a function of $CaCO_3$ addition.

$CaCO_3$-Coated TiO_2 Nanoparticles

Enhancement of the photoelectric performance of dye-sensitized solar cells by using a $CaCO_3$-coated TiO_2 nanoparticle film as an electrode

Abstract

Core-shell-type nanoparticles with TiO_2 cores and $CaCO_3$ shells were applied as the electrode of dye-sensitized solar cells. The performance of the cell was significantly improved (as high as 26.7%) compared to the case when un-coated TiO_2 particle film was used as electrode. The improved energy conversion efficiency has been ascribed to (i) enhanced dye adsorption due to the high isoelectric point of the overlayer, and (ii) the prevention of the back electron transfer by the insulating nature of the overlayer.

MgO-Coated TiO_2 Nanoparticles

K. Hong's group,
Langmuir (2005)

·MgO-coated TiO_2 nanoparticle (nanoporous structure)

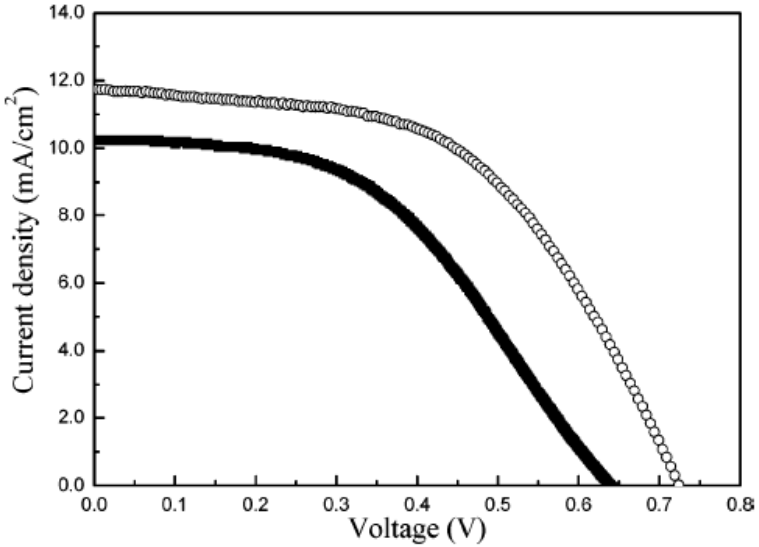

Figure 2. Photocurrent–voltage characteristics of dye-sensitized TiO_2 and MgO-coated TiO_2 electrodes (■ = 0 wt %, ○ = 0.6 wt %).

sample	V_{oc} (V)	I_{sc} (mA/cm^2)	FF (%)	η (%)
bare TiO_2	0.64	10.2	47.3	3.1
MgO-coated TiO_2	0.72	11.7	53.5	4.5

· J_{sc} enhancement: increase of the dye adsorption

· V_{oc} enhancement: suppression of the charge recombination

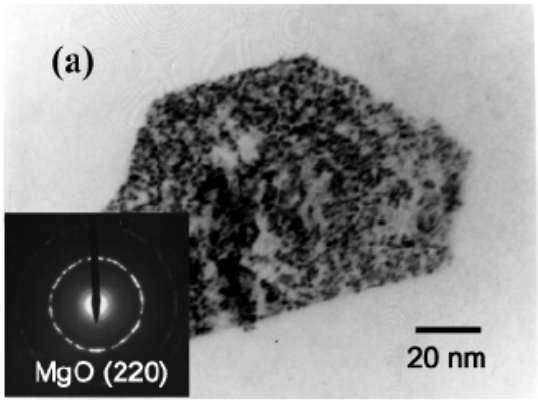

Figure 1. (a) TEM micrographs of MgO nanoparticles obtained from the thermal decomposition of $Mg(OH)_2$

MgO-Coated TiO_2 Nanoparticles

K. Hong's group,
Langmuir (2005)

Preparation of Nanoporous MgO-Coated TiO_2 Nanoparticles and Their Application to the Electrode of Dye-Sensitized Solar Cells

Sol−gel-derived $Mg(OH)_2$ gel was coated onto TiO_2 nanoparticles, and the subsequent thermal topotactic decomposition of the gel formed a highly nanoporous MgO crystalline coating. The specific surface area of the electrode that was prepared from the core−shell-structured TiO_2 nanoparticles significantly increased compared with that of the uncoated TiO_2 electrode. The increase in the specific surface area of the MgO-coated TiO_2 electrode was attributed to the highly nanoporous MgO coating layer that resulted from the topotactic reaction. Dye adsorption behavior and solar cell performance were significantly enhanced by employing the MgO-coated TiO_2 electrode. Optimized coating of a MgO layer on TiO_2 nanoparticles enhanced the energy conversion efficiency as much as 45% compared to that of the uncoated TiO_2 electrode. This indicates that controlling the extrinsic parameters such as the specific surface area is very important to improve the energy conversion efficiency of TiO_2-based solar cells.

Metal-Oxide Coating on TiO_2 Nanoparticles

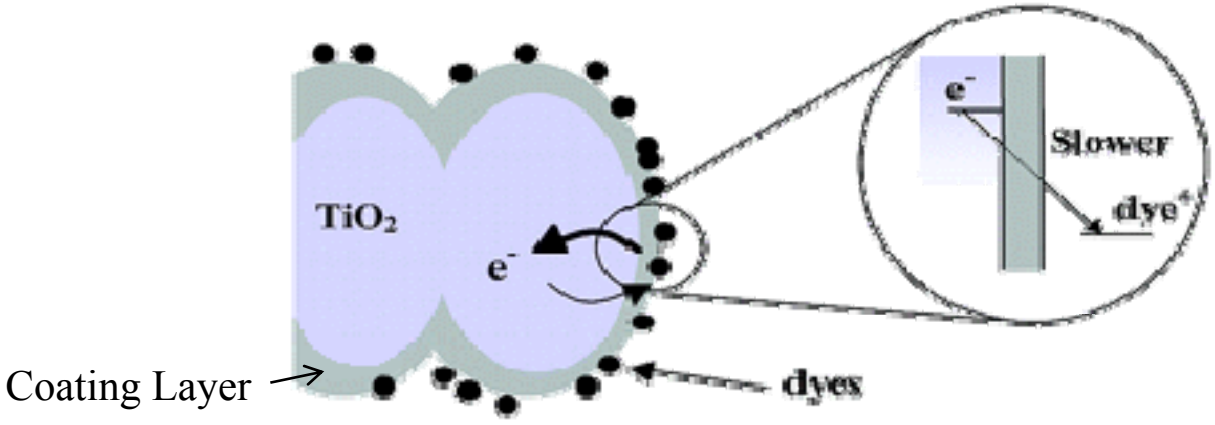

• **Effect of TiO_2 Coating Layer**

1. The insulating layers with wide band gap and high conduction band edge can retard the back transfer of electrons from TiO_2 to the electrolytes or dye molecules (decrease trap state).
2. The enhanced dye adsorption by the oxide layers can improve the cell performance
   → The coated surface favors the dye adsorption through the carboxylic acid group of the dye.

Sujuan Wu *et al.* (Wuhan University)
Nanotechnology **19**, 215704 (2008)

MgO-Coated TiO_2

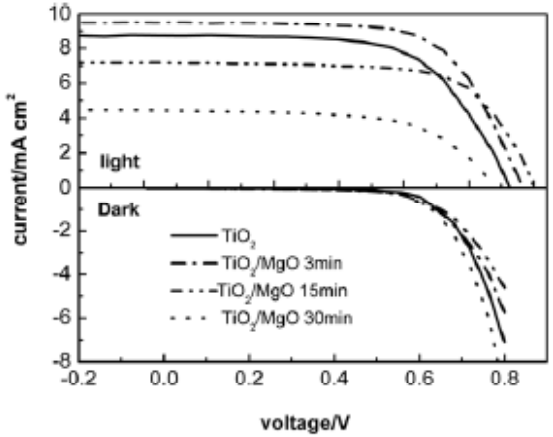

Figure 3. *I–V* curves for TiO_2 and TiO_2/MgO cells in the dark and under illumination with a light intensity of 60 mW cm^{-2}.

Sujuan Wu *et al.* (Wuhan University)
Nanotechnology **19**, 215704 (2008)

Table 1. DSSCs performance for TiO_2 and TiO_2/MgO cells under a light intensity of 60 mW cm^{-2}.

Electrode	J_{sc} (mA cm^{-2})	V_{oc} (V)	FF	η (%)
TiO_2	8.74	0.662	0.669	6.45
TiO_2/MgO 3 min	9.51	0.682	0.700	7.57
TiO_2/MgO 15 min	7.16	0.701	0.716	5.99
TiO_2/MgO 30 min	4.47	0.643	0.648	3.10

Excessively thick MgO layer beyond the tunneling distance plays a negative role in the photoelectron conversion process.

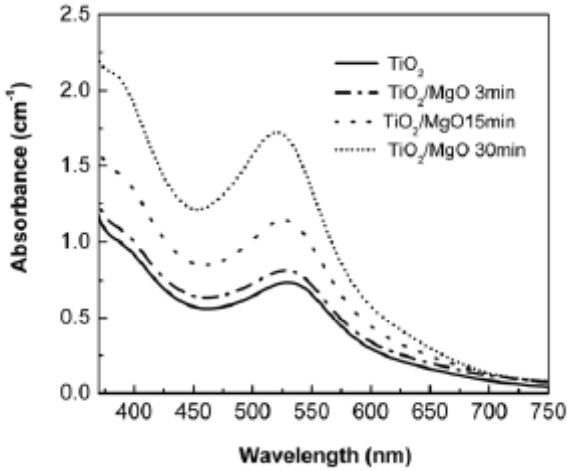

Figure 5. UV–vis absorption spectra for N719-loaded TiO_2 and TiO_2/MgO electrodes.

Dye adsorption increase with sputtering time

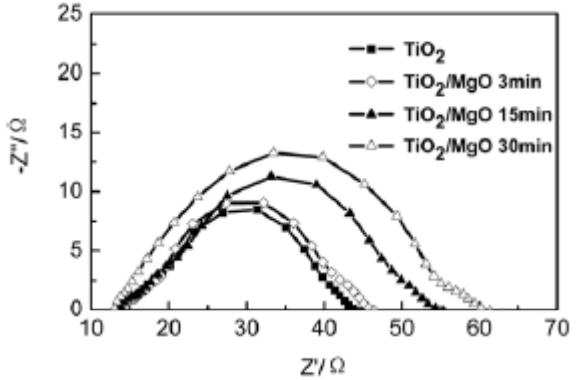

Figure 7. Impedance spectra for TiO_2 and TiO_2/MgO cells measured at −0.75 V in the dark.

Resistance at the TiO_2/dye/electrolyte increase with sputtering time

MgO-Coated TiO_2

IOP PUBLISHING NANOTECHNOLOGY

Nanotechnology 19 (2008) 215704 (6pp) doi:10.1088/0957-4484/19/21/215704

Enhancement in dye-sensitized solar cells based on MgO-coated TiO_2 electrodes by reactive DC magnetron sputtering

Sujuan Wu, Hongwei Han, Qidong Tai, Jing Zhang, Sheng Xu, Conghua Zhou, Ying Yang, Hao Hu, BoLei Chen, Bobby Sebo and Xing-Zhong Zhao[1]

Abstract

A surface modification method was carried out by reactive DC magnetron sputtering to fabricate TiO_2 electrodes coated with insulating MgO for dye-sensitized solar cells. The MgO-coated TiO_2 electrode had been characterized by x-ray photoelectron spectroscopy (XPS), energy-dispersive x-ray spectroscopy (EDX), scanning electron microscopy (SEM), UV–vis spectrophotometer, cyclic voltammetry (CV) and electrochemical impedance spectroscopy (EIS). The study results revealed that the TiO_2 modification increases dye adsorption, decreases trap states and suppresses interfacial recombination. The effects of sputtering MgO for different times on the performance of DSSCs were investigated. It indicated that sputtering MgO for 3 min on TiO_2 increases all cell parameters, resulting in increasing efficiency from 6.45% to 7.57%.

FTO/Blocking Layer/Porous TiO_2

• Introduction

Porous interfaces between FTO substrate and TiO_2 layers can be electron recombination site, i.e., electron leakage sites exist especially when solid or highly viscous redox species such as ionic liquid iodides once infiltrate into the interfaces.

→ **Blocking layer can suppress back electron transfer from FTO to electrolytes.**

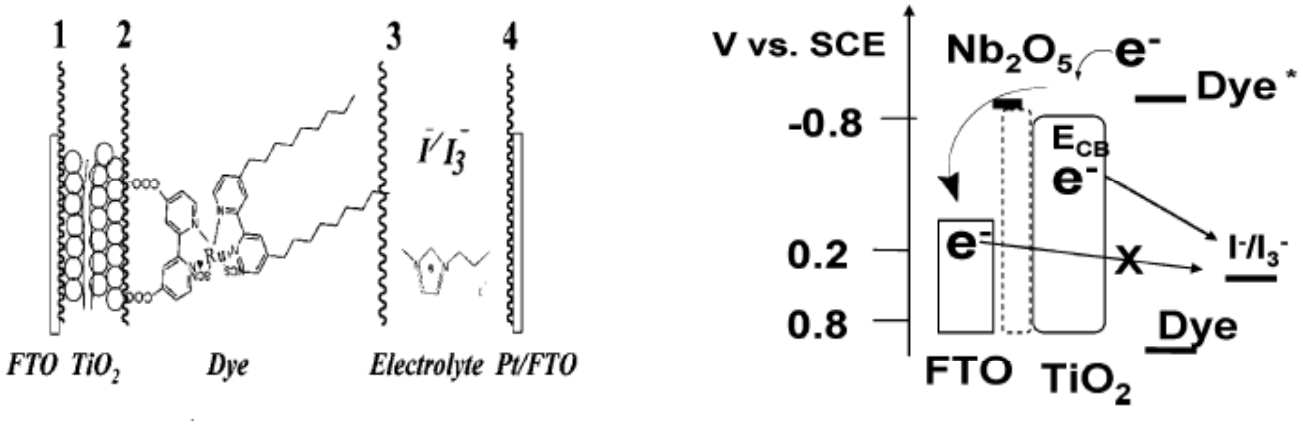

Figure 1. Schematic views of interfaces in the DSC device and the electron transfer of the new structured electrode.

Shozo Yanagida Group (Osaka University)
J. Phys. Chem. C **111**, 8092 (2007)

FTO/Nb_2O_5/Porous TiO_2

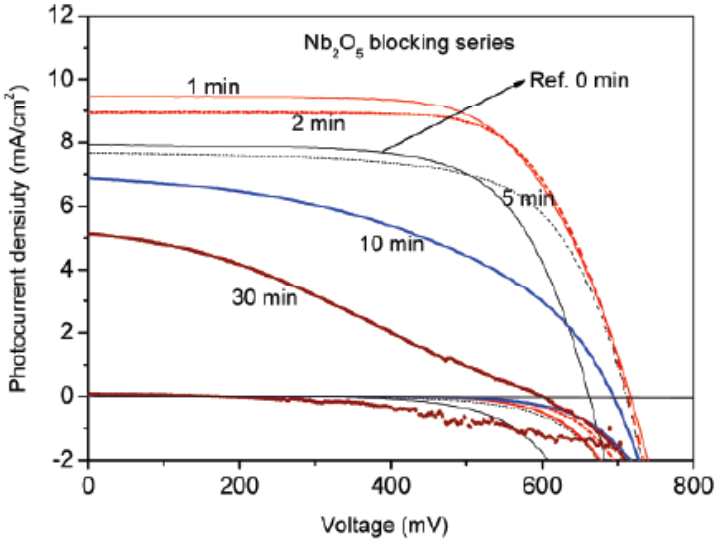

Figure 2. $J-V$ curves of the cells employing Z-907 sensitized FTO/nanoTiO_2 and FTO/Nb_2O_5/nanoTiO_2 electrodes under AM 1.5 irradiation. (Electrolyte: PMImI:EMImI-DCA = 2:1, 0.2 M I_2, 0.5 M TBP, and 0.1 M LiI; 5.5 μm of nanoTiO_2 was employed).

Sputtering method has the merits of good reproducibility, of homogeneous coverage and suitability for the large scale production.

Excessively thick blocking layers beyond tunneling distance would play a negative role in the photoelectron conversion process.

Shozo Yanagida Group (Osaka University)
J. Phys. Chem. C **111**, 8092 (2007)

TABLE 1: Comparison of $J-V$ Characteristics of the Devices with and without a Nb_2O_5-Blocking Layer

thickness of blocking layer	electrodes	V_{oc}/mV	J_{sc}/mA cm^{-2}	FF	η (%)
	bare FTO	663 ± 5	7.91 ± 0.2	0.66 ± 0.01	3.5 ± 0.1
2−3 nm	Nb_2O_5 1 min	711 ± 3	9.22 ± 0.3	0.68 ± 0.01	4.4 ± 0.1
5 nm	Nb_2O_5 2 min	710 ± 4	9.32 ± 0.4	0.68 ± 0.02	4.5 ± 0.1
13 nm	Nb_2O_5 5 min	710 ± 7	7.58 ± 0.3	0.66 ± 0	3.6 ± 0.1
26 nm	Nb_2O_5 10 min	694 ± 10	7.31 ± 0.4	0.47 ± 0.02	2.4 ± 0.1
80 nm	Nb_2O_5 30 min	589 ± 20	5.13 ± 0.3	0.32 ± 0.01	1.0 ± 0.1

FTO/Nb_2O_5/Porous TiO_2

J. Phys. Chem. C **2007**, *111*, 8092−8097

Sputtered Nb_2O_5 as a Novel Blocking Layer at Conducting Glass/TiO_2 Interfaces in Dye-Sensitized Ionic Liquid Solar Cells

Jiangbin Xia, Naruhiko Masaki, Kejian Jiang, and Shozo Yanagida*

Center for Advanced Science and Innovation, Osaka University, Suita, Osaka 565-0871, Japan

Received: January 28, 2007; In Final Form: March 7, 2007

The preparation of a novel Nb_2O_5 blocking layer deposited between fluorine-doped tin oxide (FTO) and nanocrystalline TiO_2 layer and its application for dye-sensitized ionic liquid solar cell have been studied. The Nb_2O_5 blocking layer prepared by the sputtering method on FTO has been characterized by scanning electron microscopy (SEM), cyclic voltammetry (CV), and X-ray photoelectron spectroscopy. Thin Nb_2O_5 films work as a potential blocking layer between FTO and TiO_2 nanocrystalline film in ionic liquid electrolyte cells, improving V_{oc} and finally giving a better conversion efficiency of dye-sensitized TiO_2 solar cells. The remarkable improvements of V_{oc} and the fill factor for the dye-sensitized solar cells suggest that such a thin Nb_2O_5 layer is an effective blocking layer at FTO and TiO_2 interface, contributing to the suppression of recombination processes between unidirectional transporting electron and redox electrolytes in the process of TiO_2 photoelectron conversion systems. SEM and CV reveal that the Nb_2O_5 blocking layer is electronic blocking rather than morphological blocking at the FTO/nanoTiO_2 interface, which may give another direction on the suppression of charge recombination during photoelectron conversion process.

FTO / TiO_2 Thin-Film Layer / TiO_2 Nanoparticles

FTO/TiO_2 compact layer/TiO_2

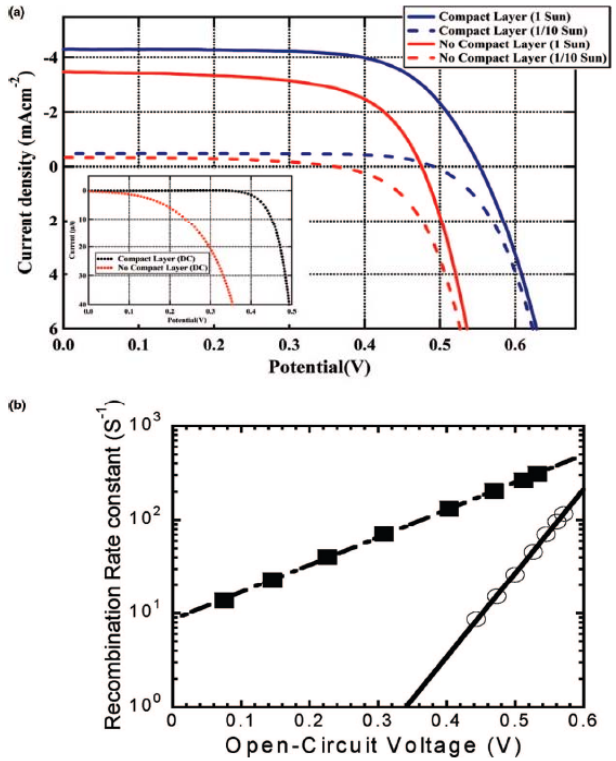

Figure 1. (a) *IV* curves of two cells both in the presence (blue) and absence (red) of a compact TiO_2 blocking layer on the FTO. The thick lines and dashed lines represent the performance at 1 Sun and 1/10 Sun, respectively. The inset shows the dark currents with (black) and without (red) the compact layer. (b) Charge recombination rate constant derived from transient open-circuit voltage decay measurements for a DSSC with a blocking layer (open circles, solid line) and without a blocking layer (solid squares, dot−dashed line).

Recombination rate decrease between FTO / Electrolyte
→ J_{SC} , V_{OC} increase

Efficiency (1 Sun)
With compact layer : 1.6%
Without compact layer : 1.0 %

Efficiency (1/10 Sun)
With compact layer : 1.6%
Without compact layer : 0.6 %

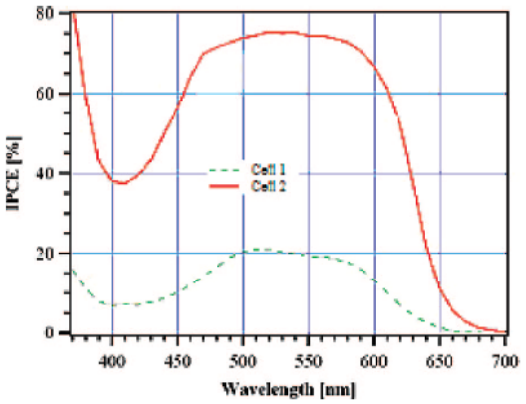

Figure 4. Example of an IPCE of two solar cells sensitized with a merocyanine dye (Mc2, see Supporting Information.). The cell incorporating a blocking layer is shown as cell 2 (red line).

Michael Grätzel *et al*. (Ecole Polytechnique)
Nano Lett. Vol. 8, No. 4, (2008)

FTO / TiO_2 Thin-Film Layer / TiO_2 Nanoparticles

The Function of a TiO_2 Compact Layer in Dye-Sensitized Solar Cells Incorporating "Planar" Organic Dyes

Anthony Burke,*,† Seigo Ito,† Henry Snaith,† Udo Bach,‡ Joe Kwiatkowski,§ and Michael Grätzel†

Laboratory for Photonics and Interfaces, Institute of Chemical Sciences and Engineering, Ecole Polytechnique Fédérale de Lausanne, Station 6, CH-1015 Lausanne, Switzerland, ARC Australian Centre for Electromaterials Science, Monash University, Victoria 3800, Australia, and Department of Physics, Imperial College London, London SW7 2BW, England

Received July 3, 2007; Revised Manuscript Received February 11, 2008

ABSTRACT

We present a device based study into the operation of liquid electrolyte dye-sensitized solar cells (DSSC's) using organic dyes. We find that, for these systems, it is entirely necessary to employ a compact TiO_2 layer between the transparent fluorine doped SnO_2 (FTO) anode and the electrolyte in order to reduce charge recombination losses. By incorporation of a compact layer, the device efficiency can be increased by over 160% under simulated full sun illumination and more than doubled at lower light intensities. This is strong evidence that the more widely employed ruthenium based sensitizers act as to "insulate" the anode against recombination losses and that many planar organic dyes employed in DSSC's could greatly benefit from the use of a compact TiO_2 blocking layer. This is in strong contrast to DSSC's sensitized with ruthenium based systems, where the introduction of compact TiO_2 has only marginal effects on conversion efficiencies.

Quantum-Dot Sensitized Solar Cell

• **Quantum-Dot Sensitized Solar Cell (QDSSC)**

→ Narrow-bandgap semiconductor quantum dots QDs (such as CdS, CdSe, PbS, and InAs) have been the subject of considerable interest as promising candidates for replacing the sensitizer dyes in DSSCs. These devices are called QD-sensitized solar cells (QDSSC).

• **Advantages**

1. The **bandgap of the QDs can be tuned** by controlling their size, and therefore, the absorption spectra of the QDs can be tuned to match the spectral distribution of sunlight.
2. Semiconductor QDs have large extinction coefficients due to the **quantum confinement effect**.
3. QDs have large intrinsic dipole moments, which may lead to **rapid charge separation**.

Quantum-Dot Sensitized Solar Cell

• Effect of Size and Morphology

Scheme 1. Random versus Directed Electron Transport through Support Architectures, (a) TiO_2 Particle and (b) TiO_2 Nanotube Films Modified with CdSe Quantum Dots

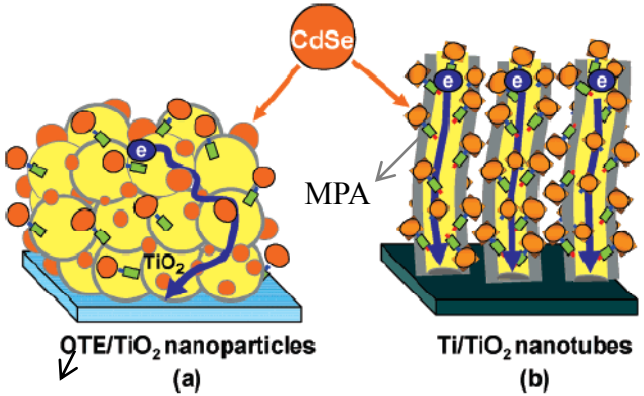

Optically transparent electrode

TiO_2 + HOOC-CH2-CH2-SH (MPA) + CdSe

Link TiO_2 and CdSe

• Morphology

Tube type is advantageous to the fast electronic conduction, due to shorter diffusion path compared with the particle type.

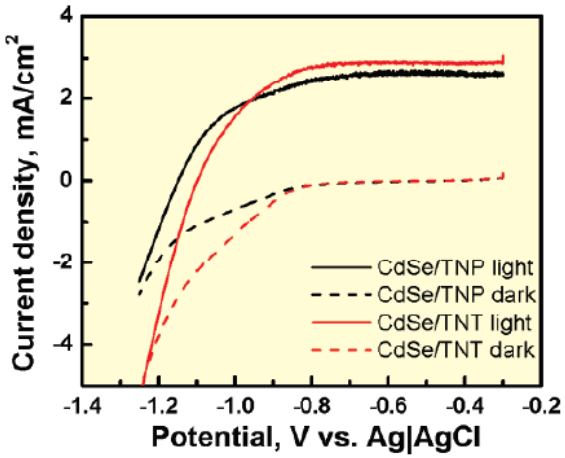

Figure 7. I–V characteristics of (A) OTE/TiO_2(NP)/CdSe and (B) (Ti/TiO_2(NT)/CdSe electrodes (excitation >420 nm; intensity 100 mW/cm^2; electrolyte, 0.1 M Na_2S solution.)

Power-conversion efficiency

OTE / TiO_2(Nanoparticles) / CdSe: 0.6%
Ti / TiO_2 (Nanotubes) / CdSe: 0.7%

Anusorn Kongkanand *et al.*
Notre Dame Radiation Laboratory
JACS **130**, 4007 (2008)

Quantum-Dot Sensitized Solar Cell

Scheme 2. Schematic Diagram Illustrating the Energy Levels of Different-Sized CdSe Quantum Dots and TiO_2[a]

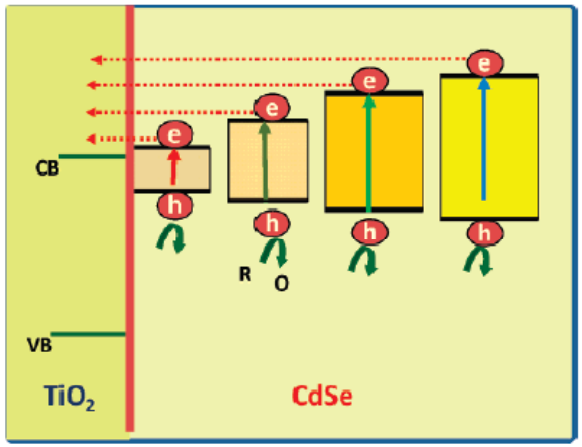

[a] The injection of electrons from CdSe quantum dots into TiO_2 is influenced by the energy difference between the two conduction bands. (Note that band positions are for reference only and not drawn to scale.)

- Size effect

  Size↓ → Band gap↑

Smaller-sized CdSe quantum dots show **greater charge injection rates** and also higher IPCE at the excitonic band.

Larger particles have **better absorption in the visible region**, but cannot inject electrons into TiO_2 as effectively as smaller-sized CdSe quantum dots.

→ Optimum size (3 nm)

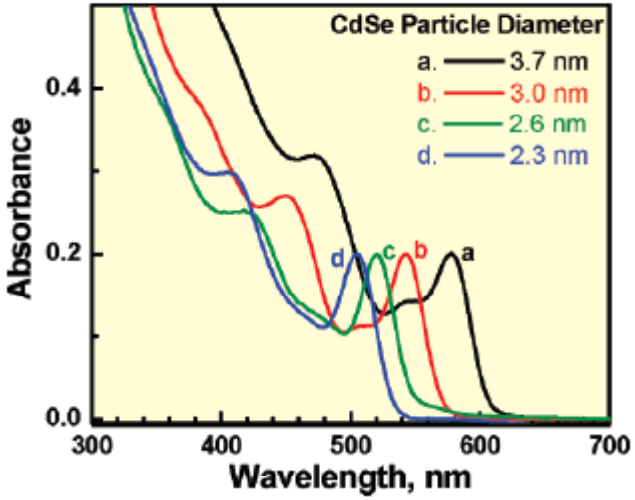

Figure 1. Absorption spectra of 3.7, 3.0, 2.6, and 2.3 nm diameter CdSe quantum dots in toluene.

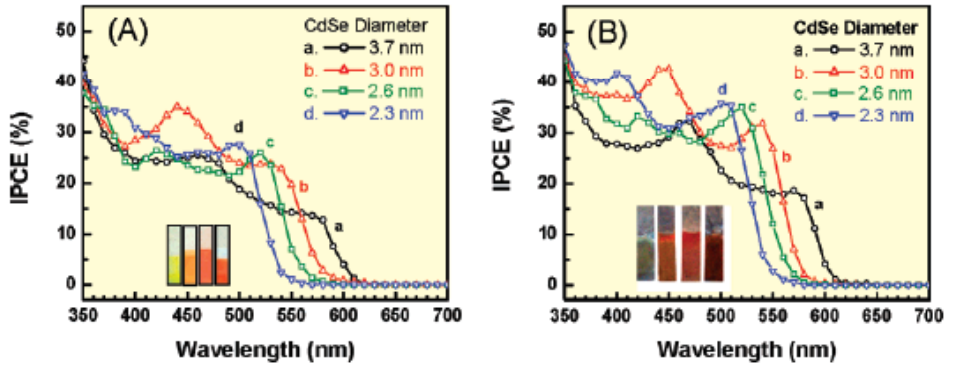

Figure 8. Photocurrent action spectra recorded in terms of incident photon to charge carrier generation efficiency (IPCE) of (A) OTE/TiO_2(NP)/CdSe and (B) (Ti/TiO_2(NT)/CdSe electrodes. The individual IPCE responses correspond to (a) 3.7, (b) 3.0, (c) 2.6, and (d) 2.3 nm diameter CdSe quantum dots anchored on nanostructured TiO_2 films.

A. Kongkanand *et al.* (*Notre Dame Radiation Laboratory*)
JACS **130**, 4007 (2008)

Quantum-Dot Sensitized Solar Cell

Quantum Dot Solar Cells. Tuning Photoresponse through Size and Shape Control of CdSe−TiO_2 Architecture

Anusorn Kongkanand,† Kevin Tvrdy,†,‡ Kensuke Takechi,† Masaru Kuno,†,‡ and Prashant V. Kamat*,†,‡,§

Notre Dame Radiation Laboratory, the Department of Chemistry and Biochemistry, and the Department of Chemical Engineering, University of Notre Dame, Notre Dame, Indiana 46556-0579

Received October 29, 2007; E-mail: pkamat@nd.edu

Abstract: Different-sized CdSe quantum dots have been assembled on TiO_2 films composed of particle and nanotube morphologies using a bifunctional linker molecule. Upon band-gap excitation, CdSe quantum dots inject electrons into TiO_2 nanoparticles and nanotubes, thus enabling the generation of photocurrent in a photoelectrochemical solar cell. The results presented in this study highlight two major findings: (i) ability to tune the photoelectrochemical response and photoconversion efficiency via size control of CdSe quantum dots and (ii) improvement in the photoconversion efficiency by facilitating the charge transport through TiO_2 nanotube architecture. The maximum IPCE (photon-to-charge carrier generation efficiency) obtained with 3 nm diameter CdSe nanoparticles was 35% for particulate TiO_2 and 45% for tubular TiO_2 morphology. The maximum IPCE observed at the excitonic band increases with decreasing particle size, whereas the shift in the conduction band to more negative potentials increases the driving force and favors fast electron injection. The maximum power-conversion efficiency ≤ 1% obtained with CdSe−TiO_2 nanotube film highlights the usefulness of tubular morphology in facilitating charge transport in nanostructure-based solar cells. Ways to further improve power-conversion efficiency and maximize light-harvesting capability through the construction of a rainbow solar cell are discussed.

Quantum-Dot Sensitized Solar Cell

ZnO nanowire에 CdSe QD을 adsorption 시킴

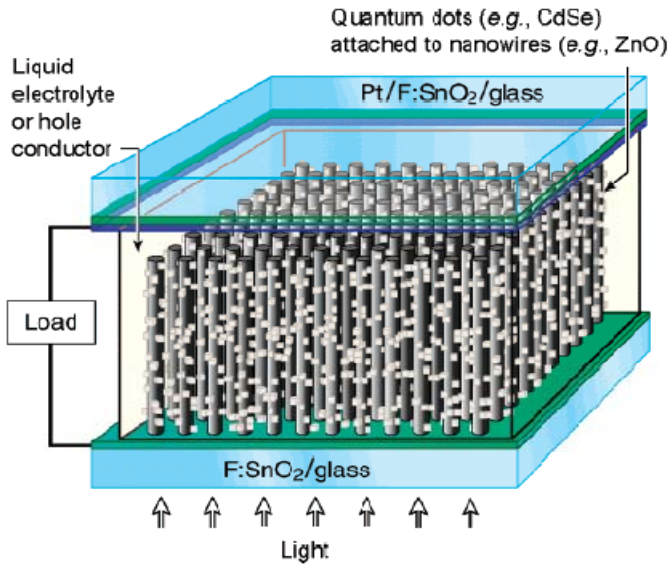

Figure 1. Schematic of the quantum-dot-sensitized solar cell. An array of ZnO nanowires, grown vertically from an F-doped SnO_2/glass substrate and decorated with CdSe quantum dots, serves as the photoanode. A second F-doped SnO_2/glass substrate, coated with a 100 Å layer of Pt, is the photocathode. The space between the two electrodes is filled with a liquid electrolyte, and the cell is illuminated from the bottom, as shown.

E. S. Aydil's group (University of Minnesota)
Nano Lett. **7**, 1793 (2007)

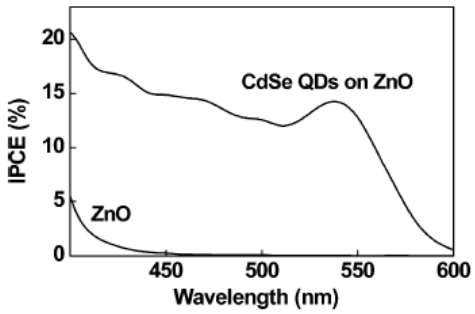

Figure 5. IPCE spectrum of the quantum-dot-sensitized and unsensitized ZnO nanowire solar cell featured in Figure 4a.

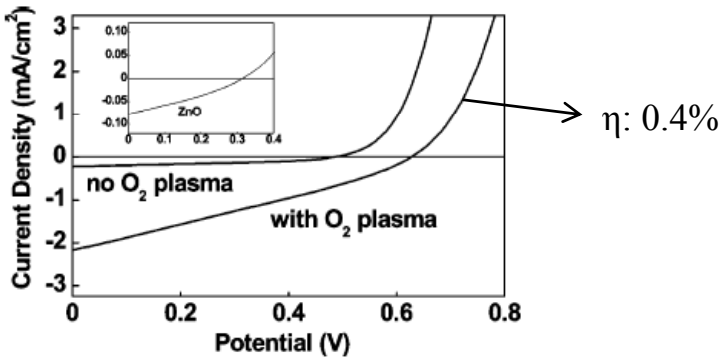

Figure 7. Current−voltage ($I-V$) characteristics of QDSSCs assembled using plasma-treated and untreated ZnO nanowires. The $I-V$ characteristics were recorded while illuminating the solar cells with 100 mW/cm^2 simulated AM1.5 spectrum. The inset shows the $I-V$ characteristics of an unsensitized ZnO nanowire solar cell. The units of the inset are the same as the large figure. The fill factor of the unsensitized nanowire solar cell is 0.27.

O_2 plasma를 통해 dangling band를 형성하여 CdSe를 ZnO에 더욱더 잘 adsorption 되도록 처리

Quantum-Dot Sensitized Solar Cell

Photosensitization of ZnO Nanowires with CdSe Quantum Dots for Photovoltaic Devices

Kurtis S. Leschkies,† Ramachandran Divakar,† Joysurya Basu,†
Emil Enache-Pommer,† Janice E. Boercker,† C. Barry Carter,†
Uwe R. Kortshagen,‡ David J. Norris,*,† and Eray S. Aydil*,†

Department of Chemical Engineering & Materials Science, University of Minnesota, 421 Washington Avenue SE, Minneapolis, Minnesota 55455, and Department of Mechanical Engineering, University of Minnesota, 111 Church Street SE, Minneapolis, Minnesota 55455

Received February 22, 2007

ABSTRACT

We combine CdSe semiconductor nanocrystals (or quantum dots) and single-crystal ZnO nanowires to demonstrate a new type of quantum-dot-sensitized solar cell. An array of ZnO nanowires was grown vertically from a fluorine-doped tin oxide conducting substrate. CdSe quantum dots, capped with mercaptopropionic acid, were attached to the surface of the nanowires. When illuminated with visible light, the excited CdSe quantum dots injected electrons across the quantum dot–nanowire interface. The morphology of the nanowires then provided the photoinjected electrons with a direct electrical pathway to the photoanode. With a liquid electrolyte as the hole transport medium, quantum-dot-sensitized nanowire solar cells exhibited short-circuit currents ranging from 1 to 2 mA/cm^2 and open-circuit voltages of 0.5–0.6 V when illuminated with 100 mW/cm^2 simulated AM1.5 spectrum. Internal quantum efficiencies as high as 50–60% were also obtained.

Organic Solar Cell

Organic Solar Cells

The main constituents of an organic solar cell are the electron donor, acceptor, anode, and cathode.

Four steps are involved in the photocurrent generation process:

1) Light absorption.
2) Exciton diffusion.
3) Exciton dissociation into free charge carriers.
4) Charges collection.

Exciton energy in polymers is ~0.5 eV, thus it is difficult to be dissociated.
Furthermore, the exciton diffusion happens at small scales (L_d ~ 10 nm).
Therefore, it is important **to increase the interface area** between the donor and the acceptor materials.

→ Effective Solution: Bulk Heterojunction (BJH)

Two-Layer Organic Photovoltaic Cell

C. W. Tang
APL (1986)

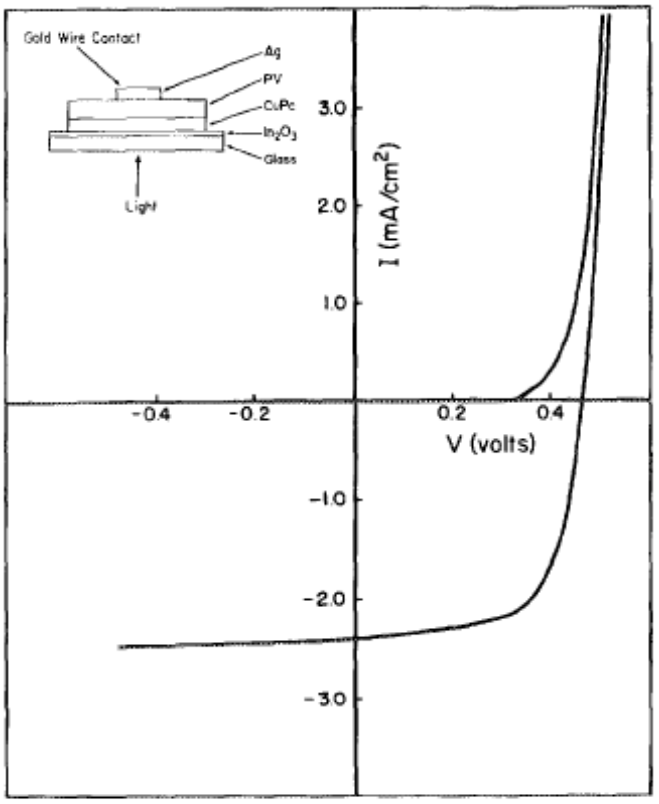

FIG. 1. Configuration and current-voltage characteristics of an ITO/CuPc (250 Å)/PV(450 Å)/Ag cell.

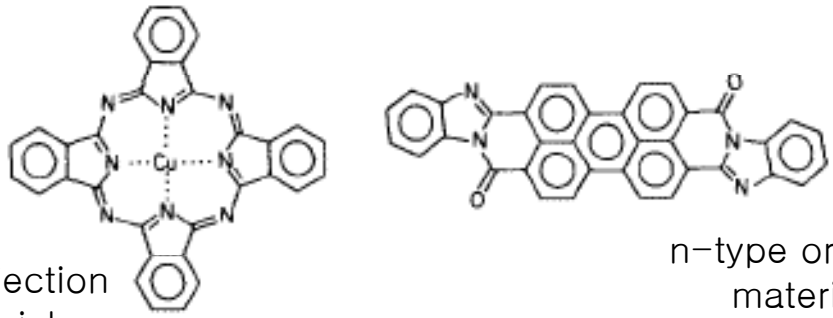

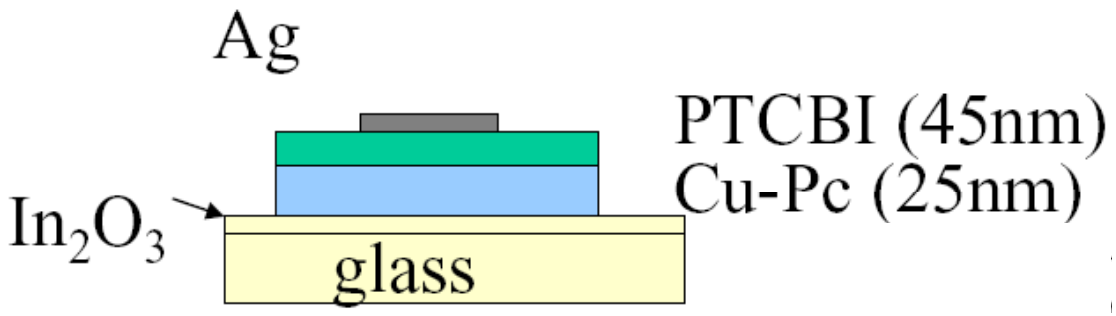

Low efficiency (~1%)
→ due to **the short exciton diffusion length (~5 nm) in organic materials**

Two-Layer Organic Photovoltaic Cell

C. W. Tang
APL (1986)

Two-layer organic photovoltaic cell

C. W. Tang
Research Laboratories, Eastman Kodak Company, Rochester, New York 14650

(Received 28 August 1985; accepted for publication 31 October 1985)

A thin-film, two-layer organic photovoltaic cell has been fabricated from copper phthalocyanine and a perylene tetracarboxylic derivative. A power conversion efficiency of about 1% has been achieved under simulated AM2 illumination. A novel feature of the device is that the charge-generation efficiency is relatively independent of the bias voltage, resulting in cells with fill factor values as high as 0.65. The interface between the two organic materials, rather than the electrode/organic contacts, is crucial in determining the photovoltaic properties of the cell.

Electron Transfer in Organic Cells

Donor and acceptor are macroscopically indistinguishable in BHJ.

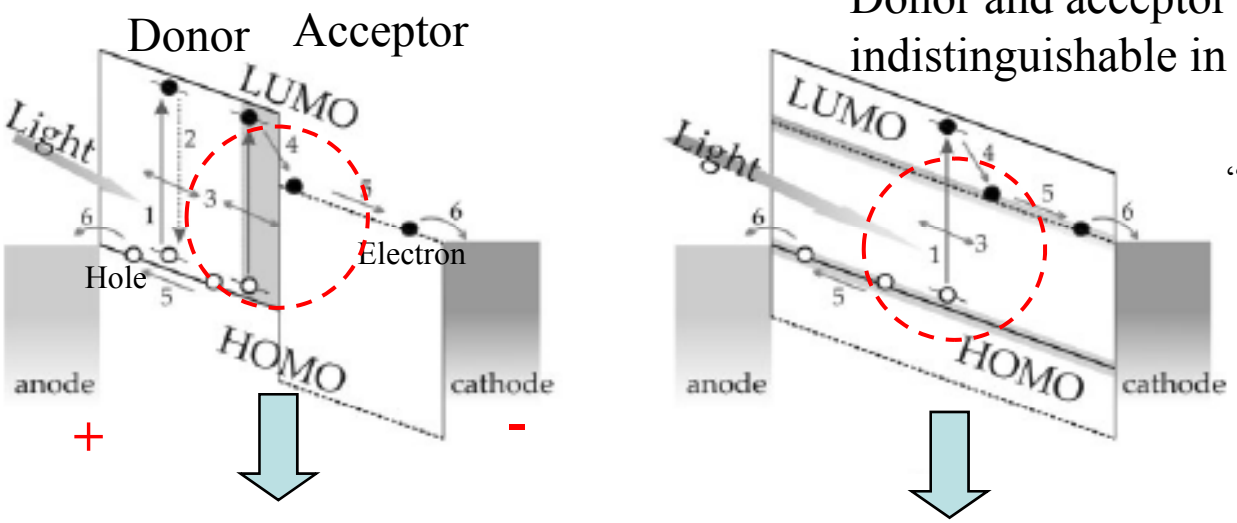

"Device Physics of Polymer: Fullerene Bulk Heterojunction Solar Cells"
P. W. M. Blom's Group,
Univ. of Groningen
Adv. Mater. (2007)

Figure 1. Schematic band diagram of a) a bilayer device and b) a bulk heterojunction. The numbers refer to the operation processes explained in the text. The dashed line represents the energy levels of the acceptor, while the full lines indicate the energy level of the donor in the PV cell. HOMO: highest occupied molecular orbital; LUMO: lowest unoccupied molecular orbital.

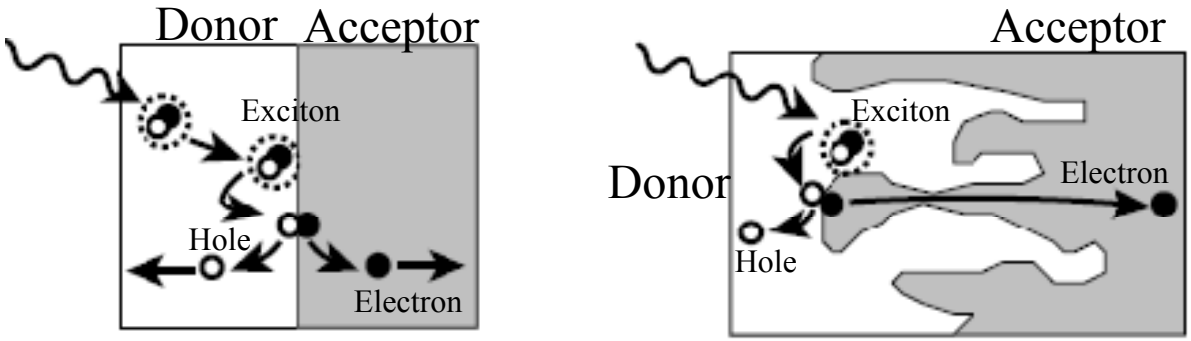

"Efficient Bulk Heterojunction Photovoltaic Cells Using Small Molecular-Weight Organic Thin Films"
S. R. Forrest's Group
Princeton Univ.
Nature (2003)

Figure 1 Diagrams of types of organic donor–acceptor photovoltaic cells and SEM images of the surface of a ~5,000-Å-thick CuPc:PTCBI film on ITO. **a**–**c**, Diagrams. **a**, Bilayer cell. **b**, Bulk heterojunction cell. **c**, Mixed-layer cell. In these diagrams, the incident light

Device Physics of Polymer:Fullerene Bulk Heterojunction Solar Cells**

By *Paul W. M. Blom,* Valentin D. Mihailetchi, L. Jan Anton Koster,* and *Denis E. Markov*

Plastic solar cells bear the potential for large-scale power generation based on materials that provide the possibility of flexible, lightweight, inexpensive, efficient solar cells. Since the discovery of the photoinduced electron transfer from a conjugated polymer to fullerene molecules, followed by the introduction of the bulk heterojunction (BHJ) concept, this material combination has been extensively studied in organic solar cells, leading to several breakthroughs in efficiency, with a power conversion efficiency approaching 5 %. This article reviews the processes and limitations that govern device operation of polymer:fullerene BHJ solar cells, with respect to the charge-carrier transport and photogeneration mechanism. The transport of electrons/holes in the blend is a crucial parameter and must be controlled (e.g., by controlling the nanoscale morphology) and enhanced in order to allow fabrication of thicker films to maximize the absorption, without significant recombination losses. Concomitantly, a balanced transport of electrons and holes in the blend is needed to suppress the build-up of the space–charge that will significantly reduce the power conversion efficiency. Dissociation of electron–hole pairs at the donor/acceptor interface is an important process that limits the charge generation efficiency under normal operation condition. Based on these findings, there is a compromise between charge generation (light absorption) and open-circuit voltage (V_{OC}) when attempting to reduce the bandgap of the polymer (or fullerene). Therefore, an increase in V_{OC} of polymer:fullerene cells, for example by raising the lowest unoccupied molecular orbital level of the fullerene, will benefit cell performance as both fill factor and short-circuit current increase simultaneously.

Efficient bulk heterojunction photovoltaic cells using small-molecular-weight organic thin films

Peter Peumans, Soichi Uchida & Stephen R. Forrest

Center for Photonics and Optoelectronic Materials (POEM), Department of Electrical Engineering and the Princeton Materials Institute, Princeton University, Princeton, New Jersey 08544, USA

The power conversion efficiency of small-molecular-weight and polymer organic photovoltaic cells has increased steadily over the past decade. This progress is chiefly attributable to the introduction of the donor–acceptor heterojunction[1,2] that functions as a dissociation site for the strongly bound photogenerated excitons. Further progress was realized in polymer devices through use of blends of the donor and acceptor materials[3–5]: phase separation during spin-coating leads to a bulk heterojunction that removes the exciton diffusion bottleneck by creating an interpenetrating network of the donor and acceptor materials. The realization of bulk heterojunctions using mixtures of vacuum-deposited small-molecular-weight materials has, on the other hand, posed elusive: phase separation induced by elevating the substrate temperature inevitably leads to a significant roughening of the film surface and to short-circuited devices. Here, we demonstrate that the use of a metal cap to confine the organic materials during annealing prevents the formation of a rough surface morphology while allowing for the formation of an interpenetrating donor–acceptor network. This method results in a power conversion efficiency 50 per cent higher than the best values reported for comparable bilayer devices, suggesting that this strained annealing process could allow for the formation of low-cost and high-efficiency thin film organic solar cells based on vacuum-deposited small-molecular-weight organic materials.

Bulk Heterojunction

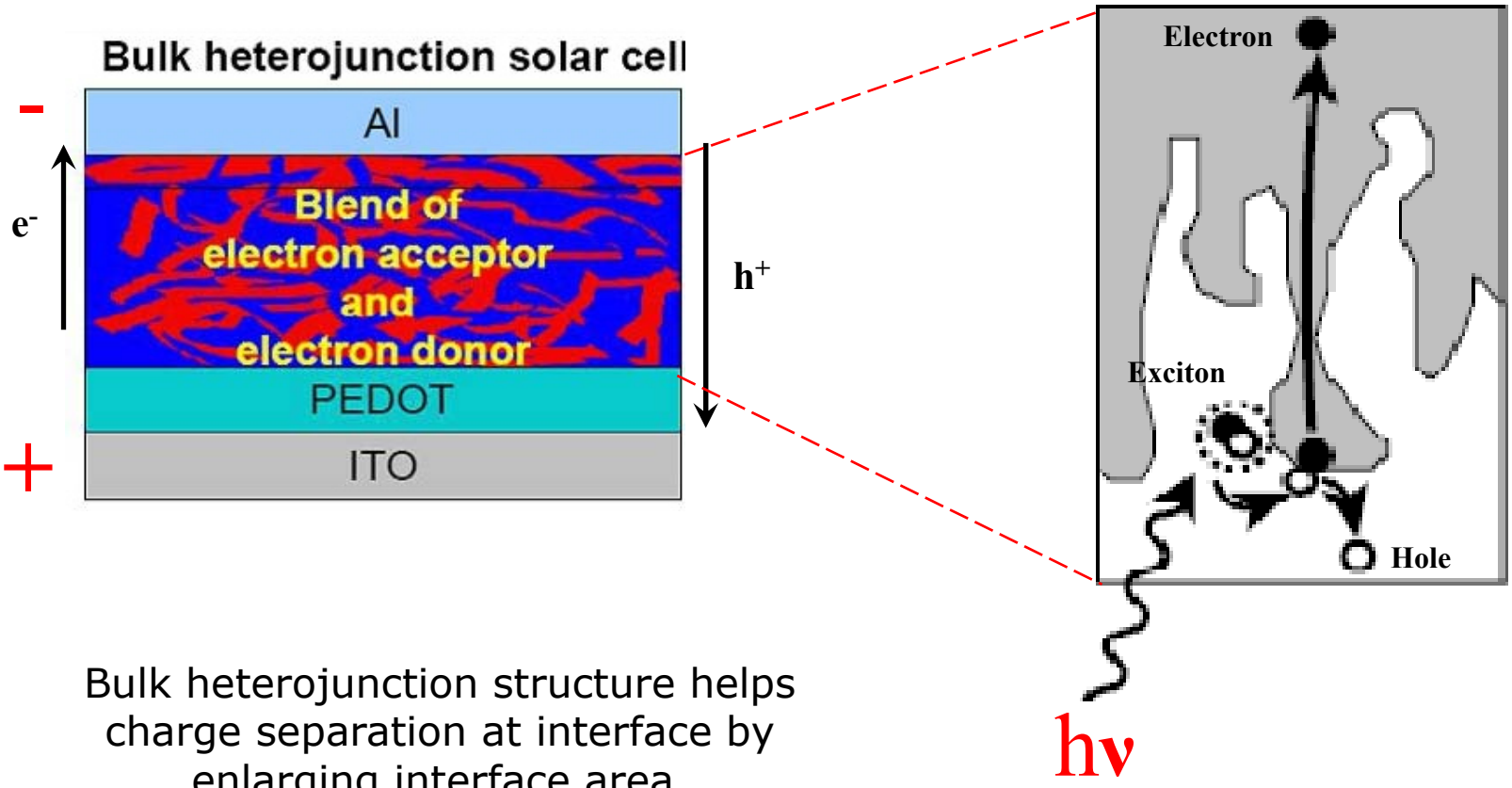

Bulk heterojunction structure helps charge separation at interface by enlarging interface area.

Structure of Organic Cells

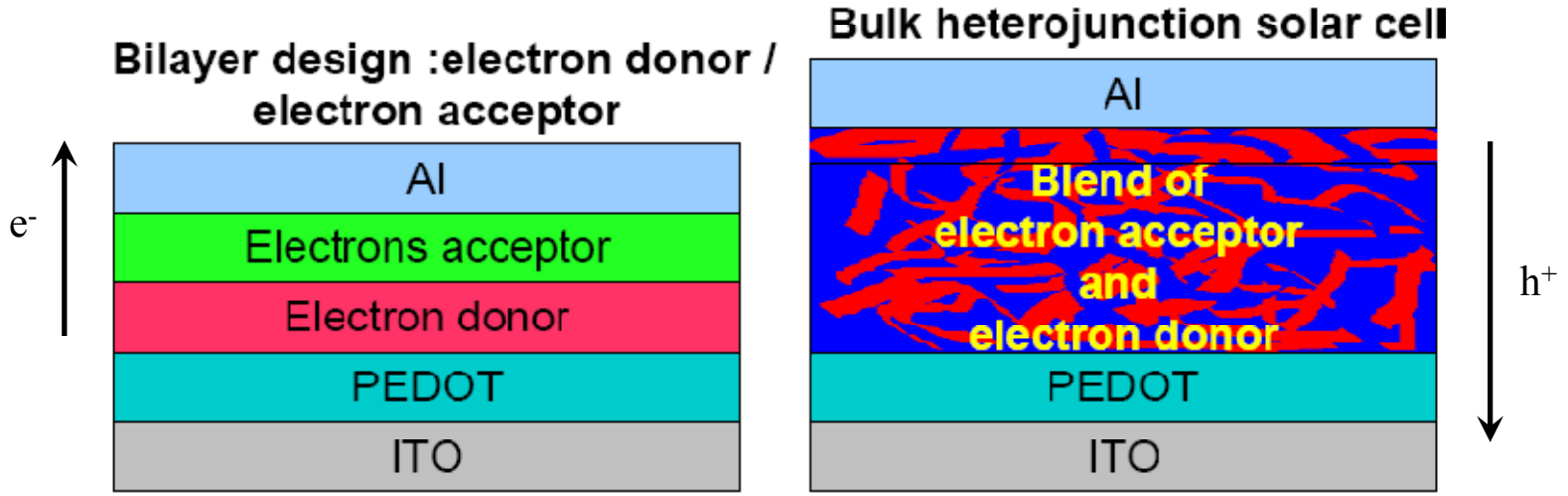

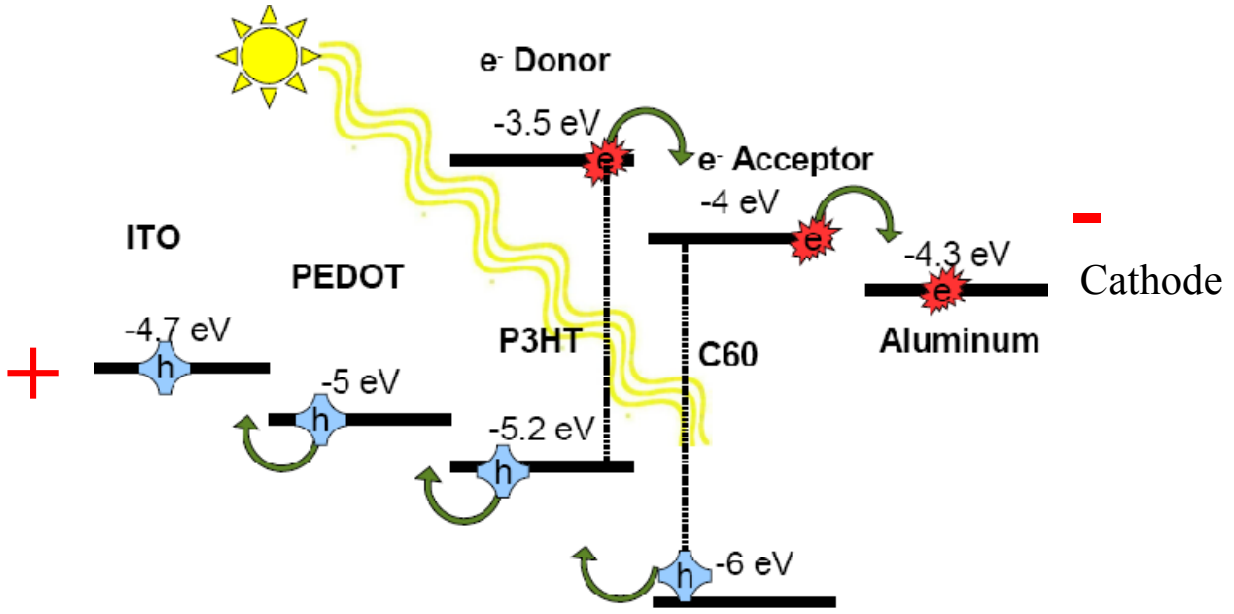

Tandem Structure

K. Lee *et al.*

Science (2007)

·V_{oc} improvement: sum of the V_{oc}'s of the individual cells

active layer

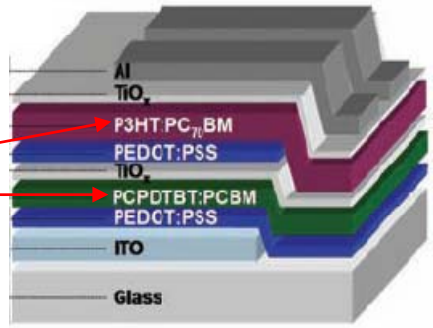

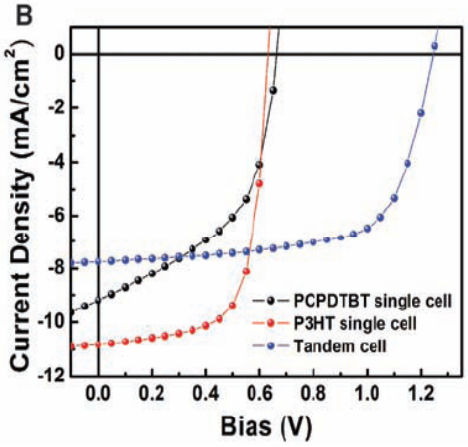

·Absorption over a broad range of solar spectrum

→ two semiconductor layers with different band gaps

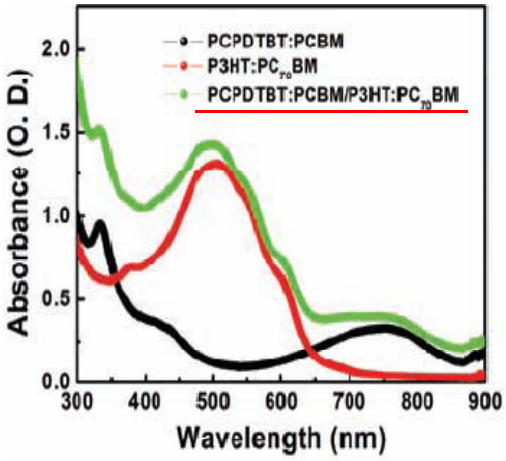

Tandem Polymer Solar Cell

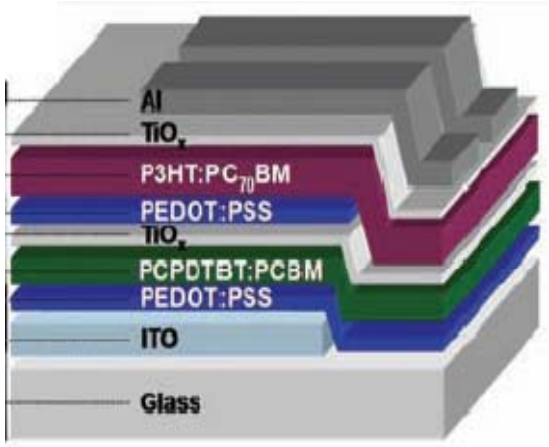

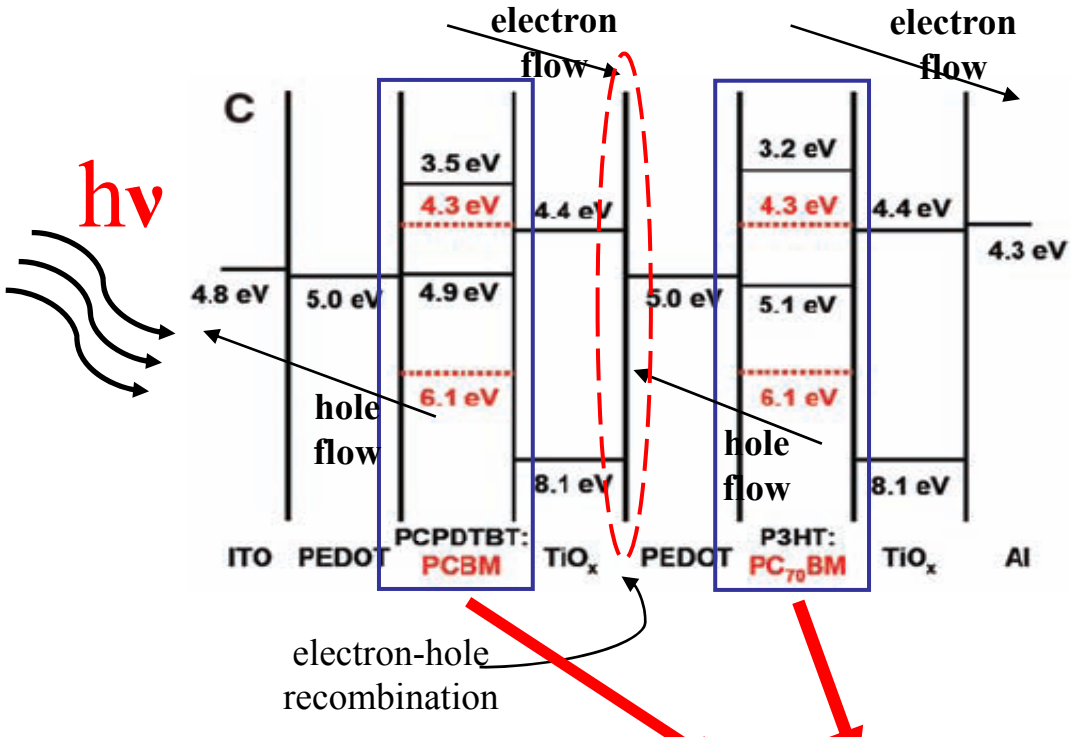

K. Lee *et al.*
Science (2007)

Tandem solar cells, in which two solar cells with different absorption characteristics are linked to use a wider range of the solar spectrum, were fabricated with each layer processed from solution with the use of bulk heterojunction materials comprising semiconducting polymers and fullerene derivatives. A transparent titanium oxide (TiO_x) layer separates and connects the front cell and the back cell. The TiO_x layer serves as an electron transport and collecting layer for the first cell and as a stable foundation that enables the fabrication of the second cell to complete the tandem cell architecture. We use an inverted structure with the low band-gap polymer-fullerene composite as the charge-separating layer in the front cell and the high band-gap polymer composite as that in the back cell. Power-conversion efficiencies of more than 6% were achieved at illuminations of 200 milliwatts per square centimeter.

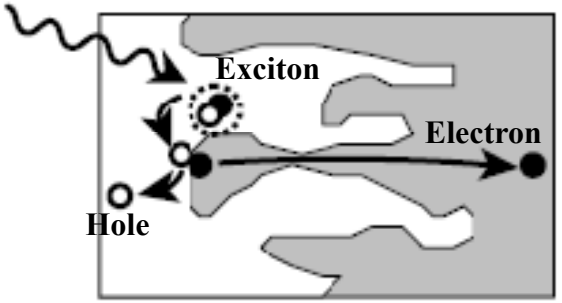

Tandem Polymer Solar Cell

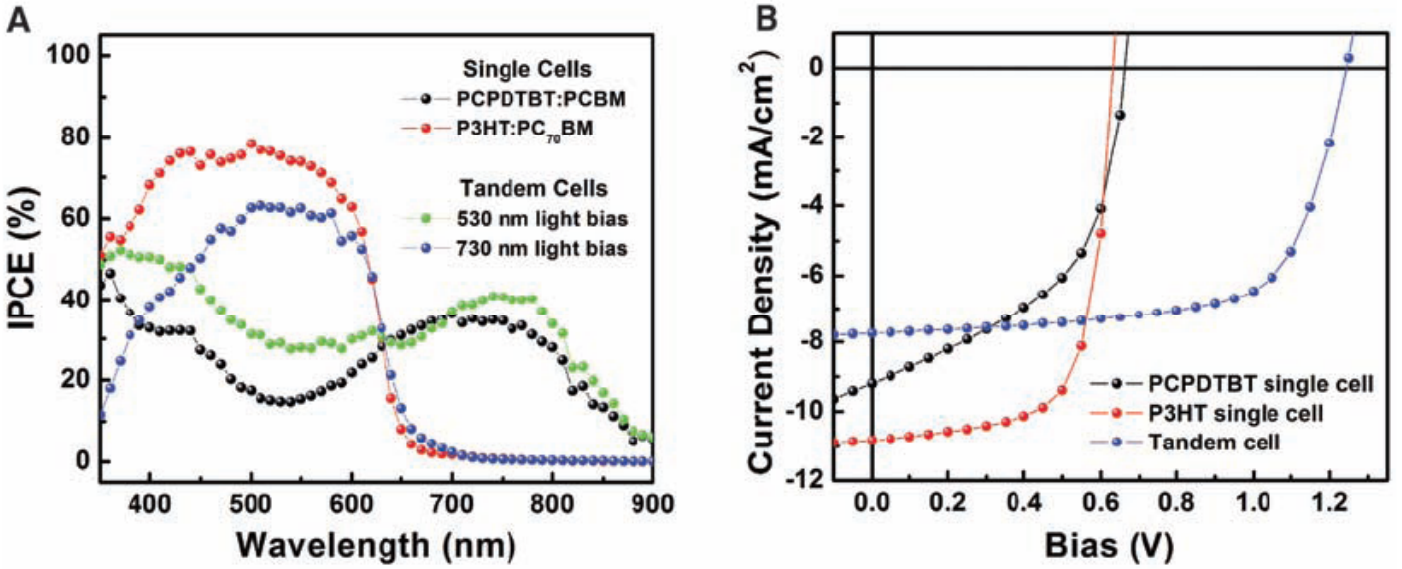

Fig. 3. (**A**) IPCE spectra of single cells and a tandem cell with bias light. We carried out the IPCE measurements using modulation spectroscopy with a lock-in amplifier for the single cells and for the tandem cell without light bias. For the tandem cell measurements made with bias light, unmodulated monochromatic light with an intensity of ~2 mW/cm^2 was used. (**B**) *J-V* characteristics of single cells and tandem cell with PCPDTBT:PCBM and P3HT:$PC_{70}BM$ composites under AM1.5G illumination from a calibrated solar simulator with irradiation intensity of 100 mW/cm^2 (about one sun) are presented. The power-conversion efficiency of a solar cell is given as $\eta_e = (J_{sc} \cdot V_{oc} \cdot FF) \cdot 100/P_{inc}$, where P_{inc} is the intensity of incident light. The device performance is summarized as follows: The PCPDTBT:PCBM single cell shows J_{sc} = 9.2 mA/cm^2, V_{oc} = 0.66 V, FF = 0.50, and η_e = 3.0%; the P3HT:$PC_{70}BM$ single cell shows J_{sc} = 10.8 mA/cm^2, V_{oc} = 0.63 V, FF = 0.69, and η_e = 4.7%; and the tandem cell shows J_{sc} = 7.8 mA/cm^2, V_{oc} = 1.24 V, FF = 0.67, and η_e = 6.5%.

K. Lee *et al.*
Science (2007)

V_{oc} = 1.24 V

J_{sc} = 7.8 mA/cm^2

FF = 67%

Efficiency = 6.5%

Double *p-i-n* Architecture

J. Drechsel's group

Appl. Phys. Lett. (2005)

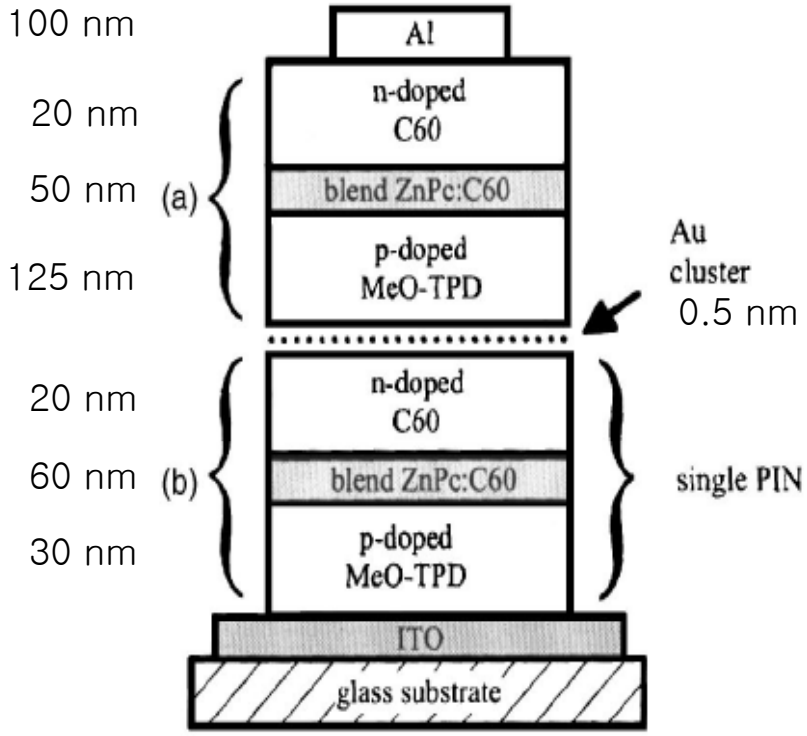

FIG. 1. Basic concept of a *p-i-n*-type organic solar cell with an active layer sandwiched between *p*- and *n*-type wide-gap transport layers: (a) The general layer sequence

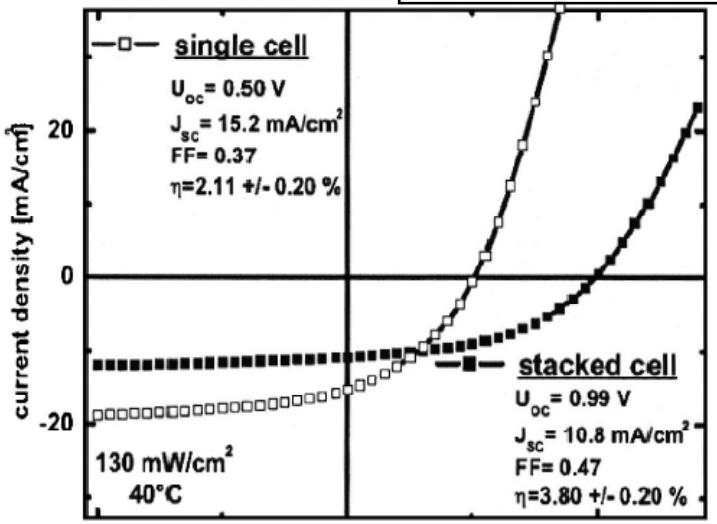

FIG. 2. *I-V* characteristics of single and tandem *p-i-n* solar cells under 130 mW/cm^2 simulated AM 1.5 solar illumination. The tandem cell has an optimized device structure according to the simulation shown in Fig. 1, and the single cell is identical to the bottom cell in the tandem configuration (Cell A) prepared simultaneously. The performance parameters are given.

electron transport layer: C_{60} doped with rhodamine B

hole transport layer: MeO-TPD doped with tetrafluorotetracyano-quinodimethane

The use of doped wide-gap charge transport layers with high conductivity and low absorption in the visible range enables one to achieve high internal quantum efficiencies and to optimize the devices with respect to optical interference effects. Here, it is shown that this architecture is particularly useful for stacking several cells on top of each other. The doping eases the recombination of the majority carriers at the interface between the cells, whereas the recombination centers are hidden for excitons and minority carriers. By stacking two *p-i-n* cells both with a phthalocyanine-fullerene blend as photoactive layer, a power efficiency of up to 3.8% at simulated AM1.5 illumination as compared to 2.1% for the respective single *p-i-n* cell has been achieved. Numerical simulations of the optical field distribution based on the transfer-matrix formalism are applied for optimization. The concept paves the way to even higher efficiencies by stacking several *p-i-n* cells with different photoactive materials that together cover the full visible spectrum. [DOI: 10.1063/1.1935771]

Summary and Representative Work

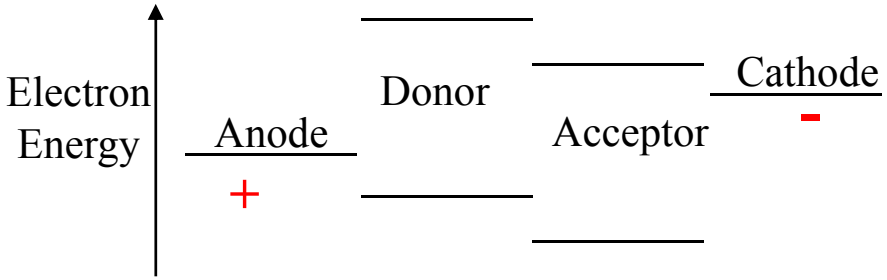

Fabrication process is simple.
Not all the excitons cannot reach the interface.
There are many dead ends.

Donor	Acceptor		Conversion Efficiency (AM 1.5)
Polymer	C_{60} Derivative	Heeger's group	4.9%
Polymer	CdSe Nanorods	Alivisatos' group	1.7%
Polymer	ZnO Nanoparticles	Janssen's group	1.6%

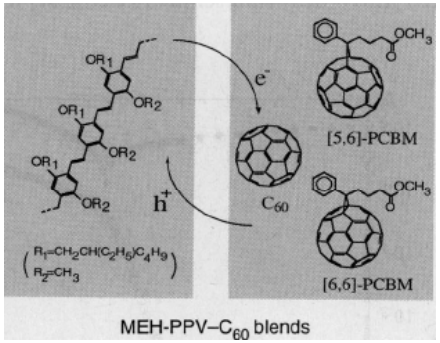

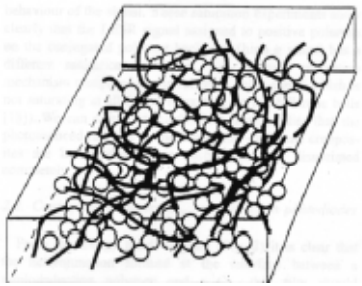

"Polymer Photovoltaic Cells … Heterojunctions"
A. J. Heeger's Group, *Science* (1995)

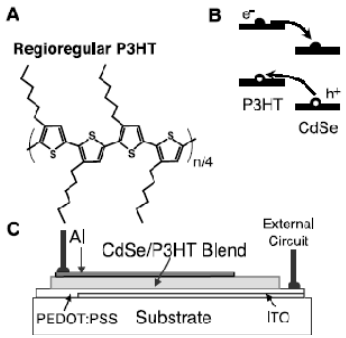

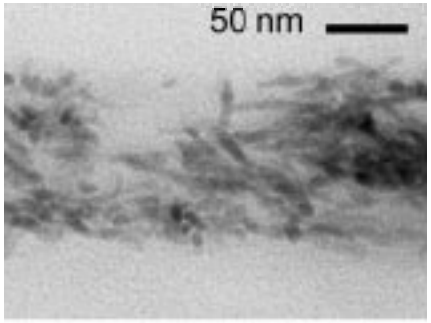

"Hybrid Nanorod-Polymer Solar Cells"
A. P. Alivisatos' Group, *Science* (2002)

Polymer Photovoltaic Cells: Enhanced Efficiencies via a Network of Internal Donor-Acceptor Heterojunctions

G. Yu,* J. Gao, J. C. Hummelen, F. Wudl, A. J. Heeger

The carrier collection efficiency (η_c) and energy conversion efficiency (η_e) of polymer photovoltaic cells were improved by blending of the semiconducting polymer with C_{60} or its functionalized derivatives. Composite films of poly(2-methoxy-5-(2′-ethyl-hexyloxy)-1,4-phenylene vinylene) (MEH-PPV) and fullerenes exhibit η_c of about 29 percent of electrons per photon and η_e of about 2.9 percent, efficiencies that are better by more than two orders of magnitude than those that have been achieved with devices made with pure MEH-PPV. The efficient charge separation results from photoinduced electron transfer from the MEH-PPV (as donor) to C_{60} (as acceptor); the high collection efficiency results from a bicontinuous network of internal donor-acceptor heterojunctions.

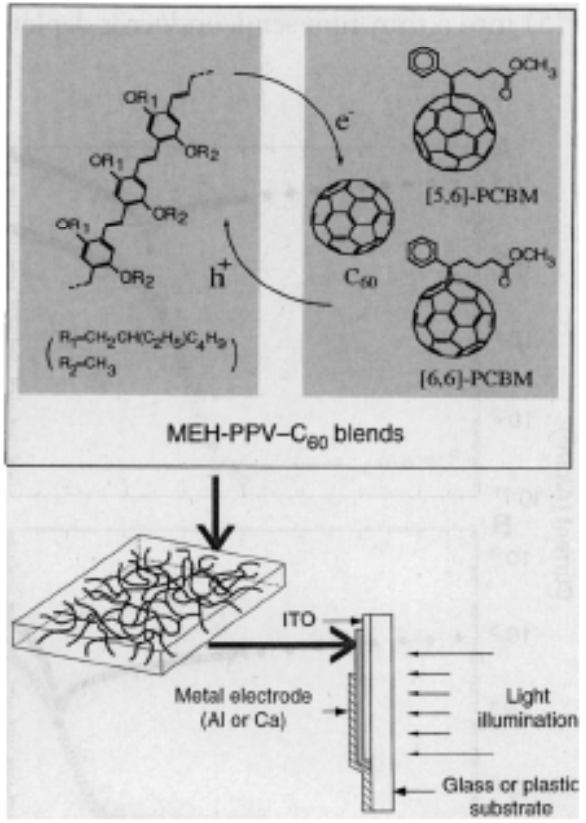

Fig. 1. Schematic diagram of the photoinduced charge transfer process in MEH-PPV:C_{60} D-A blends. The structures of the two soluble C_{60} derivatives used in this study (denoted as [6,6]PCBM and [5,6]PCBM) are included. When cast as a film, the D and A species phase-separate into a bicontinuous network (bulk heterojunction material), as shown schematically. The structure of the photovoltaic cell fabricated with this bulk heterojunction material is sketched at the bottom.

"Polymer Photovoltaic Cells … Heterojunctions"

A. J. Heeger's Group, *Science* (1995)

Hybrid Nanorod-Polymer Solar Cells

Wendy U. Huynh, Janke J. Dittmer, A. Paul Alivisatos*

We demonstrate that semiconductor nanorods can be used to fabricate readily processed and efficient hybrid solar cells together with polymers. By controlling nanorod length, we can change the distance on which electrons are transported directly through the thin film device. Tuning the band gap by altering the nanorod radius enabled us to optimize the overlap between the absorption spectrum of the cell and the solar emission spectrum. A photovoltaic device consisting of 7-nanometer by 60-nanometer CdSe nanorods and the conjugated polymer poly-3(hexylthiophene) was assembled from solution with an external quantum efficiency of over 54% and a monochromatic power conversion efficiency of 6.9% under 0.1 milliwatt per square centimeter illumination at 515 nanometers. Under Air Mass (A.M.) 1.5 Global solar conditions, we obtained a power conversion efficiency of 1.7%.

"Hybrid Nanorod-Polymer Solar Cells"

A. P. Alivisatos' Group, *Science* (2002)

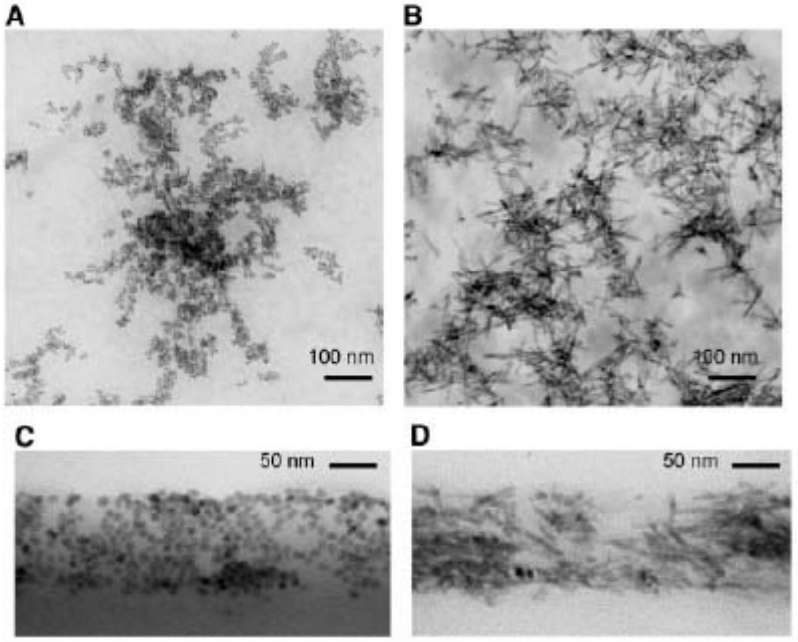

Fig. 3. Thin films of 20 wt % (**A**) 7 nm by 7 nm and (**B**) 7 nm by 60 nm CdSe nanocrystals in P3HT were studied via transmission electron microscopy. In (**C**), a TEM of a cross section of a film with 60 wt % 10 nm by 10 nm CdSe nanocrystals in P3HT reveals the distribution and organization of nanoparticles across the 110-nm-thick film. A solution of CdSe in P3HT was spin-cast onto a Polybed epoxy substrate (Ted Pella, Redding, CA) and we used an ultramicrotome to obtain ultrathin cross sections. In (**D**), a TEM of a cross section of a 100-nm-thick film consisting of 40 wt % 7 nm by 60 nm CdSe nanorods in P3HT reveals that most nanorods are partially aligned perpendicular to the substrate plane. The solutions were cast onto an Epon/Aradite epoxy substrate (Ted Pella), embedded into epoxy, cured, and sliced using an ultramicrotome. This extra support is required to slice the nanorods with the microtome, because the blend film has a tendency to tear as the rods get longer.

The Others

Triple-Junction Solar Cell

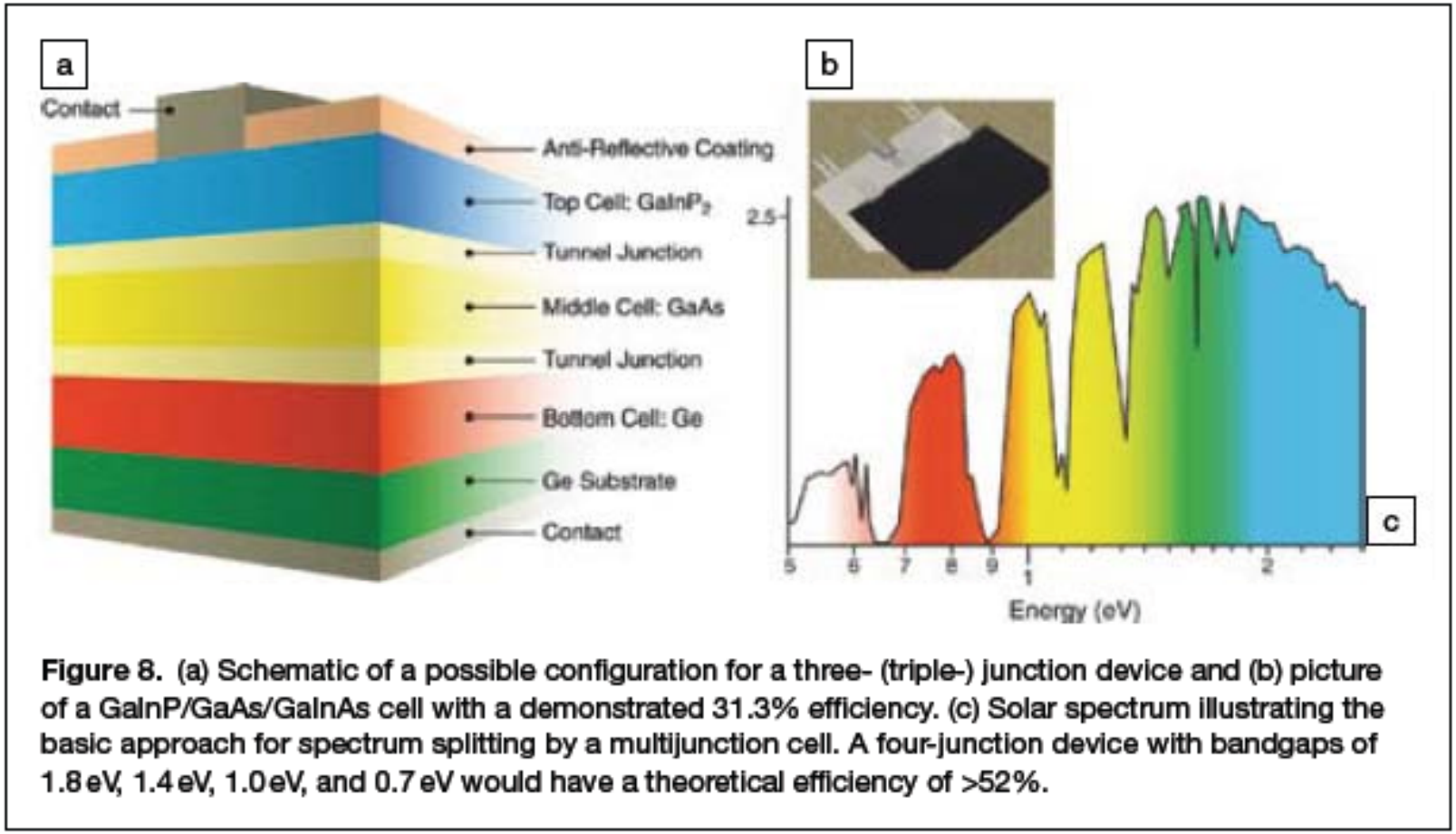

Figure 8. (a) Schematic of a possible configuration for a three- (triple-) junction device and (b) picture of a GaInP/GaAs/GaInAs cell with a demonstrated 31.3% efficiency. (c) Solar spectrum illustrating the basic approach for spectrum splitting by a multijunction cell. A four-junction device with bandgaps of 1.8 eV, 1.4 eV, 1.0 eV, and 0.7 eV would have a theoretical efficiency of >52%.

David Ginley (NREL), Matin A. Green (University of New South Wales), and Reuben Collins (Colorado School of Mines) *MRS Bulletin* (2008).

Tandem Structure

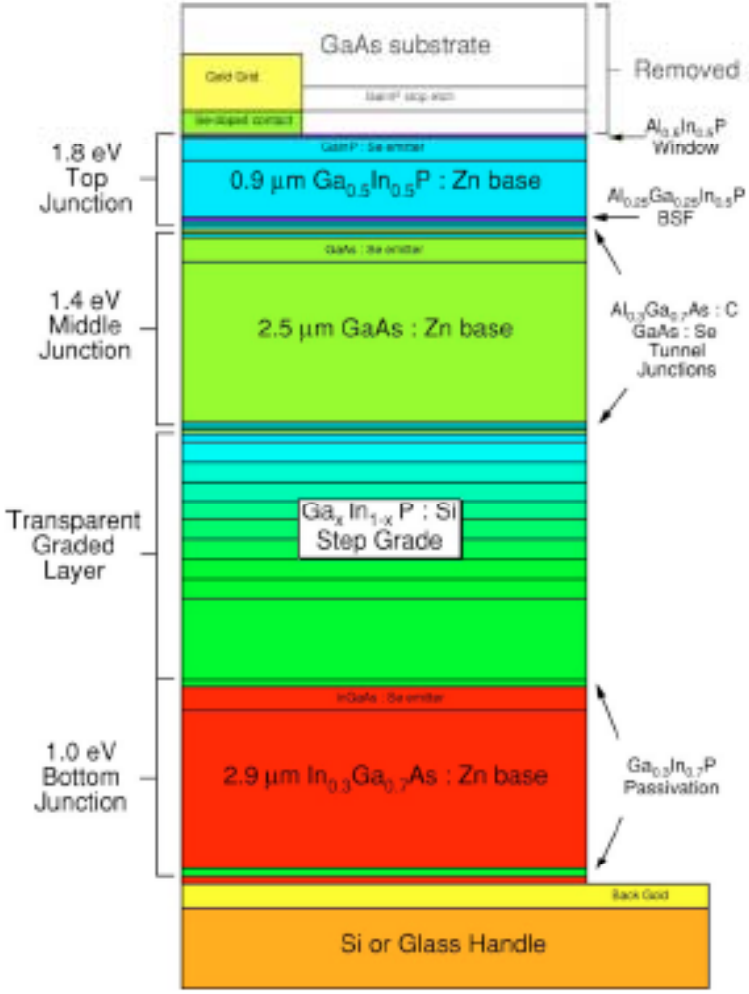

FIG. 1. Schematic of inverted triple-junction structure. The band gap of the semiconductor layers is indicated by a rainbow color scale (violet=high and red=low). The GaInP junction base thickness was 0.45 μm for the AM0 device.

TABLE I. Summary of *IV* measurements.

Solar spectrum	Irradiance (W/m^2 or suns)	Area (cm^2)	V_{oc} (V)	J_{sc} (mA/cm^2)	FF (%)	Efficiency (%)
AM1.5G (global)	1000 (1X)	0.25	2.96	13.1	86.9	33.8±1.0
AM0 (space)	1366 (1X)	0.25	3.00	16.4	85.0	30.6±0.9
AM1.5D (direct)	1000 (1X)	0.10	2.98	13.1	83.7	32.6±1.0
AM1.5D (direct)	80 757 (81X)	0.10	3.38	1059	87.7	38.9±2.3

The authors demonstrate a thin, Ge-free III–V semiconductor triple-junction solar cell device structure that achieved 33.8%, 30.6%, and 38.9% efficiencies under the standard 1 sun global spectrum, space spectrum, and concentrated direct spectrum at 81 suns, respectively. The device consists of 1.8 eV $Ga_{0.5}In_{0.5}P$, 1.4 eV GaAs, and 1.0 eV $In_{0.3}Ga_{0.7}As$ *p-n* junctions grown monolithically in an inverted configuration on GaAs substrates by organometallic vapor phase epitaxy. The lattice-mismatched $In_{0.3}Ga_{0.7}As$ junction was grown last on a graded $Ga_xIn_{1-x}P$ buffer. The substrate was removed after the structure was mounted to a structural "handle." The current-matched, series-connected junctions produced a total open-circuit voltage over 2.95 V at 1 sun. [DOI: 10.1063/1.2753729]

J. F. Geisz's group

Appl. Phys. Lett.

(2007)

Multiple-Junction Polymer Solar Cell

J. Janssen's group,
Appl. Phys. Lett.
(2007)

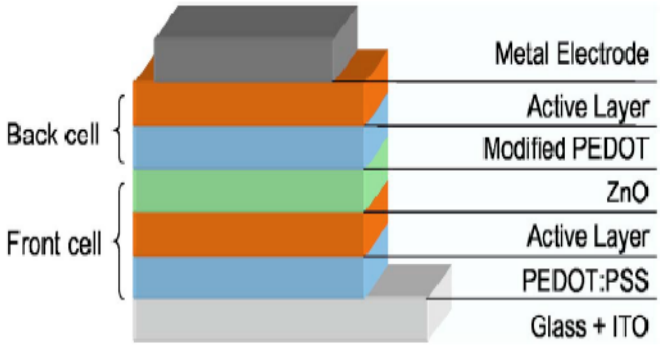

FIG. 1. (Color online) Device setup for a solution processed tandem solar cell.

Cell fabrication by solution process
+ spin coating

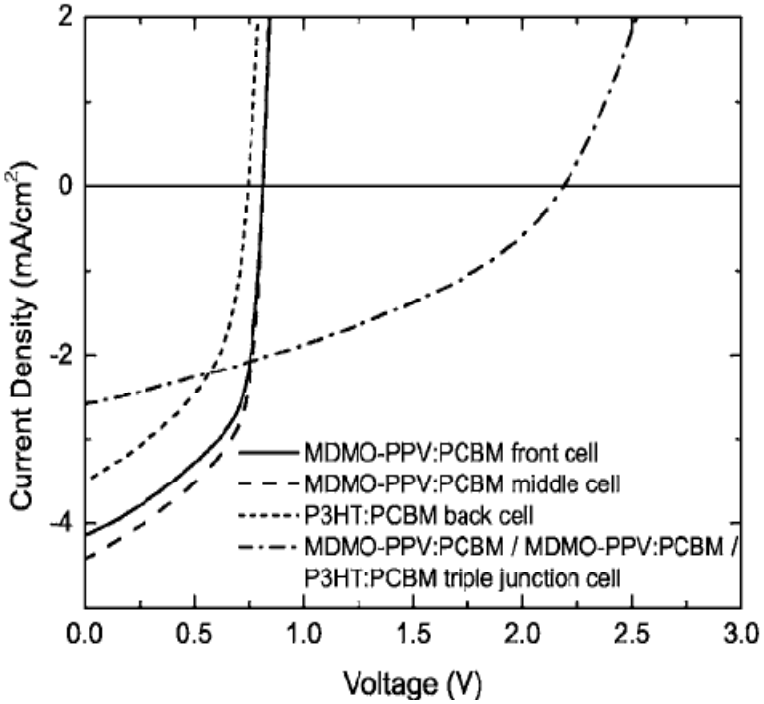

FIG. 4. Current density–voltage characteristics of the front, middle, and back cells and of the resulting triple junction cell after UV illumination.

Multiple junction solar cells incorporating polymer:fullerene bulk heterojunctions as active layers and solution processed electron and hole transport layers are presented. The recombination layer, deposited between the active layers, is fabricated by spin coating ZnO nanoparticles from acetone, followed by spin coating neutral *p*H poly(3,4-ethylenedioxythiophene) from water and short UV illumination of the completed device. The key advantage of this procedure is that each step does not affect the integrity of previously deposited layers. The open-circuit voltage (V_{oc}) for double and triple junction solar cells is close to the sum of the V_{oc}'s of individual cells. © *2007 American Institute of Physics*. [DOI: 10.1063/1.2719668]

V_{oc}: 2.19 V
→ correspond closely to the sum of single cell V_{oc}'s.

Third-Generation Solar Cell Options

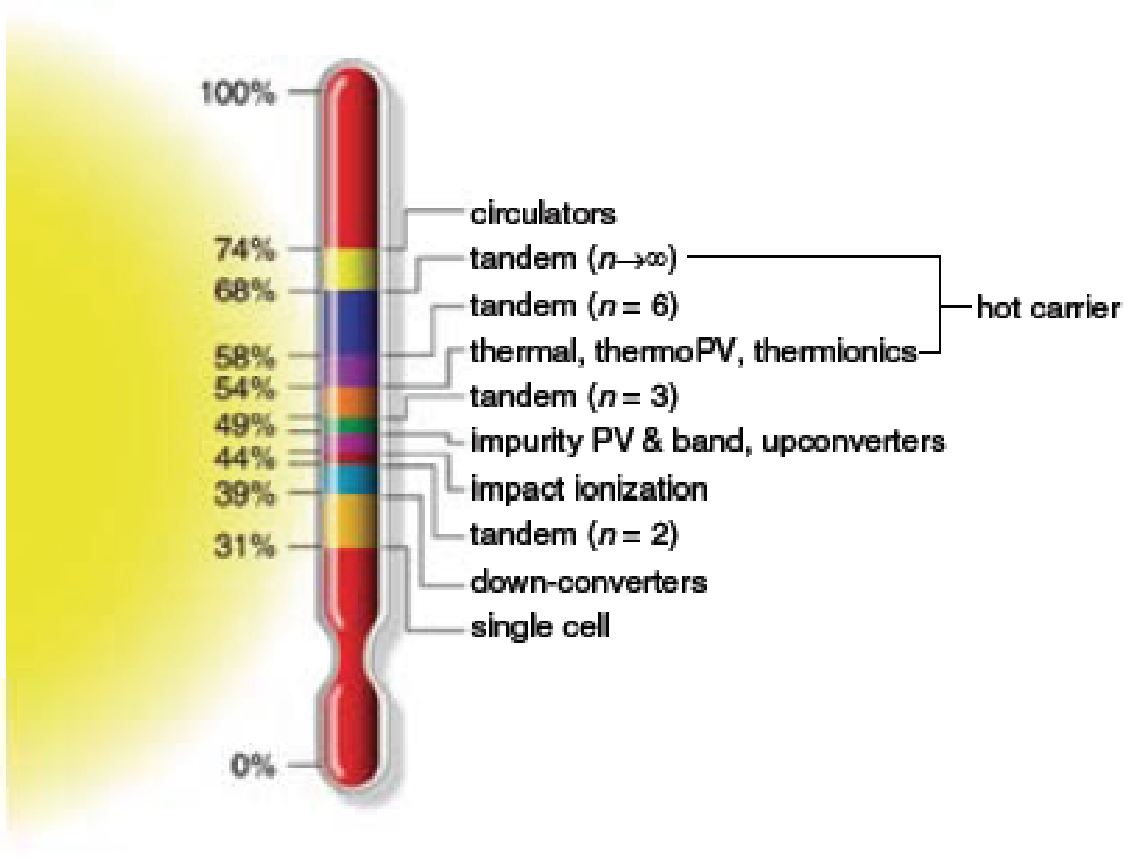

Figure 13. Third-generation options and thermodynamic limits on their efficiency. Upconverters include multi-excitonic approaches. *Note: n* is the number of cells in the stack.

David Ginley (NREL), Matin A. Green (University of New South Wales), and Reuben Collins (Colorado School of Mines) *MRS Bulletin* (2008).

Transparent Conducting Oxide (TCO)

Introduction of Transparent Conducting Oxide (TCO)

Transparent conducting oxide는 가시광선 영역의 빛을 투과시켜 사람의 눈에 투명하게 보이는 동시에 전기전도도가 좋은 물리적 특성을 나타내는 재료를 일컬으며, 보통은 줄여서 TCO, 우리말로는 투명전극이라는 단어를 사용하기도 한다.

1880년대 TCO의 개념이 처음 도입: Se을 사용한 태양전지의 전면 전극에 Ag, Pt을 얇게 증착하여 사용

→ 태양전지의 전면 전극은 외부에서 들어오는 태양빛을 되도록 많이 투과시켜 빛 에너지가 Se 태양전지에 많이 도달하도록 하여야 하며, 동시에 빛 에너지를 받아 생성된 전자와 홀을 잘 이동시켜서 유용한 에너지로 사용하여야 하므로 전기전도도 역시 좋아야 함.

1990년대 후반부터 LCD, PDP를 필두로 FPD 시장이 폭발적으로 증가하고 태양전지 시장 또한 성장. 이에 따라 TCO에 대한 수요가 증가하며 현재까지 연구가 활발히 진행.

A pellet of Indium Tin Oxide sample (left) and this same material in thin film form (right)

Physical Properties of Transparent Conducting Oxide (Transmittance)

가시광선 영역 (일반적으로 400nm ~ 700nm 파장의 전자기파)에서 투명하기 위해서는 electronic energy band gap이 400nm 파장의 전자기파 에너지인 3.1 eV 이상 되어야 한다.

band gap 3.1 eV 이상인 대표적인 산화물 반도체: ZnO (3.3 eV), In_2O_3 (3.7 eV), MgO (3.6 eV), SnO_2 (3.6 eV)

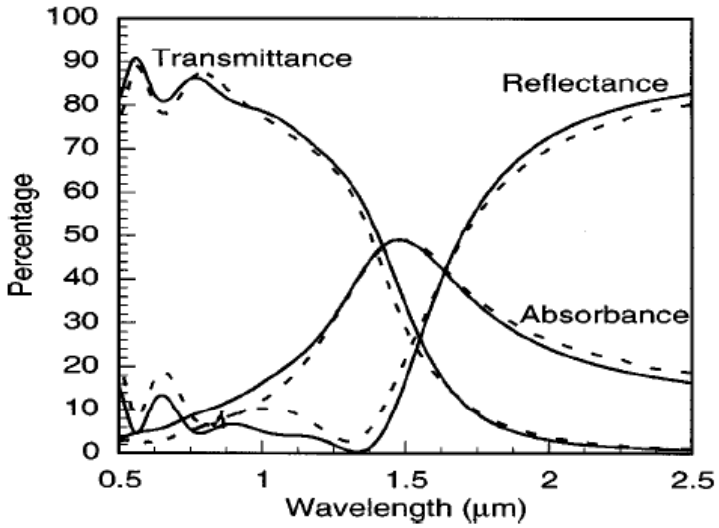

FIG. 18. Measured and modeled reflectance, transmittance, and absorbance of a Cd_2SnO_4 film as functions of wavelength.

J. Vac. Sci. Technol. A **18** (Nov/Dec 2000)

→TCO의 한 종류인 Cd_2SnO_4 박막의 transmittance 측정 결과.
가시광선 영역에서 80~90 % 수준의 transmittance를 나타낸다. Energy band gap 보다 큰 에너지의 빛의 파장의 경우에는 생략되었으나, band to band transition에 의해 빛이 흡수되면서 transmittance 가 급감한다. 또한 energy 가 작은 적외선 영역에서는 plasma resonance frequency를 기점으로 reflectance가 증가함으로 인해 transmittance가 감소한다. 이러한 transmittance 측정 결과는 대부분 연구되고 있는 TCO 물질들에서 거의 유사한 양상을 나타낸다. Cd_2SnO_4의 경우 Cd에 독성이 있어 상용화 할 수 없다.
일반적으로 TCO 물질이 상업적으로 사용되기 위해서는 가시광선 영역에서의 transmittance가 85% 이상 되어야 가능하다.

Search for improved transparent conducting oxides: A fundamental investigation of CdO, Cd_2SnO_4, and Zn_2SnO_4

T. J. Coutts,[a] D. L. Young, and X. Li
National Renewable Energy Laboratory, Golden, Colorado 80401

W. P. Mulligan
Sun Power Corporation, Sunnyvale, California 94086

X. Wu
National Renewable Energy Laboratory, Golden, Colorado 80401

J. Vac. Sci. Technol. A **18** (Nov/Dec 2000)

(Received 10 March 2000; accepted 5 July 2000)

The bulk of developmental work on transparent conducting oxides (TCOs) has been somewhat empirical. This statement applies both to more familiar materials such as indium tin oxide (ITO) and to less-well-known materials that have emerged in recent years. In this article, we place a greater emphasis on more fundamental research. Our eventual goal is to gain a thorough understanding of these materials, their potential for further improvement, whether or not they suggest new and potentially superior materials, and the way their properties are influenced by structural and other issues. We also hope to provide guidelines to other researchers working in this area. We have investigated films of cadmium oxide (CdO), cadmium stannate (Cd_2SnO_4 or CTO), and zinc stannate [Zn_2SnO_4 (ZTO)]. The CdO was prepared by chemical-vapor deposition, whereas the stannates were prepared by rf sputtering. In both cases, Corning 7059 glass substrates were used. However, some depositions were also made onto tin oxide, which had a profound effect on the nucleation of CdO, in particular. It is well known that a high free-carrier mobility is essential for a TCO with near-ideal electro-optical properties. Increasing the free-carrier concentration also increases the free-carrier absorbance but a higher mobility reduces it. We have achieved free-electron mobilities in CdO ($E_g \sim 2.4$ eV) of greater than 200 $cm^2\ V^{-1}\ s^{-1}$, of almost 80 $cm^2\ V^{-1}\ s^{-1}$ in CTO ($E_g \sim 3.1$ eV), but of only 10–15 $cm^2\ V^{-1}\ s^{-1}$ in ZTO ($E_g \sim 3.6$ eV). We have characterized these materials, and will show key data, using techniques as diverse as the Nernst–Ettingshausen effect; Mössbauer, Raman, optical, and near-infrared spectroscopies; atomic-force and high-resolution electron microscopy; and x-ray diffraction. These measurements have enabled us to determine the effective mass of the free carriers and their relaxation time, the probable distributions of cations between octahedral and tetrahedral sites, the role of the deposition parameters on the carrier concentrations, and the nature of the dominant scattering mechanisms. We also consider issues relating to toxicity of cadmium and to reserves of indium. Both are of great significance to prospective large-volume manufacturers of TCO films and must be taken into account by researchers. [S0734-2101(00)00206-2]

Physical Properties of Transparent Conducting Oxide (Resistivity)

TCO의 resistivity는 약 **10^{-4} Ωcm** 이하의 값을 가져야 한다.

$$\sigma = nq\mu$$

Conductivity (σ)는 위의 식에 따라 **carrier concentration (*n*)을 증가시키거나 mobility (*μ*)를 증가시킴** 으로써 향상시킬 수 있다.
물질에 impurity (donor)를 doping함으로써 carrier concentration을 증가 시킬 수 있고, 물질의 crystallinity를 좋게 하여 carrier mobility를 증가시킬 수 있다. 그러나 impurity를 어떤 critical value 이상으로 doping하면 crystal structure를 변화시키고 impurity에 의한 scattering을 증가시켜 conductivity의 저하요소가 될 수도 있다. 또한 conduction band내의 전자에 의해 free carrier absorption이 일어나 transmittance 마저 감소 시킬 수 있다.

$$\mu = \frac{q\tau}{m^*}$$

Carrier mobility (*μ*)는 위의 식에 따라 **relaxation time (*τ*)를 증가시키거나 effective mass (*m**)를 감소시킴** 으로써 늘릴 수 있다. 그러나 일반적으로 가시광선에 투명한 wide bandgap material의 경우 effective mass가 크다. 따라서 relaxation time을 늘려 carrier mobility를 증가 시킬 수 있다. Relaxation time은 재료의 crystallinity 를 좋게 하여 carrier의 scattering을 감소 시킴으로서 증가 시킬 수 있다.

Current Research on TCO

현재까지 TCO로서 많이 연구되고 있는 물질은 In_2O_3, SnO_2, ZnO 등이 대표적이다. 이 물질들은 doping effect가 비교적 두드러지게 나타나, 전기적 광학적 특성이 다른 Ga_2O_3, Al_2O_3, MgO 등의 material보다 TCO로의 응용가능성이 높다.

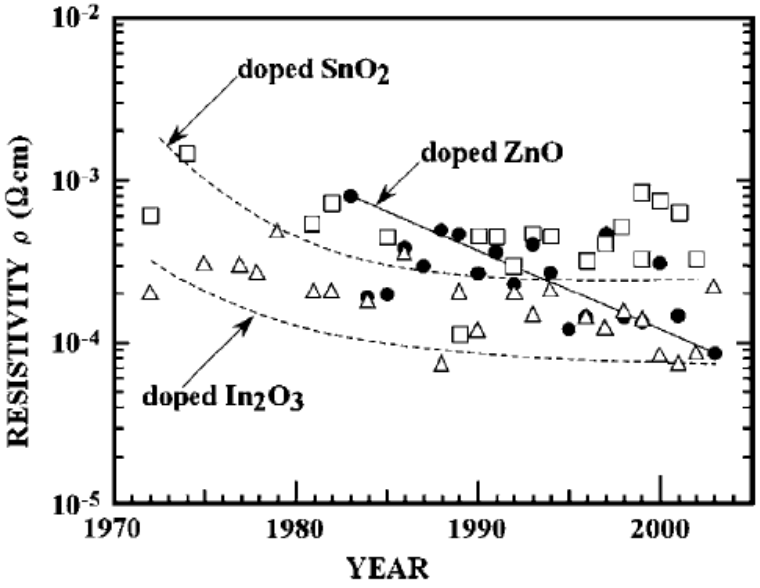

Figure 2. Reported resistivity of impurity-doped binary compound TCO films, 1972–present: impurity-doped SnO_2 (□), In_2O_3 (Δ) and ZnO (●).

Semicond. Sci. Technol. 20 (2005) S35–S44

In_2O_3 의 경우 SnO_2 와 ZnO보다 낮은 resistivity 값을 가져 가장 먼저 상용화 되고 현재 Sn doped In_2O_3 (ITO) 가 TCO로서 쓰인다. 그러나 ITO의 경우 In이 희귀원소로서 가격이 비싸다는 단점이 있다.

ZnO는 band gap이 3.3 eV 정도이며, direct band gap을 가지고 있어 optoelectronic device로서 활용가능성이 높다. 특히 Al, Ga 등의 impurity doping 시에 우수한 전기적 특성을 얻을 수 있다.

Al doped ZnO (AZO)는 Al이 doping 됨으로써 낮은 resistivity 가 얻어지고 지구상에 풍부하게 존재 하며 값이 싼 재료로 제작될 수 있다. 또한 독성이 없으며 가시광선 영역에서 transmittance가 높아 (~90%) solar cell의 전극으로서 유망한 물질로 기대된다.

Transparent conducting oxide semiconductors for transparent electrodes

Tadatsugu Minami

Optoelectronic Device System R&D Center, Kanazawa Institute of Technology,
7-1 Ohgigaoka, Nonoichi, Ishikawa 921-8501, Japan

Semicond. Sci. Technol. 20 (2005) S35–S44

Received 6 October 2004
Published 15 March 2005
Online at stacks.iop.org/SST/20/S35

Abstract

The present status and prospects for further development of polycrystalline or amorphous transparent conducting oxide (TCO) semiconductors used for practical thin-film transparent electrode applications are presented in this paper. The important TCO semiconductors are impurity-doped ZnO, In_2O_3 and SnO_2 as well as multicomponent oxides consisting of combinations of ZnO, In_2O_3 and SnO_2, including some ternary compounds existing in their systems. Development of these and other TCO semiconductors is important because the expanding need for transparent electrodes for optoelectronic device applications is jeopardizing the availability of indium-tin-oxide (ITO), whose main constituent, indium, is a very expensive and scarce material. Al- and Ga-doped ZnO (AZO and GZO) semiconductors are promising as alternatives to ITO for thin-film transparent electrode applications. In particular, AZO thin films, with a low resistivity of the order of 10^{-5} Ω cm and source materials that are inexpensive and non-toxic, are the best candidates. However, further development of the deposition techniques, such as magnetron sputtering or vacuum arc plasma evaporation, as well as of the targets is required to enable the preparation of AZO and GZO films on large area substrates with a high deposition rate.

AZO Characteristic

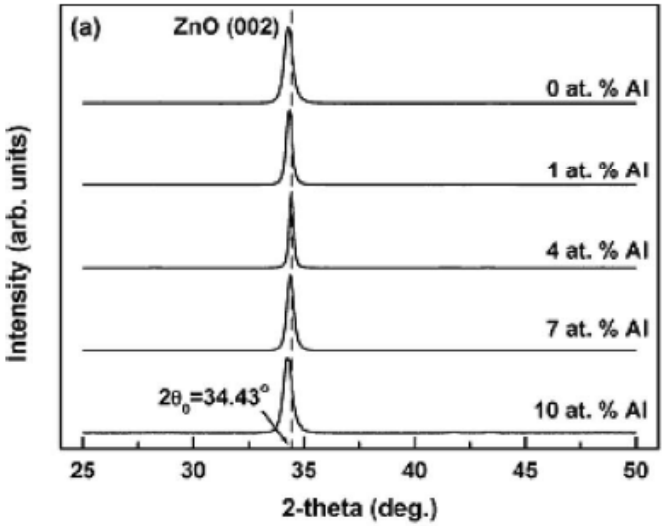

FIG. 4. XRD profiles of (Zn,Al)O films prepared with the Al contents of 0, 1, 4, 7, 10, 15, 20, 30, and 50 at. %. They are shown in (a) and (b) for convenient illustrations.

→Al의 doping 양의 변화에 따른 AZO의 X-ray diffraction (XRD) data.

Al의 doping 양이 10 at. % 가 될때 까지는 AZO의 XRD peak이 ZnO의 peak과 거의 일치함을 볼 수 있다. 즉 c-axis orientation을 가지는 crystal structure가 변하지 않는 것을 알 수 있다.

J. G. Lu's Group, Zhejiang University
J. Appl. Phys. **100**, 073714 (2006)

Structural, optical, and electrical properties of (Zn,Al)O films over a wide range of compositions

J. G. Lu,[a] Z. Z. Ye,[b] Y. J. Zeng, L. P. Zhu, L. Wang, J. Yuan, and B. H. Zhao
State Key Laboratory of Silicon Materials, Zhejiang University, Hangzhou 310027, People's Republic of China

Q. L. Liang
Quality Engineering Division, Semiconductor Manufacturing International Corp., Shanghai 201203, People's Republic of China

J. G. Lu's Group, Zhejiang University

J. Appl. Phys. **100**, 073714 (2006)

(Received 1 March 2006; accepted 31 July 2006; published online 13 October 2006)

(Zn,Al)O thin films have been prepared by a dc reactive magnetron sputtering system with the Al contents in a wide range of 0–50 at. %. The structural, optical, and electrical properties of (Zn,Al)O films were detailedly and systematically studied. The amount of Al in the film was nearly the same as, but often lower than, that in the sputtering target. The growth rate of films monotonically decreased as the Al content increased. In a low Al content region (<10 at. %), Al-doped ZnO (AZO) thin films could be obtained at 400 °C in an $Ar-O_2$ ambient with good properties. The optimal results of *n*-type AZO films were obtained at an Al content of 4 at. %, with low resistivity $\sim 10^{-4}$ Ω cm, high transmittance ~90% in the visible region, and acceptable crystal quality with a high *c*-axis orientation. The band gap could be widened to 3.52 eV at 4 at. % Al due to the Burstein-Moss shift [E. Burstein, Phys. Rev. **93**, 632 (1954)] modulated by many-body effects. An appropriate Al-doping concentration served effectively to release the residual, compressive stress in film, which may be the reason for the improvement in film stability and the increment in grain size as well. In a medium Al content region (10–30 at. %), however, the film quality was degraded, which was presumably due to the formation of clusters or precipitates in the grains and boundaries. Besides the (002) plane, other diffraction peaks such as (100) and (101) planes of ZnO were observed, but the (Zn,Al)O films still exhibited a single-phase wurtzite ZnO structure. An intragrain cluster scattering mechanism was proposed to interpret the reduction of carrier mobility in films with the Al contents in the 7–20 at. % region. The solubility limit of Al in ZnO film was identified to be in the 20–30 at. % range, much higher than the thermodynamic solubility limit of 2–3 at. % in ZnO. In a high Al content region (≥30 at. %), there were distinct observations for (Zn,Al)O films. As the Al content was 30 at. %, the film appeared in a two-phase nature with ZnO hexagonal and Al_2O_3 rhombohedral structures. At the 50 at. % Al content, the matrix of the (Zn,Al)O film was Al_2O_3, and no evident trace of wurtzite ZnO was observed. The electrical and optical properties for both cases were also very different from those at the Al contents below 30 at. %. [DOI: 10.1063/1.2357638]

AZO Characteristics

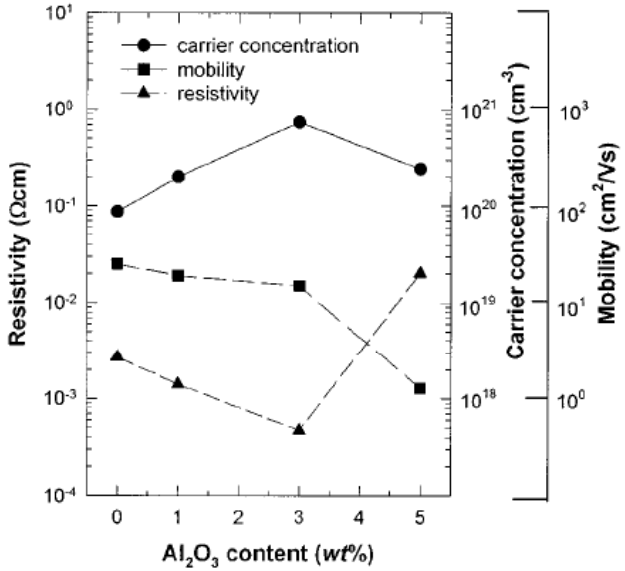

FIG. 8. Plot of the carrier concentration, Hall mobility and resistivity of AZO films as a function of Al_2O_3 content in the target (T_s= 150 °C, rf power= 150 W, P_w= 2 mTorr).

→ Al의 doping 양의 변화에 따른 AZO의 resistivity.

Impurity (Al)가 어떤 critical value 까지 doping될 때는 resistivity가 낮아지지만 그 이상 doping 될 때는 resistivity가 증가하는 것을 볼 수 있다. 이는 Al의 doping 양이 critical value이상으로 높아지면 Al이 donor로서 작용하지 않고 grain boundary등에 segregation되기 때문이다.

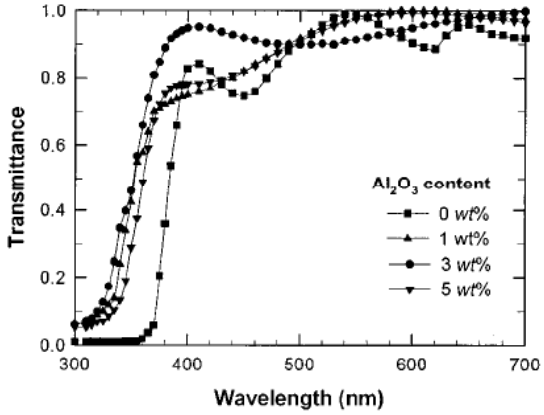

FIG. 13. Optical transmission of AZO films prepared by different amounts of Al_2O_3 in the target (T_s=150 °C, rf power=150 W, P_w= 2 mTorr).

→ Al의 doping 양의 변화에 따른 AZO의 transmittance.

Al의 doping양에 관계 없이 가시광선 영역에서 약 90%의 transmittance를 보인다.

Kun Ho Kim's Group (Gyeongsang National University)
Journal of Applied Physics **81**, 7764 (1997)

AZO Images

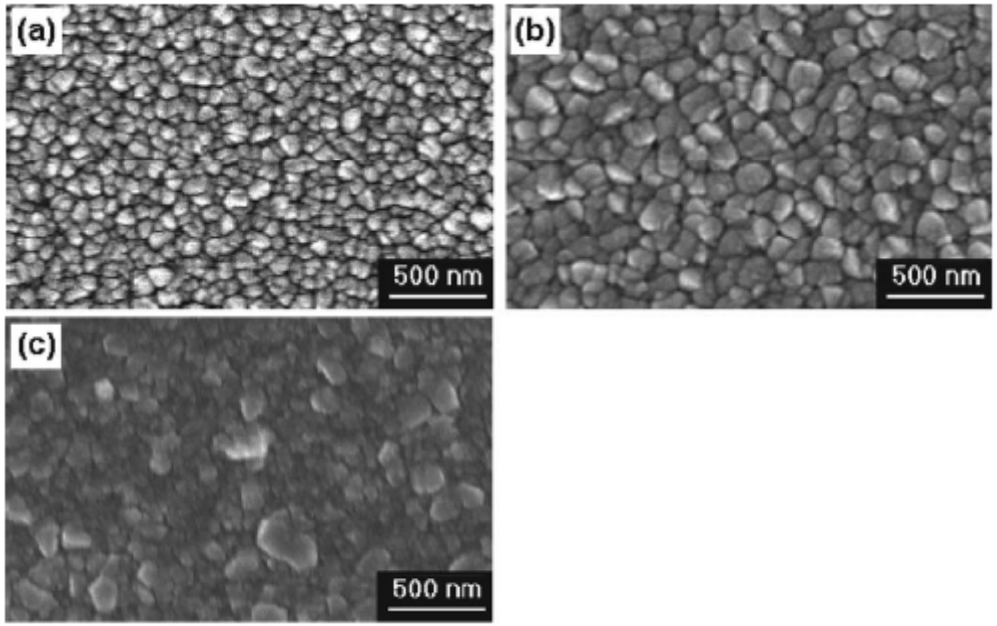

FIG. 7. SEM images of the (Zn,Al)O films prepared at different Al contents: (a) 0 at. %, (b) 4 at. %, (c) 15 at. %

→Al의 doping양에 따른 AZO의 surface SEM images.
AZO 내의 Al contents가 4 at. % 일 때는 undoped ZnO의 image와 비교했을 때 grain이 커지고 grain distribution이 더 uniform 해진다. Al contents가 15 at. % 일 때는 grain distribution이 inhomogeneous 해지며 많은 pore가 보인다. 따라서 15 at. %의 Al doping 시에는 crystallinity가 나빠지며 conductivity가 감소한다.

J.G. Lu's Group., Zhejiang University,
Journal of Applied Physics 100 (2006) 073714

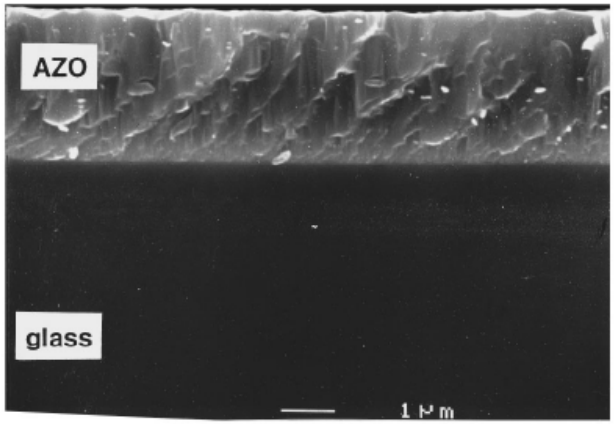

FIG. 6. Cross-sectional SEM micrograph of the AZO film prepared on a glass substrate at T_s = 150 °C (P_{rf} = 150 W, P_w = 2 mTorr).

→Al contents가 4 at.% 일 때 AZO의 cross-sectional SEM image.
C-axis orientation을 가진 columnar structure를 보인다.

Kun Ho Kim's Group (Gyeongsang National University)
Journal of Applied Physics **81**, 7764 (1997)

Structural, electrical and optical properties of aluminum doped zinc oxide films prepared by radio frequency magnetron sputtering

Kun Ho Kim[a)]
Department of Physics and the Research Institute of Natural Science, Gyeongsang National University, Chinju 660-701, Korea

Ki Cheol Park and Dae Young Ma
Department of Electronic Materials Engineering and Research Center for Aircraft Parts Technology, Gyeongsang National University, Chinju 660-701, Korea

(Received 15 October 1996; accepted for publication 17 March 1997)

Aluminum doped zinc oxide (AZO) films are prepared by rf magnetron sputtering on glass or Si substrates using specifically designed ZnO targets containing different amount of Al_2O_3 powder as the Al doping source. The structural, electrical, and optical properties of the AZO films are investigated in terms of the preparation conditions, such as the Al_2O_3 content in the target, rf power, substrate temperature and working pressure. The crystal structure of the AZO films is hexagonal wurtzite. The orientation, regardless of the Al content, is along the *c* axis perpendicular to the substrate. The doping concentration in the film is 1.9 at. % for 1 wt % Al_2O_3 target, 4.0 at. % for 3 wt % Al_2O_3 target, and 6.2 at. % for 5 wt % Al_2O_3 target. The resistivity of the AZO film prepared with the 3 wt % Al_2O_3 target is $\sim 4.7\times 10^{-4}$ Ω cm, and depends mainly on the carrier concentration. The optical transmittance of a 1500-Å-thick film at 550 nm is ~90%. The optical band gap depends on the Al doping level and on the microstructure of the films, and is in the range of 3.46–3.54 eV. The optical band gap widening is proportional to the one-third power of the carrier concentration. [S0021-8979(97)04312-0]

Kun Ho Kim's Group (Gyeongsang National University)
Journal of Applied Physics **81**, 7764 (1997)

- 2009-11-17